BONNER METEOROLOGISCHE ABHANDLUNGEN

Heft 70 (2015) (ISSN 0006-7156)
Herausgeber: Andreas Hense

A S M Mostaquimur Rahman

Influence of Subsurface Hydrodynamics on the Lower Atmosphere at the Catchment Scale

BONNER METEOROLOGISCHE ABHANDLUNGEN

Heft 70 (2015) (ISSN 0006-7156)
Herausgeber: Andreas Hense

A S M Mostaquimur Rahman

INFLUENCE OF SUBSURFACE HYDRODYNAMICS ON THE LOWER ATMOSPHERE AT THE CATCHMENT SCALE

Influence of Subsurface Hydrodynamics on the Lower Atmosphere at the Catchment Scale

Dissertation
zur
Erlangung des Doktorgrades (Dr. rer. nat.)
der
Mathematisch-Naturwissenschaftlichen Fakultät
der
Rheinischen Friedrich-Wilhelms-Universität Bonn

vorgelegt von
Dipl.-Met. A S M Mostaquimur Rahman
aus
Bangladesh

Bonn, März 2015

Diese Arbeit ist die ungekürzte Fassung einer der Mathematisch-Naturwissenschaftlichen Fakultät der Rheinischen Friedrich-Wilhelms-Universität Bonn im Jahr 2015 vorgelegten Dissertation von A S M Mostaquimur Rahman aus Bangladesh.

This paper is the unabridged version of a dissertation thesis submitted by A S M Mostaquimur Rahman born in Bangladesh to the Faculty of Mathematical and Natural Sciences of the Rheinische Friedrich-Wilhelms-Universität Bonn in 2015.

Anschrift des Verfassers:

A S M Mostaquimur Rahman
Meteorologisches Institut der
Universität Bonn
Auf dem Hügel 20
D-53121 Bonn

Address of the author:

1. Gutachter: Prof. Dr. Stefan Kollet, Forschungszentrum Jülich
2. Gutachter: Prof. Dr. Clemens Simmer, Rheinische Friedrich-Wilhelms-Universität Bonn

Tag der Promotion: 09. Oktober 2015

To my family

Abstract

Processes (e.g., groundwater flow, evapotranspiration, precipitation) in different compartments of the hydrological cycle (e.g., subsurface, land surface, and atmosphere) show characteristic variability at different space-time scales and interact with each other through complex non-linear feedback mechanisms. In the hydrologic cycle, subsurface hydrodynamics that may be expressed through the presence of a free water table, interact with land surface mass and energy balance components (e.g., shallow soil moisture and evapotranspiration), which may significantly affect atmospheric processes (e.g., atmospheric boundary layer height and convective precipitation). This thesis aims to understand and quantify the feedback mechanisms between groundwater dynamics and the atmosphere via land surface processes at the catchment scale by analyzing the space-time variability of the fluxes and states of the coupled water and energy cycles. Both modeling and observations of various mass and energy balance components of the hydrological cycle are applied in order to achieve this goal. A coupled simulation platform consisting of a subsurface model (ParFlow), a land surface model (CLM3.5), and an atmospheric model (COSMO-DE) is applied over a model domain encompassing the Rur catchment, Germany, to simulate the fluxes from the subsurface across land surface into the atmosphere over multiple years. The coupled model continuously simulates the mass and energy fluxes over space and time for all three compartments of the hydrological cycle. A comprehensive comparison between the model results and observations demonstrates the model's capability to reproduce the dynamics as well as the absolute values of the mass and energy fluxes (e.g., shallow soil moisture, groundwater table depth, latent heat flux, sensible heat flux, near-surface temperature). Statistical, geostatistical, and spectral analysis techniques are used to explore the inherent variability of the compartmental mass and energy fluxes, which reveals the interconnections of the compartmental processes at various space-time scales. In this thesis, a novel concept of a *dual-boundary forcing* is introduced to represent and quantify the interactions between the compartmental mass and energy balance components at the relevant space and time scales. According to this concept, atmosphere and

groundwater act as the upper and lower boundary conditions, respectively, for the land surface. The dominating boundary condition controlling the variability of land surface processes is determined by space and time localized moisture and energy availability. This concept states that the space-time patterns of land surface processes can be explained by the variability of the dominating boundary condition, which is corroborated by applying continuous wavelet transform and variogram techniques on the model results and observations. In the ensuing step, the proposed *dual-boundary forcing* concept is tested considering different lower boundary conditions based on groundwater dynamics in a coupled subsurface-land surface model. The results show that there are significant and predictable differences in the variability of land surface processes at monthly to multi-month time scales from the model configurations with different lower boundary conditions, which indicates that the representation of groundwater dynamics in a numerical simulation platform affects the temporal variability of land surface processes. For example, it was demonstrated that the temporal variability of evapotranspiration simulated by a coupled subsurface-land surface model is reduced at monthly to multi-month time scales in case of a simplified representation of groundwater dynamics. Finally, fully integrated simulations of the terrestrial hydrological cycle are performed considering different groundwater dynamics in a subsurface-land surface-atmosphere model of the larger Rur catchment to study the influence of subsurface hydrodynamics on local weather generating processes. The results show that differences in groundwater dynamics in the model affect shallow soil moisture, evapotranspiration, and sensible heat transfer, which influences atmospheric boundary layer height, convective available potential energy, and precipitation especially under strong convective conditions. These results suggest that groundwater dynamics may generate systematic uncertainties in atmospheric simulations in a fully-coupled model. This thesis reveals that the presence of groundwater dynamics is important to take into account in atmospheric simulations and water resources assessments, such as, drought prediction.

Zusammenfassung

Die Prozesse (z.B. Grundwasserströmung, Evapotranspiration, Niederschlag), die in den verschiedenen Kompartimenten des hydrologischen Kreislaufs (z.B. Boden, Landoberfläche und Atmosphäre) stattfinden, zeigen eine charakteristische Variabilität auf verschiedenen Zeit- und Raumskalen. Sie interagieren miteinander durch komplexe nicht-lineare Feedback-Mechanismen. Die Hydrodynamik des Bodens kann beispielsweise durch einen frei beweglichen Grundwasserspiegel formuliert werden und interagiert mittels Komponenten der Massen- und Energiebilanz mit der Landoberfläche (z.B. oberflächennahe Bodenfeuchte und Evapotranspiration). Der Einfluss der Hydrodynamik auf die Landoberfläche kann wiederum signifikante Auswirkungen auf die atmosphärischen Prozesse herbeiführen (z.B. die Höhe der atmosphärischen Grenzschicht und konvektiven Niederschlag). Diese Arbeit fokussiert sich auf diese Feedback-Mechanismen, die zwischen Grundwasserdynamik und Atmosphäreneigenschaften via Landoberflächenprozesse auf der Einzugsgebietsskala entstehen können. Das Verständnis und die Bewertung dieser Mechanismen wird durch die Analyse der Raum-Zeitvariabilität der Zustände und Flüsse des gekoppelten Wasser- und Energiekreislaufes erzielt. Die Verwendung von Beobachtungsdaten und die Modellierung der verschiedenen Komponenten der Massen- und Energiebilanz des hydrologischen Kreislaufs sollen dabei helfen, die entsprechenden Erkenntnisse zu liefern. Eine gekoppelte Simulationsplattform, die aus einem Boden-Grundwassermodell (ParFlow), einem Landoberflächenmodell (CLM3.5) und einem Atmosphärenmodell (COSMO-DE) besteht, wird über das Einzugsgebiet der Rur (Deutschland) angewendet. In diesem gekoppelten System werden die Massen- und Energieflüsse von den untersten Bodenschichten über die Landoberfläche bis in die Atmosphäre über einen Zeitraum von mehreren Jahren durchgängig in Zeit und Raum simuliert. Ein umfassender Vergleich zwischen den Resultaten des Modells und den Beobachtungsdaten demonstriert die Eigenschaft des Modells, die Dynamik und die absoluten Werte des Massen- und Energieflusses (z.B. oberflächennahe Bodenfeuchte, Grundwasserspiegel, latenten und fühlbaren Wärmefluss, bodennahe Temperaturen) zu

reproduzieren. Statistische, geostatistische und spektrale Analysetechniken werden genutzt, um die inhärente Variabilität der Massen- und Energieflüsse der entsprechenden Kompartimente zu identifizieren. Durch diese Analysetechniken lassen sich die Zweiwegekopplungen der Prozesse der entsprechenden Kompartimente in verschiedenen Zeit- und Raumskalen bestimmen. In dieser Arbeit wird ein neues Konzept des *dual-boundary forcings* eingeführt, um die Interaktion zwischen den Komponenten der Massen- und Energiebilanz der entsprechenden Bereiche in den relevanten Raum- und Zeitskalen zu repräsentieren und quantifizieren. Die Atmosphäre und das Grundwasser agieren diesem Konzept entsprechend als obere, respektive untere Randbedingung für die Landoberfläche. Die zeitliche und räumliche Verfügbarkeit von Feuchte und Energie bestimmt hierbei die dominierende Randbedingung bezüglich der Variabilität der Landoberflächenprozesse. Das Konzept des *dual-boundary forcings* konstatiert im weiteren Verlauf, dass die zeitlichen und räumlichen Strukturen der Landoberflächenprozesse durch die Variabilität der dominierenden Randbedingung erklärt werden kann. Dieser Einfluss der Randbedingung auf die Landoberfläche wird durch die Anwendung der Kontinuierliche Wavelet-Transformation und Variogrammanalysen der Modellresultate und der Beobachtungsdaten gezeigt. Im darauffolgenden Schritt wird unter der Betrachtung verschiedener unterer Randbedingungen, basierend auf der Grundwasserdynamik des gekoppelten Boden-Landoberflächenmodells, das aufgestellte *dual-boundary forcing* Konzept getestet. Die Ergebnisse der Simulationen mit den verschiedenen unteren Randbedingungen zeigen, dass es signifikante vorhersagbare Unterschiede in der Variabilität von Landoberflächenprozessen im Bereich von monatlichen bis hin zu Zeitskalen von mehreren Monaten gibt. Dies zeigt, dass das Vorhandensein der Grundwasserdynamik in einer numerischen Simulationsplattform die zeitliche Variabilität der Landoberflächenprozesse beeinflußt. Zum Beispiel wurde gezeigt, dass die zeitliche Variabilität der Evapotranspiration durch ein gekoppeltes Boden-Grundwassermodell simuliert wird monatlich zu mehrmonatigen Zeitskalen bei einer vereinfachten Darstellung der Grunddynamik verringert. In einem letzten Schritt werden unter der Berücksichtigung verschiedener Randbedingungen der Grundwasserdynamik im Boden-Landoberflächen-Atmosphären Modell des erweiterten Rur-Einzugsgebiets komplett integrierte Simulationen des terrestrischen, hydrologischen Kreislaufs durchgeführt, um den Einfluss der Hydrodynamik des Bodens auf lokale, wetterbestimmende Prozesse zu analysieren. Die Ergebnisse zeigen, dass unterschiedliche Grundwasserdynamiken des Modells einen signifikanten Einfluß auf die landoberflächennahe Bodenfeuchte, die Evapotranspiration und fühlbaren Wärmeströme ausüben. Diese weisen wiederum einen Einfluss auf die

Grenzschichthöhe, CAPE (convective available potential energy) und den Niederschlag, besonders unter stark konvektiven Konditionen auf. Diese Resultate lassen den Schluß zu, dass die Grundwasserdynamik in vollgekoppelten Modellen systematische Unsicherheiten in atmosphärischen Simulationen generieren können. Unter der Berücksichtigung von Modellresultate und Beobachtungen zeigt diese Arbeit auf, dass das Vorhandensein der Grundwasserdynamik in numerischen Simulationsplattformen die Variabilität der Prozesse durch Massen- und Energieflüsse der entsprechenden Kompartimente an der Landoberfläche beeinflusst. Aufgrund dieser Ergebnisse ist es wichtig, das Vorhandensein der Grundwasserdynamik bei atmosphärischen Simulationen und Anwendungen in der Wasserbewirtschaftung, wie zum Beispiel Vorhersagen von Dürreperioden, zu berücksichtigen.

Contents

List of figures

List of tables

List of abbreviations

ABLH	Atmospheric Boundary Layer Height
CAPE	Convective Available Potential Energy
CBC	Constant Boundary Condition
CLM	Common Land Model
DBC	Dynamic Boundary Condition
DBF	Dual-Boundary Forcing
DSMW	Digital Soil Map of the World
DWD	Deutscher Wetterdienst
FAO	Food and Agricultural Organization of UNO
FD	Free-Drainage boundary condition
GLC2000	Global Land Cover 2000
IGBP	International Geosphere-Biosphere Program
LANUV	Landesamt für Natur, Umwelt und Verbraucherschutz NRW
LBC	Lower Boundary Condition
MODIS	Moderate-Resolution Imaging Spectroradiometer
PFT	Plant Functional Type
TERENO	Terrestrial Environmental Observatories
TerrSysMP	Terrestrial Systems Modeling Platform
TR32	Transregional Collaborative Research Centre

Chapter 1

Introduction

1.1 Background

The terrestrial hydrological cycle comprises numerous complex processes (e.g., groundwater flow, evapotranspiration, precipitation) in the subsurface, land surface, and atmosphere compartments. These processes exhibit inherent variability at different space-time scales [e.g., *Kumar and Georgiou*, 1993; *Haddad et al.*, 2004; *Gundogdu and Guney*, 2007; *Táany et al.*, 2009; *Beecham and Chowdhury*, 2010]. Examining the variability of the aforementioned processes in the coupled water and energy cycles is important for water resources assessment and management practices, such as, drought prediction and irrigation management under dry conditions.

Figure 1.1 shows characteristic space-time scales of various processes in different compartments of the hydrological cycle based on experimental data and heuristic considerations [*Blöschl and Sivapalan*, 1995]. This figure depicts that the space-time scale of precipitation in the atmospheric compartment of the hydrological cycle ranges from 1 km and several minutes (cumulus convection) to 1000 km and more than a day (frontal systems). While the hydrological processes (e.g., overland flow, groundwater flow) may act at similar spatial scales, they show delayed response to atmospheric forcing (i.e., precipitation). According to *Blöschl and Sivapalan* [1995], this temporal delay depends on the dominant runoff generation mechanisms and increases as the water passes through the subsurface. Figure 1.1 depicts that while processes of infiltration excess runoff are relatively fast (< 30 min), saturation excess runoff is characterized by longer time scales, because generation of a saturated layer delays runoff generation. Subsurface streamflow shows a characteristic time scale of about a day or longer. Groundwater-controlled processes, on the other hand, are associated with significantly longer time scales of months to hundreds or even thousands of years. In terms of spatial scale, infiltration excess runoff generation can be defined as a very

small scale process. Saturation excess runoff generation and subsurface stormflow, in contrast, requires a certain minimum catchment area to operate. Channel flow generally occurs at larger spatial scales above a channel initiation area up to the length scales of the largest river basins [*Blöschl and Sivapalan*, 1995].

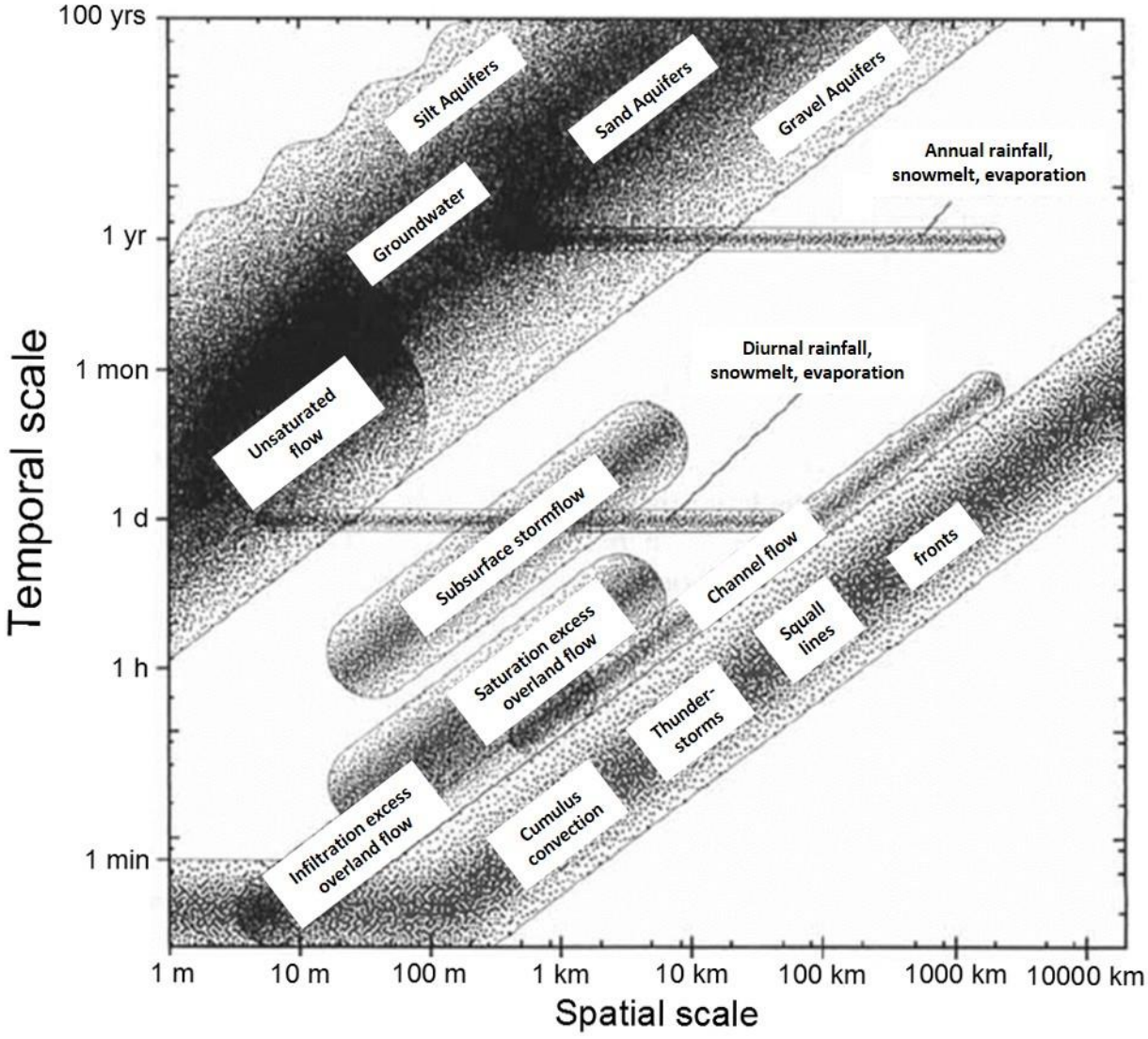

Figure 1.1. Characteristic space-time scales of the compartmental processes (adapted from *Blöschl and Sivapalan*, 1995).

In the terrestrial hydrological cycle, the aforementioned processes interact via complex non-linear feedback mechanisms [e.g., *Betts et al.*, 1996]. For example, Figure 1.2 illustrates some important land-atmosphere feedbacks across various time scales [*Betts et al.*, 1996]. This figure shows interconnection between incoming solar radiation and land surface energy balance components at the diurnal time scale, which is intuitive. A seasonal time scale is also observed in Figure 1.2, which is associated with long-term memory of soil moisture and

temperature. The century time scale connection between vegetation and aerosol indicates periodic burning of forest, which eventually reduces incoming radiation [*Betts et al.*, 1996]. Figure 1.1 and 1.2 show that the processes in different compartments of the hydrological cycle and their non-linear interactions are associated with various space-time scales (from centimeters to thousands of kilometers, and seconds to centuries, respectively), which makes the study of these interconnections difficult. However, characterizing the interactions between the compartmental processes is important in order to understand the overall mechanisms of the hydrological cycle.

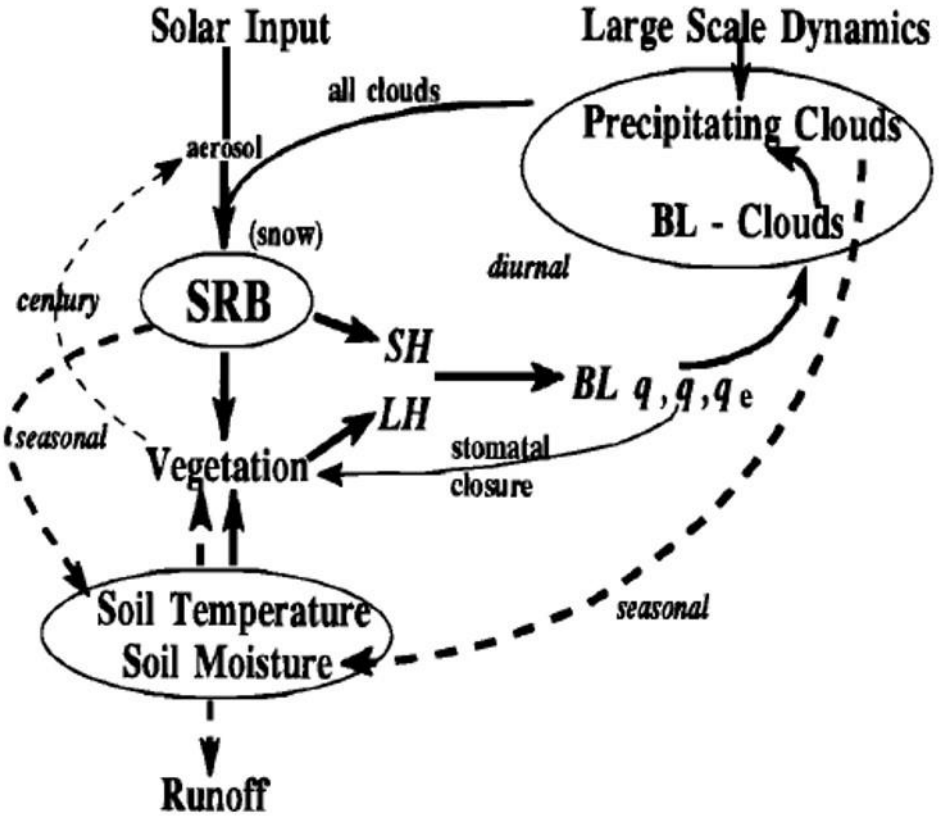

Figure 1.2. Schematic of some important land-atmosphere interactions at different time scales (adapted from *Betts et al.*, 1996). (BL - atmospheric Boundary Layer; SRB - Surface Radiation Budget; LH - Latent Heat flux; SH - Sensible heat flux; q - mixing ratio).

Several efforts have been made previously to study the feedback mechanisms between the compartmental mass and energy fluxes in the context of subsurface-land surface [e.g., *Levine and Salvucci*, 1999; *Liang et al.*, 2003; *Fan and Miguez-Macho*, 2010] and land surface-atmosphere [e.g., *Brubaker and Entekhabi*, 1996; *Betts et al.*, 1996; *Koster et al.*, 2003; *Porporato et al.*, 2000; *Santanello et al.*, 2009; *Ferguson and Wood*, 2011] interactions. Previous studies show that the moving free groundwater table influences land surface mass

and energy fluxes [e.g., *Kollet and Maxwell*, 2008; *Maxwell and Kollet*, 2008; *Soylu et al.*, 2011]. *Liang et al.* [2003] showed that the interactions between surface and groundwater dynamics play an important role on land surface mass and energy fluxes. *Maxwell and Miller* [2005] demonstrated the effect of including detailed subsurface hydrodynamics in the Common Land Model (CLM) for simulating the fluxes and states of the coupled water and energy cycles.

The influence of groundwater on surface runoff has been demonstrated using both, observations [e.g., *Yeh and* Eltahir, 2005] and model results [e.g., *Miguez-Macho and Fan*, 2012a]. *Sklash and Farvolden* [1979] discussed the effect of groundwater on surface runoff generation using both observations and simulation results. *Yeh and Eltahir* [2005] demonstrated a significant non-linear relationship between groundwater table depth (*WTD*) and streamflow at the monthly time scale using observations from Illinois, USA. *Decharme et al.* [2010] argued that groundwater storage may be a significant source of uncertainty in simulating continental hydrological processes. Adapting a numerical modeling approach, *Miguez-Macho and Fan* [2012a] showed that the streamflow dominance in the Amazon region can be explained by the variability of groundwater table depth (*WTD*). This study summarized several important findings, such as, 1) groundwater dominates streamflow in the headwater catchment, 2) the direction and magnitude of two-way exchange between groundwater and floodwater is controlled by *WTD*, and 3) groundwater buffers surface water systems through seasonal drought periods. The studies by *Little and Bloomfield* [2010] and *Schilling and Zhang* [2012] have demonstrated the scaling properties of groundwater dynamics and showed the connection with surface water systems.

The effect of the moving free groundwater table on evapotranspiration (*ET*) through land surface soil moisture has also been discussed previously [e.g., *Chen and Hu*, 2004; *Soylu et al.*, 2011]. *Chen and Hu* [2004] discussed the influence of groundwater on *ET* via root zone moisture and argued that this effect is significant in the areas characterized by shallow *WTD*. The important role of groundwater on dry season *ET* was discussed by *Lam et al.* [2011], who argued that simulating groundwater flow in climate models has the potential to augment multi-year memory. *Tian et al.* [2012] demonstrated that representation of groundwater table influences the *ET* simulation of a numerical model. *Miguez-Macho and Fan* [2012b] showed the influence of groundwater on *ET* at a seasonal scale and discussed different mechanisms responsible for this phenomenon. This study demonstrated that capillary rise from groundwater table can maintain high dry season *ET* near the valleys. *Kollet and Maxwell*

[2008] studied the influence of groundwater dynamics on land surface energy fluxes and demonstrated a framework to examine the spatial correlation between groundwater dynamics and land surface energy fluxes. This study proposed a critical *WTD* zone (1-5 m) where this correlation is significant along hillslopes. *Kollet and Maxwell* [2008] also demonstrated that the interconnection between subsurface hydrodynamics and land surface energy fluxes depends seasonally and spatially on the spatial variability of *WTD*. *Soylu et al.* [2011] argued that root zone soil moisture, which can be a significant mediator of land-atmosphere interactions, is influenced by *WTD*. This study re-corroborated the concept of the critical *WTD* zone discussed by *Kollet and Maxwell* [2008]. A similar relationship between *ET* and *WTD* was found by *Szilagyi et al.* [2013], who used remotely sensed observations over the Platte river valley, USA. *Amenu and Kumar* [2005] demonstrated the controlling effect of the low frequency variability of groundwater dynamics on land surface energy fluxes and argued that this influence may be significant under dry conditions. The study by *Rahman et al.* [2014], discussed a framework to examine the coherence between *WTD* and land surface processes and demonstrated that groundwater dynamics affects space-time variability of *ET* under moisture limited conditions in summer. The aforementioned studies show that subsurface hydrodynamics influences the magnitude and dynamics of land surface mass and energy balance components, which may reciprocally affect the feedback mechanisms between the land surface and atmosphere.

The land-atmosphere interaction has been the subject of research for some time [e.g., *Manabe*, 1969; *Shukla and Mintz*, 1982; *Abramopoulus et al.*, 1988; *Manabe and Delworth*, 1990]. *Manabe et al.* [1969] discussed the importance of surface hydrology on the atmosphere and described a method to include surface hydrology into General Circulation Models (GCMs). *Shukla and Mintz* [1982] demonstrated the influence of *ET* on global rainfall and temperature. *Manabe and Delworth* [1990] discussed the connection between of land surface soil moisture dynamics and atmosphere indicating as the previous studies the importance of soil moisture for atmospheric processes.

In the following, numerous previous studies demonstrated the influence of land surface soil moisture on precipitation [e.g., *Findell and Eltahir*, 1997; *Koster et al.*, 2003; *Hohenegger et al.*, 2009; *Hauck et al.*, 2011; *Taylor et al.*, 2012]. *Cook et al.* [2006] showed that dry areas with lower *ET* enhance atmospheric instability and, thus, precipitation formation. *Emori* [1998] argued that spatial soil moisture variability induces local atmospheric circulation and may aid the initiation of afternoon convective precipitation. Local atmospheric circulation

induced by spatial soil moisture variability was also discussed by *Patton et al.* [2005], who demonstrated the influence of land surface heterogeneity on atmospheric boundary layer using idealized simulations. *Findell and Eltahir* [1997] studied the correlation between land surface soil moisture and subsequent rainfall and argued that knowledge of late spring/early summer soil moisture can facilitate drought and flood prediction. *Schär et al.*, [1999] demonstrated that shallow soil moisture affects precipitation via land surface energy fluxes. *Hohenegger et al.* [2009] demonstrated that there exist both positive (i.e., precipitation over regions with high soil moisture) and negative (i.e., precipitation over regions with low soil moisture) correlation between soil moisture and convective precipitation, which is of high relevance for the simulations performed in this thesis. The study by *Froidevaux et al.* [2014] indicated that background wind may be a potential mechanism for the aforementioned positive and negative correlations between soil moisture and convective precipitation.

The interconnections between land surface and atmospheric processes have also been studied previously through observations of the fluxes and states of the terrestrial system. *Zhang et al.* [2008] used soil moisture from the Global Land Data Assimilation System (GLDAS [*Rodell et al.*, 2004]) in combination with observed precipitation to study spatially varying land-atmosphere coupling strength. *Ferguson and Wood* [2011] used satellite remote sensing data in order to examine land-atmosphere coupling. Satellite remote sensing data was also used by *Taylor et al.* [2012], who demonstrated a negative feedback between land surface soil moisture and afternoon convective precipitation (i.e., probability of afternoon convective rainfall is higher over dry regions).

Because of the important role of land surface processes on the atmosphere, several previous studies have examine the effect of including land surface heterogeneity in climate models to improve local weather prediction [e.g., *Rowell and Blondin*, 1990; *Findell and Eltahir*, 1997; *Seuffert et al.*, 2002; *Gedney and Cox*, 2003; *Zhang et al.*, 2008]. *Rowell and Blondin* [1990] demonstrated that the variability of land surface soil moisture significantly affects short-range precipitation forecasts. The study by *Seuffert et al.* [2002] suggested that the inclusion of lateral water transport in soil may be important to consider in local weather prediction models.

The aforementioned studies illustrate the subsurface-land surface and land surface-atmosphere interactions through modeling and measurements. Therefore, a connection between subsurface hydrodynamics and the local weather generating processes via land surface mass and energy fluxes can be conceptualized, which has also been attempted previously. The

study by *York et al.* [2002] demonstrated seasonal to inter-annual feedbacks between groundwater and atmospheric processes. This study suggested that only a physics based model can reproduce the behavior of *WTD* and resultant influence on land-atmosphere mechanisms. *Maxwell et al.* [2007] discussed the connection between subsurface hydrodynamics and atmosphere via land surface processes. In this study, space-time correlation between *WTD* and surface and lower atmospheric processes was demonstrated. *Anyah at al.* [2008] showed the influence of subsurface hydrodynamics on precipitation via land-atmosphere interaction. *Yuan et al.* [2008] argued that groundwater dynamics influences atmospheric boundary layer processes by affecting surface heat and moisture fluxes, which may eventually affect convection. *Williams et al.* [2010] studied the connection between subsurface hydrodynamics and atmospheric processes and demonstrated that an uncertainty reduction in subsurface parameterization (i.e., hydraulic conductivity) results in reduced uncertainty in atmospheric variables (e.g., wind speed) simulated by a numerical model. Using a fully coupled scale-consistent subsurface-land surface-atmosphere simulation platform, Shrestha et al. [2014] showed that the systematic patterns in root zone soil moisture, which are the results of subsurface and land surface hydrology, affect atmospheric boundary layer development. *Bonetti et al.* [2015] examined the role of groundwater dynamics on atmospheric boundary layer processes and demonstrated that *WTD* influences the predisposition of convective rainfall via *ET*.

1.2 Objectives and outline

While the aforementioned studies showed that the compartmental processes of the hydrological cycle interact with each other, the space-time scales of these interactions remain largely unresolved. In this context, the objective of this thesis is to explain and quantify the feedback mechanisms between groundwater dynamics and lower atmospheric processes via land surface mass and energy balance components at the catchment scale. The underlying hypothesis is that the subsurface hydrodynamics modifies the patterns and structures of land surface mass and energy balance components, which may influence the atmospheric processes at various space-time scales. This thesis aims to study this influence by analyzing the space-time patterns of the fluxes and states of the coupled water and energy cycles from aquifers into the atmosphere. Both modeling and observations of mass and energy balance components of the hydrological cycle are used in this thesis to achieve the aforementioned objective and test the hypothesis. Statistical, geostatistical, and spectral analysis techniques are used to

explore the inherent variability of the compartmental processes, which reveals their interconnections at various space-time scales.

The subsequent chapters of this thesis are organized as follows:

In chapter 2, the fluxes and states of the coupled water and energy cycles are simulated from aquifers across the land surface using an integrated numerical model and the results are presented. The coupled subsurface-land surface model ParFlow.CLM [e.g., *Maxwell and Miller*, 2005; *Kollet and Maxwell*, 2008] is applied over a model domain encompassing the Rur catchment (Figure 1.4), Germany, in order to simulate the mass and energy fluxes of the hydrological cycle continuously over space and time. Model runs are performed over multiple years (2009-2011) at an hourly time step using atmospheric forcing data from the German Weather Service (DWD). The simulation results are compared with spatially distributed observations obtained from various sources (e.g., Z1/INF and Z3 projects of TR32, TERENO, LANUV, Erftverband). Statistical techniques are used to perform this comprehensive comparison, which demonstrates the model's capability to reproduce the dynamics and absolute values of the mass and energy balance components without major calibration.

In chapter 3, the model results and observations from chapter 2 are used to analyze the coherence between various processes of the coupled water and energy cycles. In this chapter, the new concept of a *dual-boundary forcing* (DBF) is introduced, which connects the processes in different compartments of the hydrological cycle at various space-time scales. According to the DBF concept, the atmosphere and groundwater act as the upper and the lower boundaries, respectively for the land surface processes. The space-time localized availability of energy and moisture determines the dominating boundary condition for the exchange processes. The land surface reacts and interacts at the interface between the free atmosphere and subsurface to adapt or transform the variability of the processes associated with those boundaries. Thus, according to this concept, when accounting for major non-linear feedbacks, the space-time patterns in land surface processes can be in large parts explained by the variability of the dominant boundary condition at the respective space and time scales. The DBF concept is substantiated applying geostatistical and spectral analysis techniques on the simulation results and observations described in chapter 2. The results suggest that the variability of latent heat flux is driven by the radiative atmospheric forcing (i.e., net radiation) at the daily time scale. This variability of latent heat flux is propagated to the subsurface compartment and creates the diurnal *WTD* fluctuation through daily water uptake under moisture limited conditions, which is analogous to periodic pumping of groundwater. Because

of this withdrawal, groundwater storage depletes and influences latent heat flux starting at monthly to multi-month time scale under soil moisture limited conditions in summer. The geostatistical analysis demonstrates that under energy limited conditions, the spatial pattern of latent heat flux is determined by net radiation. Strong influence of *WTD* on the spatial variability of latent heat flux is observed under soil moisture limited conditions. These findings suggest that, the spatial pattern of latent heat flux may be predicted from net radiation measurements alone under energy limited conditions. On the other hand, *WTD* observations are useful in predicting the spatial pattern of latent heat flux in summer. A version of this chapter has been published in the journal Water Resources Research [*Rahman et al.*, 2014].

Chapter 3 describes groundwater dynamics as the lower boundary condition of the coupled water and energy cycles in the framework of the DBF concept, which is tested in chapter 4. For chapter 4, the underlying hypothesis is that a parameterization of groundwater dynamics via simple constant head or free drainage boundary conditions may lead to an alteration (reduction) of variance in land surface processes, which may ultimately affect the prognostic capabilities of a numerical model. This hypothesis is tested considering three different lower boundary conditions (LBCs), namely, dynamic, constant, and free-drainage lower boundary conditions (DBC, CBC, and FD, respectively) in the coupled model ParFlow.CLM. The dynamic lower boundary condition (DBC) allows the temporal evolution of the groundwater table, while constant lower boundary condition (CBC) maintains a temporally constant *WTD* throughout the simulation period. The free drainage (FD) configuration, on the other hand, mimics the classical description of soil water flow in land surface models at the bottom of the model domain and allows water to leave via gravity drainage in purely one-dimensional vertical parameterization. Except for the LBCs, the three model configurations are identical in terms of inputs, initial, and boundary conditions. Therefore, the differences in land surface processes simulated by the aforementioned model configurations can be attributed directly to the differences in groundwater dynamics. The results demonstrate differences in spatial and temporal variability of shallow soil moisture and latent heat flux from the three model configurations, which are significant especially under soil moisture limited conditions in summer. Continuous wavelet transform analysis reveals the characteristic one-day scale temporal variability in latent heat flux and net radiation from all three configurations, indicating the connection between atmospheric radiative forcing and *ET* at the daily time scale. On the other hand, significant differences in time localized variance of latent heat flux from the three model configurations are observed at monthly to multi-month time scales in the

summer months. These results support the statement of the DBF concept that groundwater dynamics influence the variability of the land surface processes under soil moisture limited conditions at monthly to multi-month time scales. A version of this chapter is submitted for publication to the journal Hydrological Processes [*Rahman et al.*, 2015a].

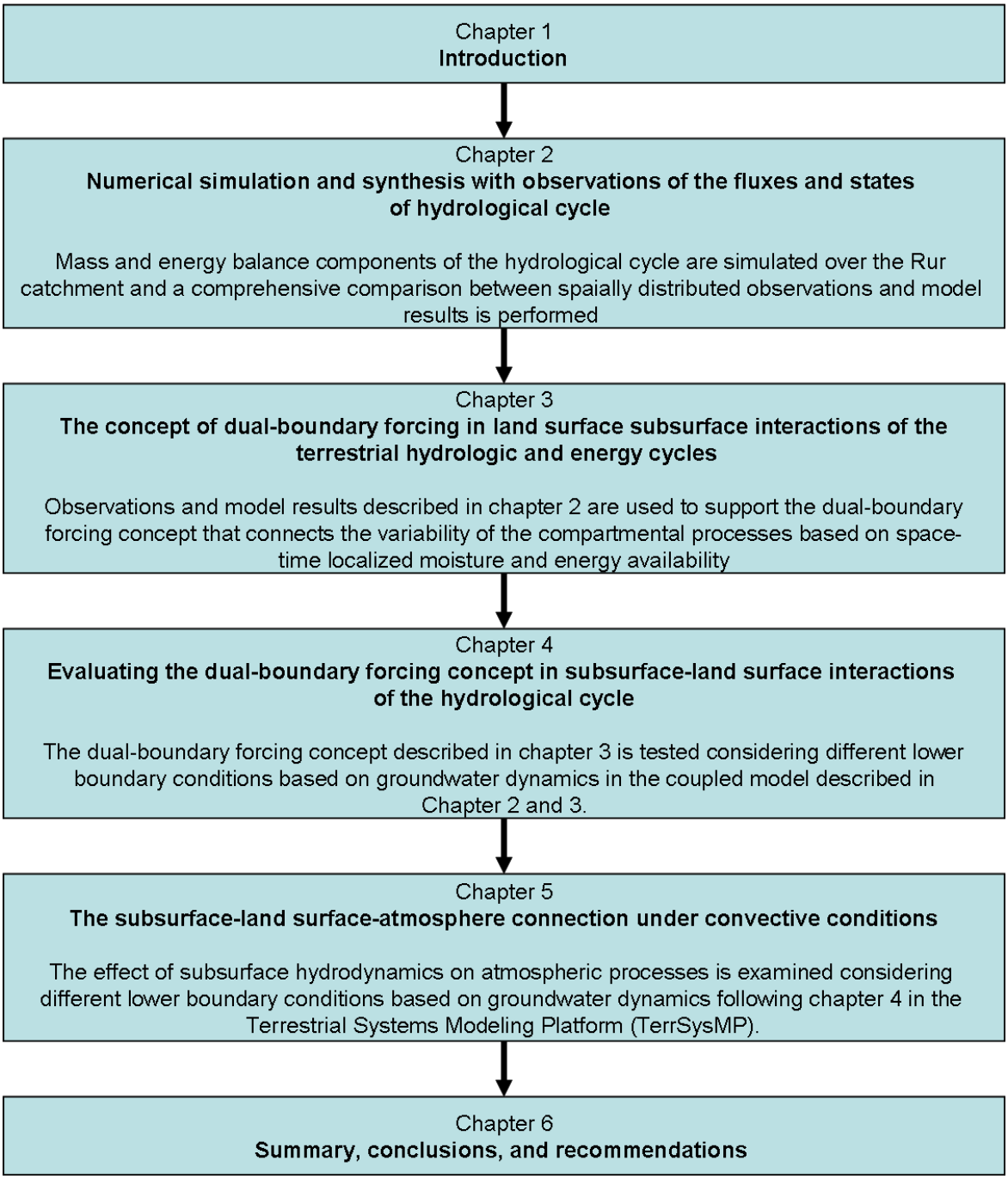

Figure 1.3. Schematic of the thesis organization.

The influence of groundwater dynamics on land surface mass and energy fluxes described in chapter 3 and 4 may reciprocally affect the atmospheric, which is examined in chapter 5. A fully coupled subsurface-land surface-atmosphere model (Terrestrial Systems Modeling Platform, TerrSysMP [*Shrestha et al.*, 2014]) is applied over a study area encompassing the Rur catchment and simulations are performed over two convective precipitation events considering the DBC and CBC model configurations described in chapter 4. Ensemble simulations are performed by varying the model initial conditions following the prescribed ensemble generation method by the German Weather Service (DWD) in order to account for the intrinsic, internal atmospheric variability. The results demonstrate that groundwater dynamics affect atmospheric boundary layer height, convective available potential energy, and precipitation via the coupling with land surface soil moisture and energy fluxes especially under strong convective conditions. A mechanism of subsurface-land surface-atmosphere interaction is also discussed in this chapter, which may be interpreted as the potential reason of sensitivity of atmospheric processes to subsurface hydrodynamics. The results suggest that groundwater dynamics introduces systematic uncertainties in atmospheric simulations, which may be important to consider in local weather prediction simulations. A version of this chapter is under review in the journal Advances in Water Resources [*Rahman et al.*, 2015b].

Finally, conclusions are drawn by summarizing the major findings of this thesis and concrete recommendations for future research are put forth in chapter 6. Figure 1.3 presents a schematic that shows the organization of this thesis. This figure also depicts the thematic connection between different chapters of this thesis.

1.3 Description of the Rur catchment

The Rur catchment (Figure 1.4) is the central research area of the Transregional Collaborative Research Centre (TR32) and the Terrestrial Environmental Observatories (TERENO), which is coordinated at the Research Centre Juelich (Forschungszentrum Juelich). This catchment is located in Western Germany with an area of approximately 2,350 km^2. The Rur River has a length of ~165 km with headwaters in Belgium and the mouth into the Meuse River near Maastricht. The main tributaries for the upper, middle, and lower reaches are the Urft, Inde, and Wurm, respectively. The northern part of this catchment is flat and situated in the Rhine lowlands. The southern part of the catchment, in contrast, is characterized by the mountainous Eifel region. Geologically, the northern flat regions of the Rur catchment is formed of

quaternary and tertiary unconsolidated rock deposits. The southern Eifel region, on the other hand, is predominantly formed of Devonian and Carboniferous sedimentary rocks.

Agriculture is the major land use in the northern part of the catchment, while the Eifel is heavily forested with coniferous trees. The Eifel is characterized by high annual precipitation rate (>1000mm/a) and a moderate potential evapotranspiration of approximately 500 mm/a. In contrast, the northern lowlands receive less annual precipitation (600-800 mm/a) and contribute to higher potential evapotranspiration of approximately 550-600 mm/a [*Bogena et al.*, 2005]. A distinct difference in the mean annual temperature between the northern (8.5-10.5 °C) and the southern (7.0-9.0 °C) part of the catchment is observed because of a ~600 m difference in elevation.

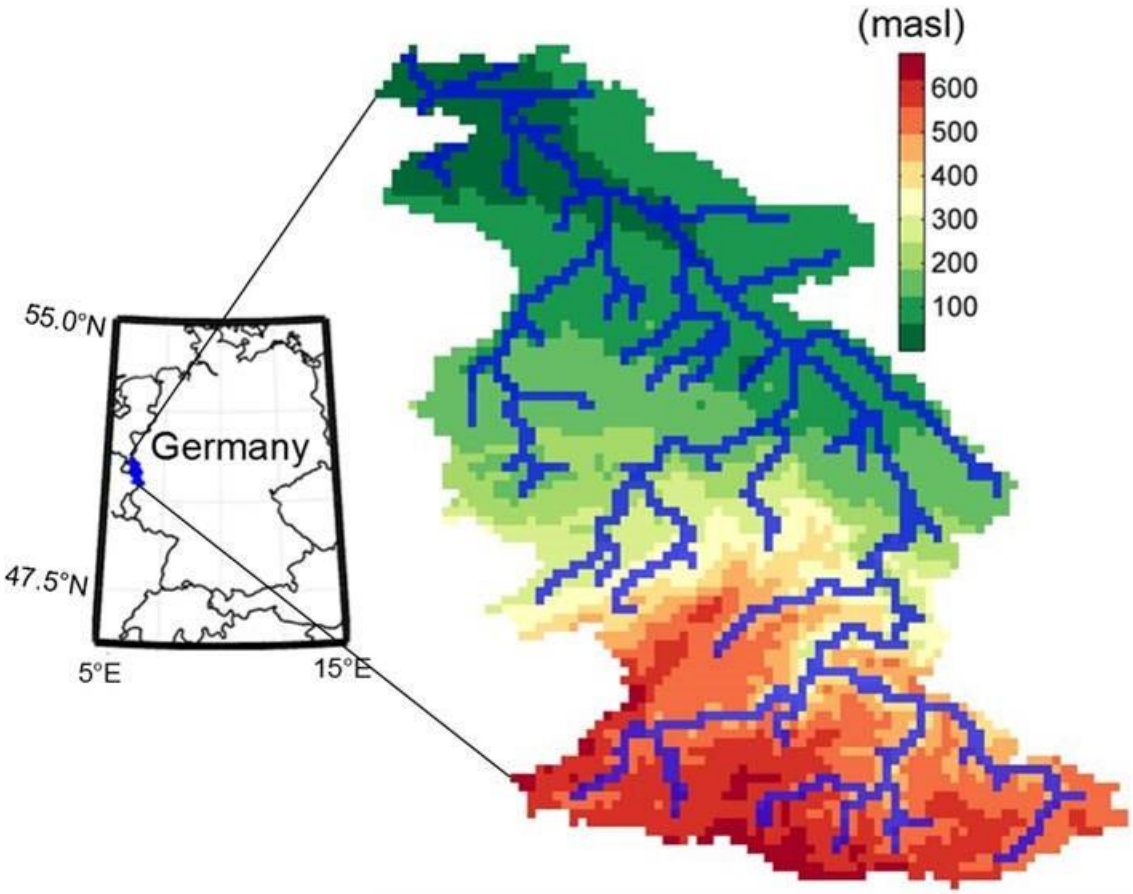

Figure 1.4. Location and topography of the Rur catchment. The blue lines on the topography represents the river network.

1.4 Description of the numerical models

In this thesis, the ParFlow.CLM model [e.g., *Maxwell and Miller*, 2005; *Kollet and Maxwell*, 2008] is used to simulate the subsurface and land surface processes in a coupled manner and the Terrestrial Systems Modeling Platform (TerrSysMP [*Shrestha et al.*, 2014]) is used to simulate the fluxes and states from the subsurface across the land surface into the atmosphere. The ParFlow.CLM model consists of a subsurface model ParFlow [e.g., *Ashby and Falgout*, 1996; *Jones and Woodward*, 2001; *Kollet and Maxwell*, 2006] and a land surface model CLM [*Dai et al.*, 2003; *Oleson et al.*, 2008]. TerrSysMP consists of the atmospheric model COSMO in addition to the aforementioned subsurface and land surface models. A brief description of the aforementioned numerical models is provided below.

1.4.1 The subsurface model ParFlow

The integrated, parallel, variably saturated groundwater/surface water flow model ParFlow [e.g., *Ashby and Falgout*, 1996; *Jones and Woodward*, 2001] solves the Richards' equation [*Richards*, 1931] in three spatial dimensions:

$$S_s\theta\frac{\partial\psi}{\partial t}+\phi\frac{\partial\theta(\psi)}{\partial t}=\nabla\cdot\mathbf{q}+S \tag{1.1}$$

$$\mathbf{q}=-k(x)k_r(\psi)\nabla(\psi-z) \tag{1.2}$$

where S_s is specific storage (m^{-1}), θ is soil moisture (-), ψ is pressure head (m), t is time (s), ϕ is porosity (-), $\mathbf{q}$ is water flux (ms^{-1}), S is general source/sink term (s^{-1}), $k(x)$ is saturated hydraulic conductivity (ms^{-1}), $k(r)$ is relative permeability (-), and z is depth below surface (m). ParFlow uses a finite volume scheme with two point flux approximation in space and an implicit backward Euler scheme in time to solve equation 1.1. The overland flow is integrated by applying a free surface overland flow boundary condition at the land surface [*Kollet and Maxwell*, 2006]. The kinematic wave equation is solved maintaining the continuity of pressure and flux at the boundary. A terrain following vertical grid can be used in ParFlow honoring the topographic slopes in an approximate fashion [*Maxwell*, 2013].

1.4.2 The land surface model CLM

The Common Land Model (CLM [*Dai et al.*, 2003; *Oleson et al.*, 2008]) simulates the mass and energy fluxes at the land surface. The energy balance equation in CLM can be written as:

$$R_{net}(\theta) = LE(\theta) + H(\theta) + G(\theta) \quad (1.3)$$

where R_{net} is net radiation (Wm^{-2}), LE is latent heat flux (Wm^{-2}), H is sensible heat flux (Wm^{-2}), and G is ground heat flux (Wm^{-2}). This equation is written here as a function of θ to demonstrate the connection between land surface energy balance and subsurface hydrodynamics. Vertical mass, energy, and momentum fluxes are described by the Monin-Obukhov similarity principle in CLM.

In CLM, LE is described as

$$LE = L_v E \quad (1.4)$$

where L_v is the latent heat of vaporization (Jkg^{-1}). E is calculated as

$$E = E_c + E_g \quad (1.5)$$

where E_c is evaporation from vegetation canopy ($kgm^{-2}s^{-1}$) and E_g is evaporation from ground ($kgm^{-2}s^{-1}$). In this equation, E is connected to the non-linear source/sink term (S) in equation 1.1 because of the interconnection of land surface mass and energy fluxes and subsurface hydrodynamics via shallow soil moisture discussed earlier in this chapter.

In equation 1.3, H is calculated as the sum of sensible heat flux from vegetation, H_c (Wm^{-2}) and ground, H_g (Wm^{-2}).

$$H = H_c + H_g \quad (1.6)$$

CLM obtains ground heat flux from one-dimensional transient heat conduction equation. The net radiation is described as

$$R_n = S_c + S_g + L_{in} - L_{out} \quad (1.7)$$

where S_c is absorbed solar radiation by vegetation (Wm^{-2}), S_g is absorbed solar radiation by ground (Wm^{-2}), L_{in} is incoming long wave radiation, and L_{out} is outgoing long wave radiation.

1.4.3 The atmospheric model COSMO

The atmospheric model COSMO is used as the numerical weather prediction system by the German Weather Service (DWD). The COnsortium of Small-scale MOdeling, which is an association of several European weather services, develops and maintains this model. The horizontal model grid in COSMO is based on a rotated coordinate system with the model

equator intersecting the centre of the model domain. Vertically, COSMO employs a hybrid coordinate system, which is parallel to the orography in the lower atmospheric levels. The prognostic variables of COSMO includes wind vector, pressure perturbation, air temperature, water vapor specific humidity, cloud liquid water content, cloud ice content, specific snow water content, and specific graupel content.

The convection permitting configuration of COSMO (referred to as COSMO-DE [e.g., *Baldauf et al.*, 2011]) is used in this thesis. COSMO-DE uses the split-explicit time-stepping method [e.g., *Wicker and Skamarock*, 2002] in order to solve the nonhydrostatic compressible Euler equations. The parameterization in COSMO-DE includes a surface transfer scheme to calculate heat and momentum transfer coefficients [e.g., *Raschendorfer*, 2001], a radiation scheme after *Ritter and Geleyn* [1992], a single-momentum cloud microphysics scheme [e.g., *Lin et al.*, 1983; *Reinhardt and Seifert*, 2006], a level-2.5 turbulence parameterization after *Mellor and Yamada* [1982], and a shallow convection scheme after *Tiedtke* [1982].

1.4.4 The coupled subsurface-land surface model ParFlow.CLM

In ParFlow.CLM, ParFlow is consistently coupled to CLM over the first ten vertical model layers downward starting at the land surface. The layer thicknesses range from 4 cm at land surface to 200 cm at greater depth. ParFlow simulates the three-dimensional distribution of soil moisture in the subsurface and deeper groundwater flow and sends this information to the land surface model CLM. On the other hand, CLM calculates the non-linear source/sink terms of soil moisture (e.g., infiltration from precipitation, and soil evaporation and plant transpiration, respectively) for ParFlow, which are partitioned vertically following an exponentially decaying root density distribution in case of root water uptake. The two model components communicate through the exchange of fluxes and shallow three-dimensional hydraulic pressure and soil moisture distributions at every time step following an operator splitting approach.

With regard to subsurface energy transport, which is computed by CLM, it is important to note that CLM considers only heat conduction in simulating subsurface energy transport ignoring convection, which eventually decouples the heat transport from the moisture transport in the model [*Kollet et al.*, 2009]. At the top, CLM requires atmospheric variables including precipitation, radiation, air temperature, barometric pressure, wind speed, and specific humidity to force the model. The off-line coupling scheme considered in ParFlow.CLM assumes that, these atmospheric variables do not change due to transient land

surface conditions [*Kollet*, 2009]. This assumption may influence the mass and energy fluxes simulated by the model, which is due to the non-linear feedback mechanisms between different compartments discussed earlier in this chapter.

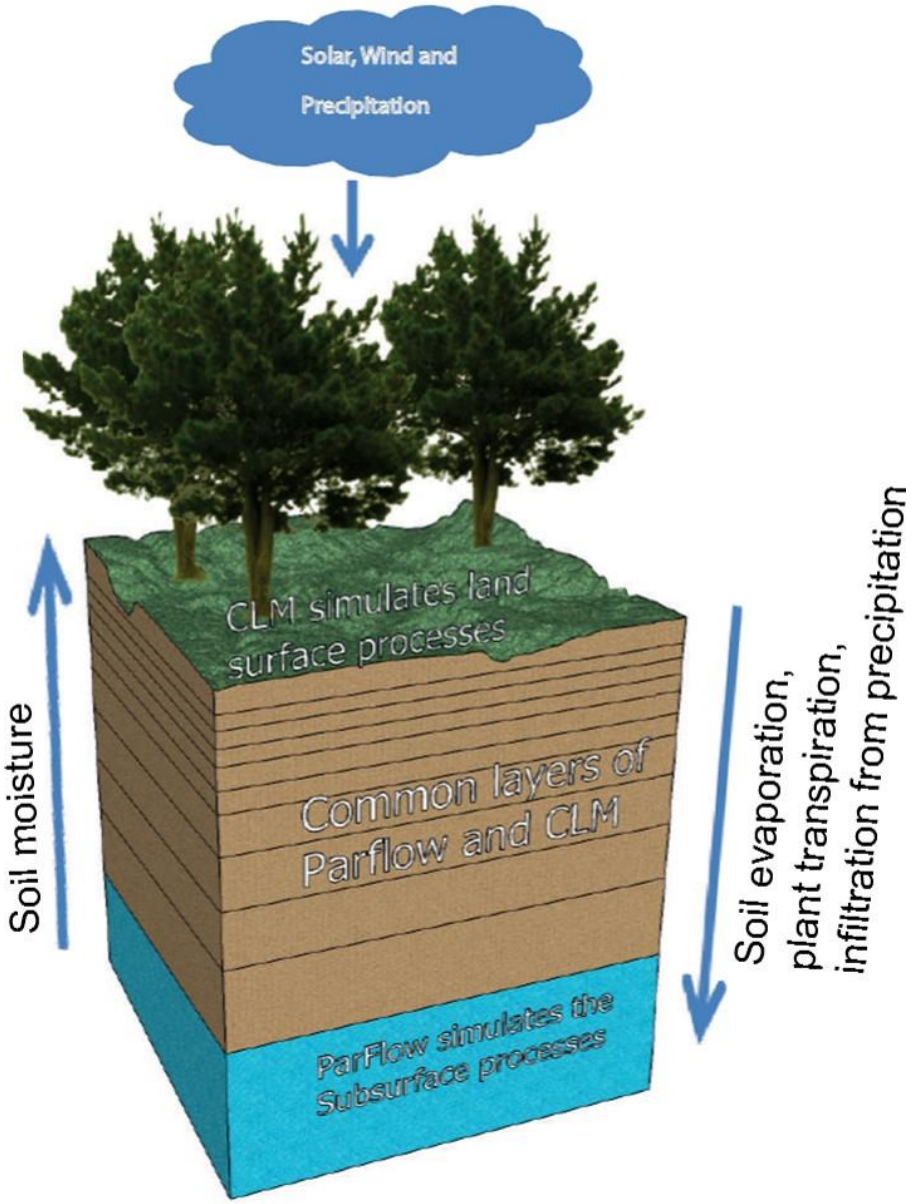

Figure 1.5. Simplified schematic of the coupled subsurface-land surface model ParFlow.CLM.

1.4.5 The Terrestrial Systems Modeling Platform (TerrSysMP)

The highly modular scale-consistent Terrestrial Systems Modeling Platform (TerrSysMP) has been discussed in *Shrestha et al.* [2014]. TerrSysMP consists of the atmospheric model COSMO-DE, the land surface model CLM3.5, and the three-dimensional variably saturated groundwater/surface water flow model ParFlow. An external coupler (OASIS3-MCT [e.g.,

Valcke, 2013; *Gasper et al.*, 2014]) is used to couple the three component models employing a multiple-process-multiple-data approach. In TerrSysMP, the model components are able to exchange fluxes at different spatial and temporal resolutions using time integration/averaging and spatial interpolation operators based on the downscaling algorithms developed by *Schomburg et al.* [2010, 2012].

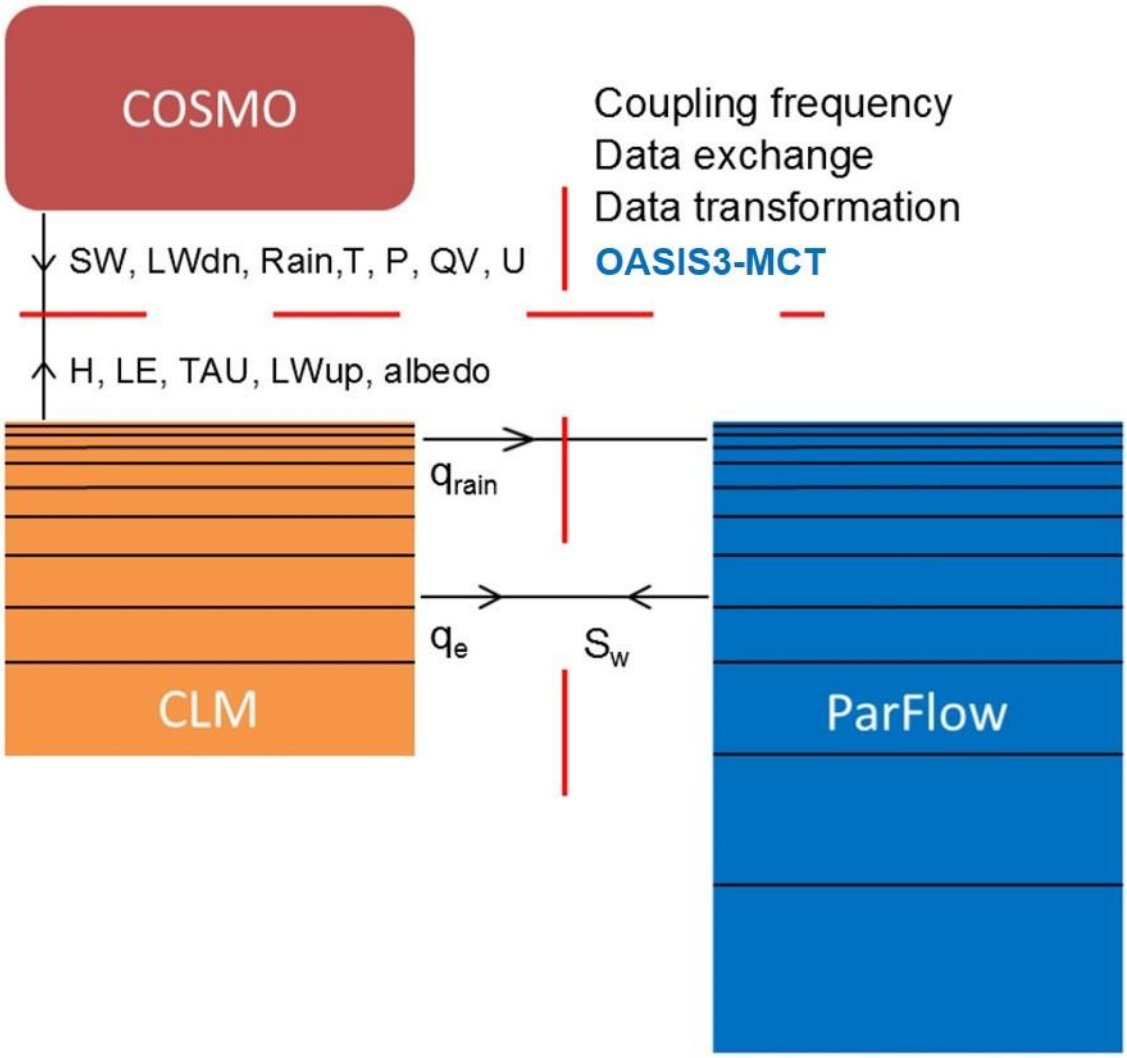

Figure 1.6. Simplified schematic of the Terrestrial Systems Modeling Platform, TerrSysMP (redrawn after *Shrestha et al*., 2014). (SW – incoming shortwave radiation, LWdn – downward longwave radiation, T – atmospheric temperature, P – atmospheric pressure, QV – specific humidity, U – wind speed, H – sensible heat flux, LE – latent heat flux, TAU – zonal momentum flux, LWup – upward longwave radiation, q_{rain} – source term from precipitation, q_e – sink term from evapotranspiration, S_w – soil moisture).

In TerrSysMP, the atmospheric model (COSMO-DE) and the land surface model (CLM3.5) exchange atmospheric and land surface fluxes in a sequential manner via the external coupler OASIS3-MCT. The atmospheric variables (i.e., wind speed, air temperature, pressure, specific humidity, incoming short and long wave radiation, precipitation, and measurement

height) at the lowest COSMO-DE layer are used to drive CLM3.5 at the current time step and the land surface mass and energy balance components are calculated. The land surface energy and momentum fluxes along with albedo and outgoing long wave radiation are then sent back to COSMO-DE in an operator splitting approach. The dimensionless surface transfer coefficients of COSMO-DE are subsequently updated inversely based on these fluxes. The vertical gradients at the lowest level are calculated based on the surface temperature from the previous time step.

The external coupler OASIS3-MCT is also used in TerrSysMP to couple the subsurface model ParFlow and the land surface model CLM3.5. Through this coupling, ParFlow replaces the simplified hydrological scheme in CLM3.5 and simulates subsurface hydrodynamics and surface runoff. The two coupled component models exchange fluxes and shallow soil moisture distributions following a sequential information exchange procedure.

Chapter 2

Numerical simulation and synthesis with observations of the fluxes and states of hydrological cycle

2.1 Introduction

Understanding the variability and interactions of different processes in the hydrological cycle has been the subject of research in the scientific community for some time [e.g., *Shukla and Mintz*, 1982; *Kovács*, 1986; *Delworth and Manabe*, 1988; *Findell and Eltahir*, 1997]. One way to study the inherent variability of these processes is the monitoring of the fluxes and states of the coupled water and energy cycles [e.g., *Entin et al.*, 2000; *Baldocchi et al.*, 2001; *Andreo et al.*, 2006]. Although this direct method examines the space-time variability in different mass and energy balance components [e.g., *Maurer et al.*, 2004; *Brunsell and Anderson*, 2011; *Renner and Bernhofer*, 2011; *Xiao et al.*, 2012], studying the interactions between various processes in the terrestrial system through observations is generally not feasible. Continuous measurements covering all the compartments (e.g., subsurface, land surface, and atmosphere) of the hydrological cycle over the same region over long time periods required for this purpose are often not available.

In order to fill this gap, physics-based distributed models are used to study fluxes and states continuously in both space and time. These models use relatively simple mathematical formulations to represent complex process in the hydrological cycle [e.g., *Vrugt et al.*, 2005], and various sources contribute uncertainty to them [e.g., *Beven and Binley*, 1992; *Beven*, 1993; *Moradkhani et al.*, 2005; *Liu and Gupta*, 2007; *Beven et al.*, 2010]. In spite of these limitations, physics-based distributed models are widely used to examine the variability of the mass and energy balance components of the terrestrial system.

Several previous studies have coupled physics-based models to examine the interconnections between the compartmental processes [e.g., *York et al.*, 2002; *Tian et al.*, 2012; *Niu et al.*,

2013]. A coupled regional climate-hydrological model RAMS-Hydro was used by *Anyah et al.* [2008] to study the role of groundwater dynamics on land surface and atmospheric processes. *Kollet and Maxwell* [2008] examined the connection between groundwater dynamics and land surface energy fluxes at the catchment scale using a coupled subsurface-land surface model ParFlow.CLM [e.g., *Maxwell and Miller*, 2005]. *Yuan et al.* [2008] coupled a groundwater flow model with the regional climate model RegCM3 [*Pal et al.*, 2007] to examine the influence of groundwater dynamics on regional climate. *Leung et al.* [2011] used the coupled model MM5-VIC to demonstrate the interactions between subsurface and atmospheric processes via land surface. These studies suggest that physics-based coupled models can be used to reveal the interconnections between the compartmental processes of the hydrological cycle where sufficient direct observations are missing.

The objective of this chapter is to simulate the fluxes and states of the terrestrial hydrologic and energy cycles using the coupled simulation platform ParFlow.CLM and perform a comprehensive comparison with spatially-distributed measurements. The model results and observations described here are used in the next chapter to study the interactions between compartmental mass and energy balance components at various space-time scales. The coupled model used here consists of the three-dimensional groundwater/surface water flow model ParFlow [*Jones and Woodward*, 2001; *Kollet and Maxwell*, 2006], and the land surface model, CLM [*Dai et al.*, 2001]. The comparison between the simulation results and observations demonstrate the capability of the model to reproduce realistic dynamics as well as the absolute values of the mass and energy fluxes of the coupled water and energy cycles.

2.2 Model description

ParFlow is an integrated, parallel, variably saturated groundwater flow model that solves Richards' equation [*Richards*, 1931] in three spatial dimensions using a globalized Newton method. It applies a finite volume scheme with a two-point flux approximation in space and an implicit backward Euler scheme in time. ParFlow solves the coupled subsurface-land surface flow by applying a free surface overland flow boundary condition at the land surface [*Kollet and Maxwell*, 2006]. A terrain following vertical grid can be utilized to take advantage of a variable vertical spatial discretization while honoring the topographic slopes in an approximate fashion [*Maxwell*, 2013]. The Common Land Model (CLM) solves the mass, energy, and momentum balance equation at the land surface, forced with atmospheric

variables including precipitation rate, long/short wave radiation, air temperature, pressure, wind speeds, specific humidity, and barometric pressure.

The energy balance equation at the land surface can be written as:

$$R_{net}(\theta) = LE(\theta) + H(\theta) + G(\theta) \tag{2.1}$$

where R_{net} is net radiation (Wm^{-2}), LE is latent heat flux (Wm^{-2}), H is sensible heat flux (Wm^{-2}), G is ground heat flux (Wm^{-2}), and θ is soil moisture at the land surface ($kgkg^{-1}$). Here, the equation is written as a function of soil moisture to emphasize the connection with subsurface hydrodynamics. The different exchange terms with the atmosphere in equation (2.1) are expressed based on the Monin-Obukhov similarity principle, which describes vertical mass, energy, and momentum fluxes above a rough surface. The ground heat flux G is applied as the top boundary condition for subsurface conductive heat transport, and obtained as the residual of equation (2.1), closing the energy balance. The mass balance equation in the subsurface can be written as follows:

$$S_s\theta\frac{\partial\psi}{\partial t} + \phi\frac{\partial\theta(\psi)}{\partial t} = \nabla\cdot\mathbf{q} + Q \tag{2.2}$$

$$\mathbf{q} = -k(x)k_r(\psi)\nabla(\psi - z) \tag{2.3}$$

where S_s is the specific storage (m^{-1}), ψ is the pressure head (m), t is the time (s), ϕ is the porosity (-), $\mathbf{q}$ is the water flux (ms^{-1}), Q is the general source/sink term (s^{-1}), $k(x)$ is the saturated hydraulic conductivity (ms^{-1}), $k(r)$ is the relative permeability (-), and z is the depth below surface (m). The depth differentiated source/sink term Q describes the infiltration, ground evaporation and root water uptake by plants in equation (2.2) and is connected to the moisture dependent latent heat flux $LE(\theta)$ in equation (2.1). Thus, the coupling between the land surface-subsurface processes develops through the moisture dependence of the energy variables and the non-linear source/sink term in the equations of variably saturated subsurface flow.

In the modeling framework, ParFlow is coupled to CLM over the first ten vertical model layers downward starting at the land surface. ParFlow, which replaces the simplified soil moisture and runoff formulation in CLM, simulates the three-dimensional subsurface distribution of soil moisture and deeper groundwater flow and sends this information to CLM. The land surface model CLM calculates the non-linear source/sink terms of soil moisture

(e.g., infiltration from precipitation, and soil evaporation and plant transpiration, respectively) for ParFlow, which are partitioned vertically following an exponentially decaying root density distribution in case of root water uptake. The two model components communicate through the exchange of fluxes and shallow three-dimensional hydraulic pressure and soil moisture distributions at every time step following an operator splitting approach.

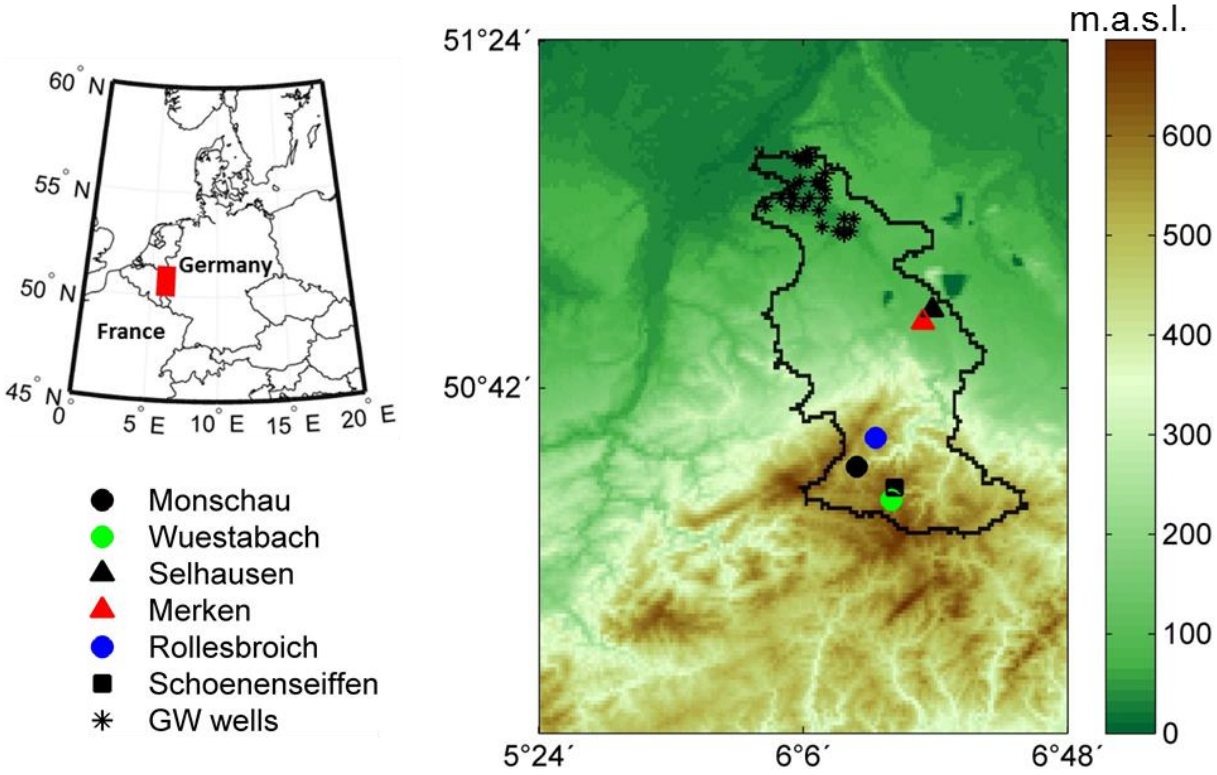

Figure 2.1. Location and topography of the model domain. The red box on the map (left) shows the location of the study area. The black line on the topography (right) indicates the border of Rur catchment. The legends show the locations of measurement stations.

2.3 Study area and model setup

The study area is the Rur catchment (Figure 2.1), which is located in Western Germany with an area of approximately 2,350 km^2. The Rur River has a length of some 165 km with headwaters located in Belgium and the mouth into the Meuse River at Roermond, Netherlands. The main tributaries for the upper, middle, and lower reaches are the Urft, Inde, and Wurm, respectively. The southern part of the Rur catchment is characterized by the mountainous Eifel region. The northern part, on the other hand, is flat and situated in the lower Rhine lowlands. Geologically, the northern part of the Rur catchment is formed of unconsolidated rock deposits, while Palaeozoic and Mesozoic rock outcrops mainly in the southern part. Agriculture is the major land use in the northern part of the catchment, while

the mountainous southern part is predominantly dense coniferous forest. Due to the difference in topographic elevation (~600 m), there is a distinct difference in the mean annual temperature between the northern (8.5-10.5 °C) and the southern (7.0-9.0 °C) part of the catchment. The mountainous part is characterized by high annual precipitation rate (>1000 mm/a) and a moderate potential evapotranspiration of approximately 500 mm/a. In contrast, the northern lowlands receive less annual precipitation (600-800 mm/a) and contribute to higher potential evapotranspiration of approximately 550-600 mm/a [*Bogena et al.*, 2005].

The ParFlow.CLM model is applied over an area encompassing the Rur catchment (Figure 2.1). A larger model domain is considered in order to account for cross-watershed flow. A uniform lateral grid resolution of $\Delta x=\Delta y=1$km and the aforementioned terrain following grid implementation is used, which allows a variable vertical discretization ranging from 4×10^{-2} to 2×10^{0}m at the land surface to the bottom of the model domain, respectively. The total depth of the subsurface is 50m in this model.

The model includes spatially distributed topography, vegetation cover, soil types, and atmospheric forcing data. Information from the Global Land Cover 2000 digital database (GLC2000, European Commission, Joint Research Centre, 2003) is used to represent the spatially distributed vegetation cover of the model domain (Figure 2.2). The plant parameters for different vegetation types are derived following the International Geosphere-Biosphere Program (IGBP) standard. Cultivated and managed area occupies around 47% of the model domain, while forest covers around 26% of the total area.

Parameter name	Parameter value	Unit
Saturated hydraulic conductivity, k_{sat}	6.4×10^{-6}	ms^{-1}
Porosity, ϕ	0.44	-
van Genuchten parameter, α	2.1	m^{-1}
van Genuchten parameter, n	3.0	-
Residual saturation, S_{res}	0.1	-

Table 2.1. Soil hydraulic parameters of the homogeneous deep subsurface.

The deeper subsurface is considered to be homogeneous with parameter values directed at the dataset by *Gleeson et al.* [2011]. The properties of the homogeneous subsurface are given in Table 2.1. DSMW (Digital Soil Map of the World) provided by FAO (Food and Agricultural Organization of UNO) along with the Euro-soil database information [e.g., *Dolfing et al.*, 1999] are used to represent the heterogeneity of soil texture in the shallow subsurface (Figure 2.2). The saturation pressure head relationship for different soil types (Table 2.2) is

represented by the vanGenuchten function [*van Genuchten*, 1980] using the parameters extracted from RAWLS database [*Schaap and Leij*, 1998].

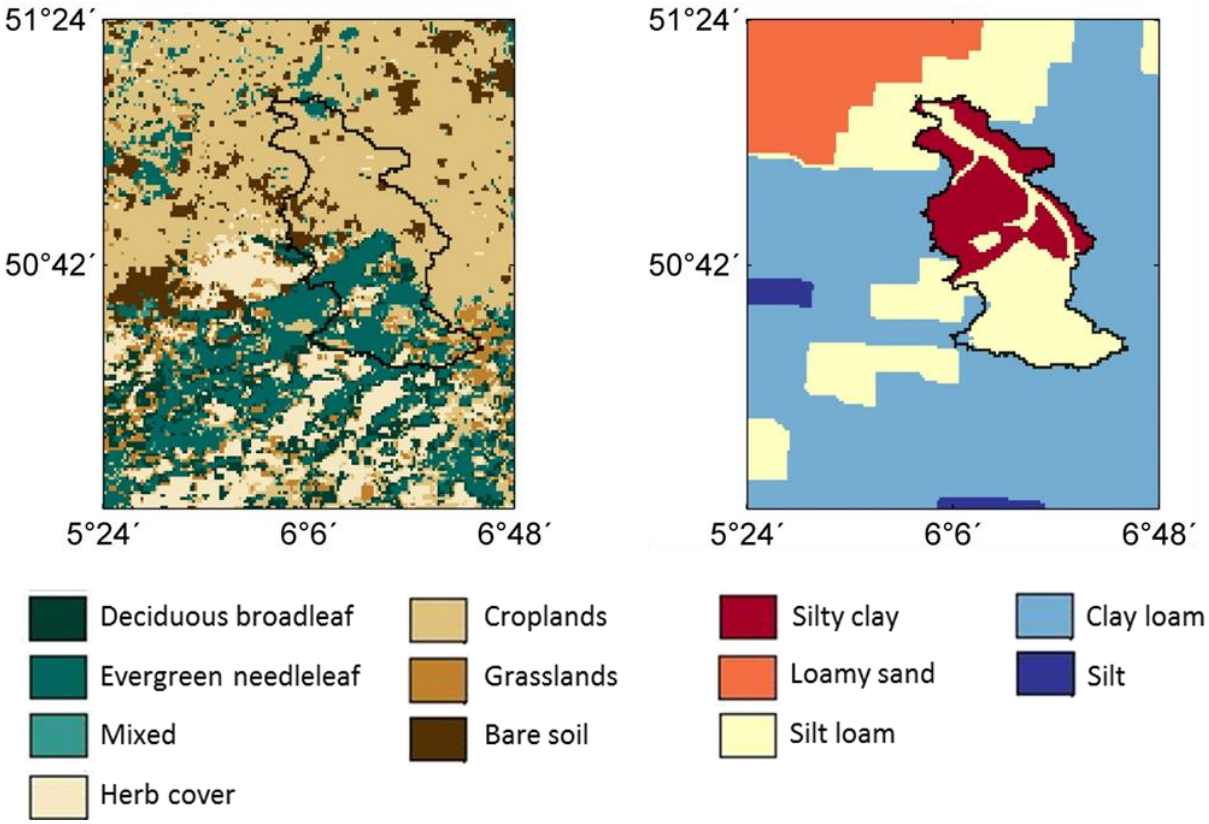

Figure 2.2. Spatially distributed vegetation (left) and soil cover (right) information used in ParFlow.CLM model. The black line indicates the border of Rur catchment in both Figures.

The simulation period for this study extends from January 2009 until December 2011 with a one-hour time step. Hourly atmospheric forcing data is obtained from COSMO-DE re-analysis data set of the German Weather Service (DWD) operating with a lateral grid resolution of 2.8km over Germany. The atmospheric forcing data is downscaled to the model grid resolution of 1km by linear interpolation. In order to obtain a realistic initial condition, the model is initialized with an arbitrary uniform water table depth of 5m below ground surface then run repeatedly using the hourly atmospheric forcing data of 2009 until a state of dynamic equilibrium is reached.

Texture	K_{sat} **[ms^{-1}]**	ϕ	α**[m^{-1}]**	n	S_{res}
Silty clay	8.3×10^{-7}	0.389	2.7	2.0	0.2
Silt loam	3.9×10^{-6}	0.441	2.1	3.0	0.1
Clay loam	1.1×10^{-6}	0.354	2.1	2.0	0.15

Table 2.2. Soil hydraulic parameters of shallow subsurface.

2.4 Field measurements

The location, temporal extent, measurement frequency, and the source of various observations used in this thesis are summarized in Table 2.3. The Rur catchment is the central research area for the Transregional Collaborative Research Centre (TR32) and the Terrestrial Environmental Observatories (TERENO), which is coordinated at the Research Centre Juelich (Forschungszentrum Juelich). Measuring stations are located throughout the catchment with an objective of gathering information on the mass and energy fluxes from the subsurface across the land surface into the atmosphere. In the forested sub-catchment Wuestebach (Figure 2.1), a state-of-the-art wireless sensor network is installed to obtain long-term continuous, spatially distributed soil moisture information [e.g., *Rosenbaum et al.*, 2012]. Spatially distributed soil moisture information is gathered at three different soil depths (5cm, 20cm and 50cm) by this sensor network. In this study, the spatially averaged soil moisture (also averaged over the three measurement depths) information is used from this network.

Data	Location	Temporal extent	Frequency	Source
Discharge	Monschau	01.01.2009 - 31.12.2009	Daily	LANUV
Soil moisture	Wuestebach	01.07.2009 - 31.12.2009	15 min	TERENO
Soil moisture	Rollesbroich	05.05.2011 - 31.12.2011	15 min	TERENO
Soil moisture	Schoenenseiffen	01.01.2010 - 31.12.2011	10 min	TERENO
Water table depth	-*	01.01.2009 - 31.12.2009	Weekly - Monthly	LANUV
Water table depth	Wuestebach	01.01.2011 - 31.12 2011	Daily	TERENO
Latent heat flux	Merken	01.04.2009 - 31.08.2009	30 min	TR32 database
Latent heat flux	Wuestebach	18.02.2011 - 31.12.2011	30 min	Uni. Trier
Latent heat flux	Merzenhausen	01.07.2011 - 31.12.2011	30 min	TERENO
Sensible heat flux	Merken	01.04.2009 - 31.08.2009	30 min	TR32 database
Net radiation	Selhausen	01.01.2009 - 31.12.2009	60 min	TERENO
Ground heat flux	Selhausen	01.01.2009 - 31.12.2009	60 min	TERENO

Table 2.3. Location, temporal extent, measurement frequency, and source of the field measurements.
(*The locations are shown in Figure 2.1).

The Nature, Environment, and Consumer Protection Agency (LANUV) of North Rhine-Westphalia collects daily average discharge information at several gauging stations along the Rur River. Large reservoir systems in the mountainous southern part of the catchment influence the downstream flow considerably. In this study, discharge information from the Monschau gauging station located in the upstream reaches of the river is used, which is arguably less influenced by management practices. Erftverband, which is a non-profit water management organization in the region, provided groundwater table depth (*WTD*) at numerous measuring stations in the catchment.

Three energy balance towers were installed at the TR32 test site Merken (Figure 2.1) in different types of agricultural fields, namely, winter wheat, sugar beet, and barley. Each tower was equipped with two eddy covariance stations at 2.5 and 6m above ground. The lower measurement height is usually more representative of the respective land use type, while the upper one provides a larger footprint and improved energy balance closure. *LE* and *H* measurements from this site collected during the TR32 FLUXPAT campaign in summer 2009 [e.g., *Graf et al.*, 2010; *van de Boer et al.*, 2013; *Kessomkiat et al.*, 2013] is use in this study. Net radiation (R_{net}), ground heat flux (G), 2m air temperature (T_{air}), and soil temperature (T_{soil}) data are obtained from the micrometeorological tower located in Selhausen (Figure 2.1).

2.5 Results and discussion

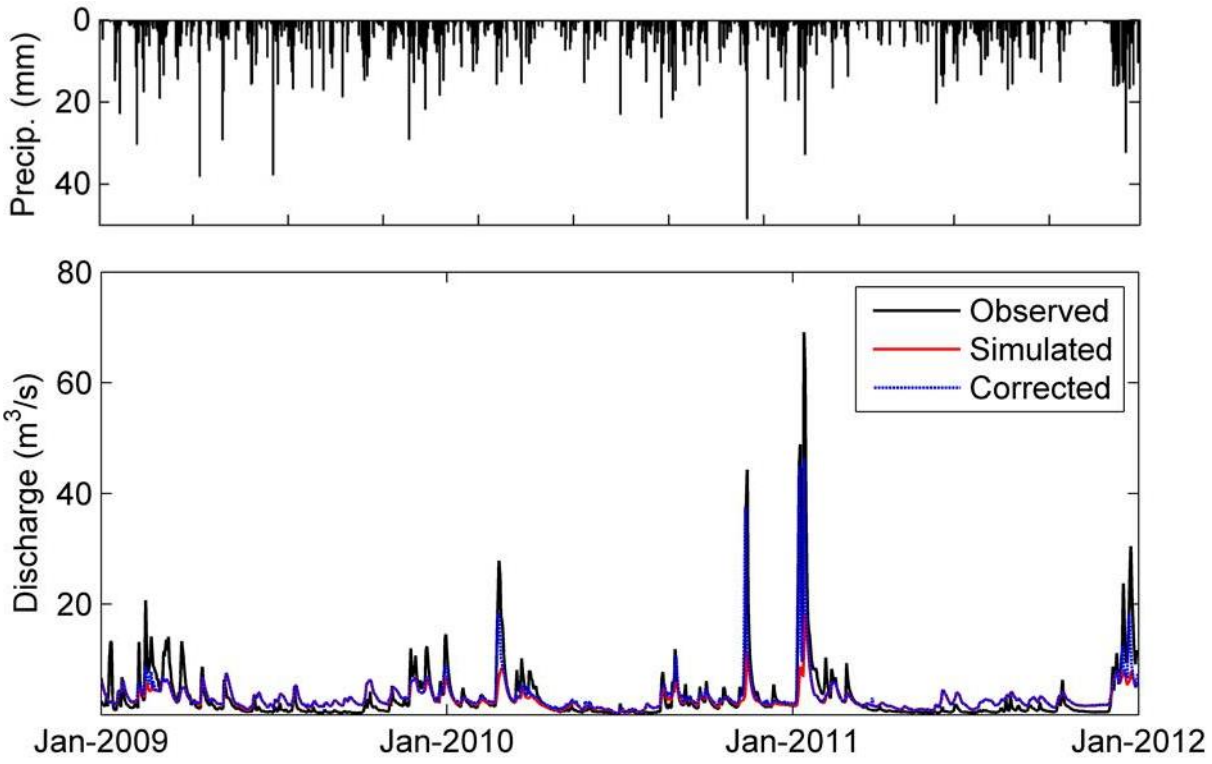

Figure 2.3. Precipitation (top) and observed and simulated hydrographs (bottom) at the Monschau discharge gauging station. The *corrected* discharge is calculated by adding measured differential releases (outflow-inflow) from the Perlenbach reservoir to the simulated data.

Figure 2.3 shows a comparison between observed and simulated hydrographs from January 2009 until December 2011 at the Monschau discharge gauging station. This figure shows that the model is generally able to capture the timing of the peaks throughout the simulation period. During low flow conditions, the simulation results show good agreement with the

observations. However, the peak discharge values are underestimated in December 2010 and January 2011. The overall model performance is depicted by a Nash-Sutcliffe value [*Nash and Sutcliffe*, 1970] of *NSE* =0.40. As mentioned earlier, the flows on the Rur River are managed with reservoir systems that are not considered by ParFlow.CLM. In order to estimate the influence of such management practices on the simulation, Figure 2.3 also shows the comparison between the observed and modeled hydrographs after correcting the simulated discharge by adding measured differential releases (outflow-inflow) from Perlenbach reservoir, which is located at the upstream reaches of the Monschau gauging station. This correction improves the agreement between the observed and simulated hydrographs, which is reflected by a considerably improved *NSE* of 0.65. Therefore, it is likely that discrepancies between the observed and simulated hydrographs result from the management practices.

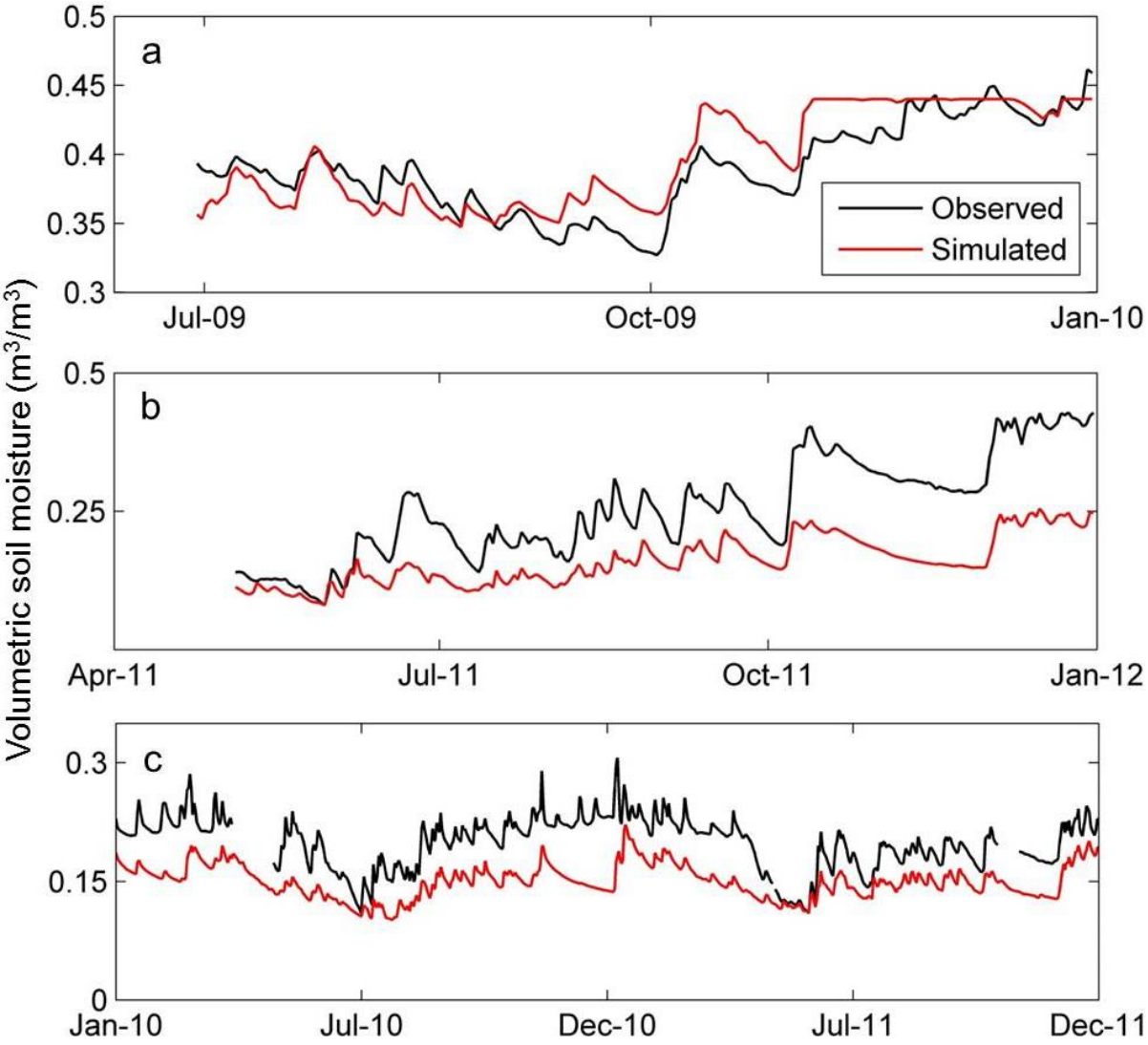

Figure 2.4. Observed and simulated soil moisture at Wuestebach (a), Rollesbroich (b), and Schoenenseiffen (c) test sites.

Figure 2.4 compares the observed and simulated soil moisture at three different test sites over the Rur catchment. Simulated values for the comparison are derived by averaging the soil moisture over the top two vertical model layers. Figure 2.4a shows the comparison at the Wuestebach test site, demonstrating reasonable agreement between the model results and observations without model calibration. Good agreement between observed and simulated soil moisture in terms of magnitude and dynamics is observed from July to October in Figure 2.4a. After this period, the model becomes saturated because the porosity value used in the simulation at this location is too low [*Rosenbaum et al.*, 2012]. Figure 2.4b and 2.4c compares observed and simulated soil moisture at Rollesbroich and Schoenenseiffen test sites, respectively. The dynamics in observed soil moisture due to wetting and drying is again reproduced well by the simulation. However, in both locations, the model generally underestimates soil moisture. Reasons of these discrepancies may include the uncertainty in model parameters and interpolation of the atmospheric forcing data.

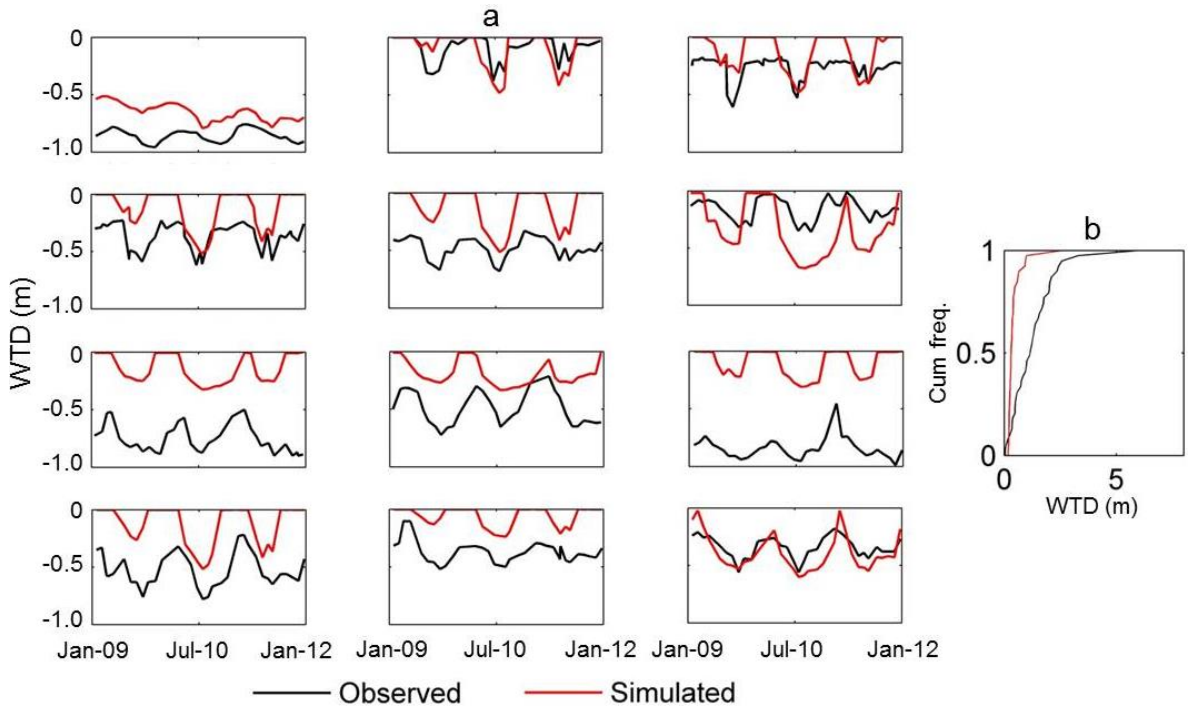

Figure 2.5. Observed and simulated groundwater table depth, *WTD* time series at 12 selected groundwater wells (a), and cumulative frequency distributions of the observed and simulated *WTD* (b).

Figure 2.5a shows a comparison between the observed and simulated groundwater table depth (*WTD*) time series from January 2009 until December 2011 at 12 selected wells. The seasonal dynamics of the observed *WTD* are reproduced reasonably well by the simulation, though the model generally predicts shallower *WTD* compared to the observations. This is also observed in Figure 2.5b, which shows the cumulative frequency distributions of the observed and

simulated mean *WTD* for all 43 wells. One possible reason for this underestimation may be the coarse lateral grid resolution of 1km, which has been discussed previously [e.g., *Zhang and Montgomery*, 1994; *Kuo et al.*, 1998; *Sulis et al.*, 2011].

Figure 2.6 shows a comparison between the average daily cycles of observed and simulated *LE* and *H* in different months of 2009 at the Merken test site. The model performance is reasonable in reproducing the daily cycles of *LE*. The dynamics in *LE* are captured well throughout the measurement period with a small overestimation in mid-day during July. The daily cycle of simulated *H* also shows reasonable agreement with the measured data in April. However, for the rest of the measurement period, a systematic over prediction of day time *H* is observed. Similar results were obtained in the study by *Baker et al.* [2005], where the Simple Biosphere Model (SiB2.5) overestimated *H* compared to eddy covariance measurements.

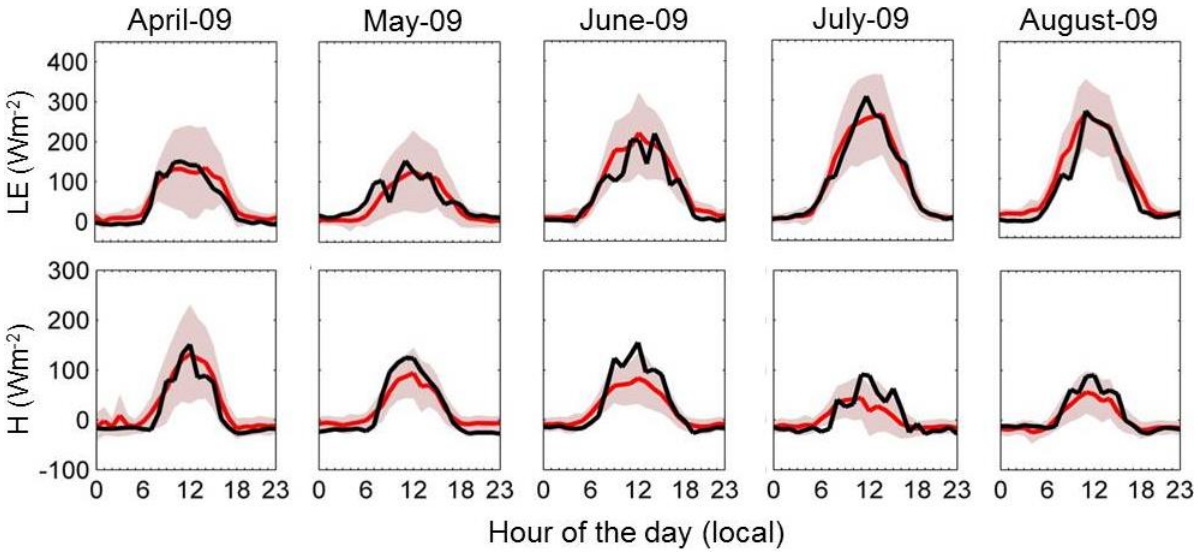

Figure 2.6. Observed and simulated average daily cycles of latent heat flux, *LE*, and sensible heat flux, *H* at the Merken test site. The solid black lines show the mean values of simulated data. The red lines and shaded areas show the mean and standard deviation of observed flux, respectively.

Continuous wavelet transform technique is applied to study the temporal dynamics of the observed and simulated *LE*; because interpreting the temporal variability of complex processes from direct inspection of the time series alone is not feasible. A brief description along with the mathematical formulation of the wavelet transform technique is given in Appendix B. Figure 2.7 show the time-localized wavelet power and the global wavelet spectra of observed and simulated *LE* at the Merzenhausen test site from July 2011 until December 2011. The observed *LE* time series shows variability at 1day time scale due to the diurnal variation of incoming solar radiation. Additionally, monthly (about 32day time scale)

variability is also observed in the measured time series. Figure 2.7 illustrates that the simulated time series also show variability at these two prominent time scales, which clearly demonstrates the model's capability of reproducing the dynamics in *LE* across different time scales.

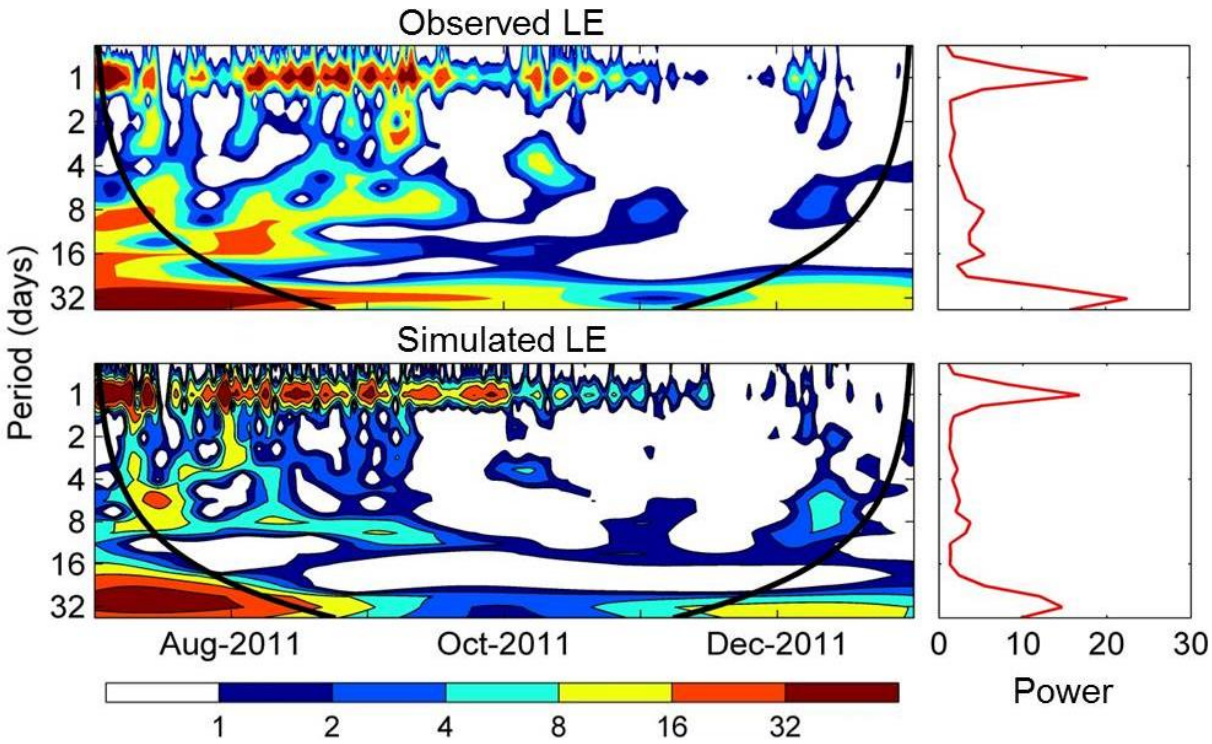

Figure 2.7. Wavelet transform of observed and simulated latent heat flux, *LE*, at the Merzenhausen test site. The time localized power is shown in the left panels. The cone of influence is indicated with the thick black lines in these plots. The right panels show the global wavelet power.

Figure 2.8a shows the comparison between daily averaged observed and simulated T_{air} at the Selhausen site. The dynamics in observed daily average T_{air} is reproduced by ParFlow.CLM throughout the year without systematic bias. Both observed and simulated time series show the same (seasonal) variability with the maxima in August and minima in January. Figure 2.8b shows the comparison between the observed and simulated T_{soil} at the same site. The model generally reproduces the overall trend as well as the absolute values, although overestimation and underestimation in T_{soil} are observed during May-July and August-October, respectively. Note that the measurements are performed at 5cm soil depth while the simulated T_{soil} is obtained from the first model layer (Δz = 4cm). This may contribute to the mismatch between the observed and simulated T_{soil}.

Figure 2.9 shows a comparison between observed and simulated net radiation at the Selhausen site. In Figure 2.9a, the overall variability in observed daily average R_{net} is captured by the

simulation. Figure 2.9b shows monthly boxplots of observed and simulated daily average R_{net}. The monthly trend is also well-reproduced by the simulation, although in the warmer months the model shows overestimation in the monthly mean values. In the model, R_{net} is calculated as the sum of absorbed solar radiation (by the canopy and the ground), and the net atmospheric long wave radiation, which depend on the canopy characteristics and surface albedo. Due to the coarse lateral spatial discretization of 1km, the albedo considered in the model may be significantly different from the true albedo at the measurement points, which may contribute to the discrepancies between observed and simulated R_{net}.

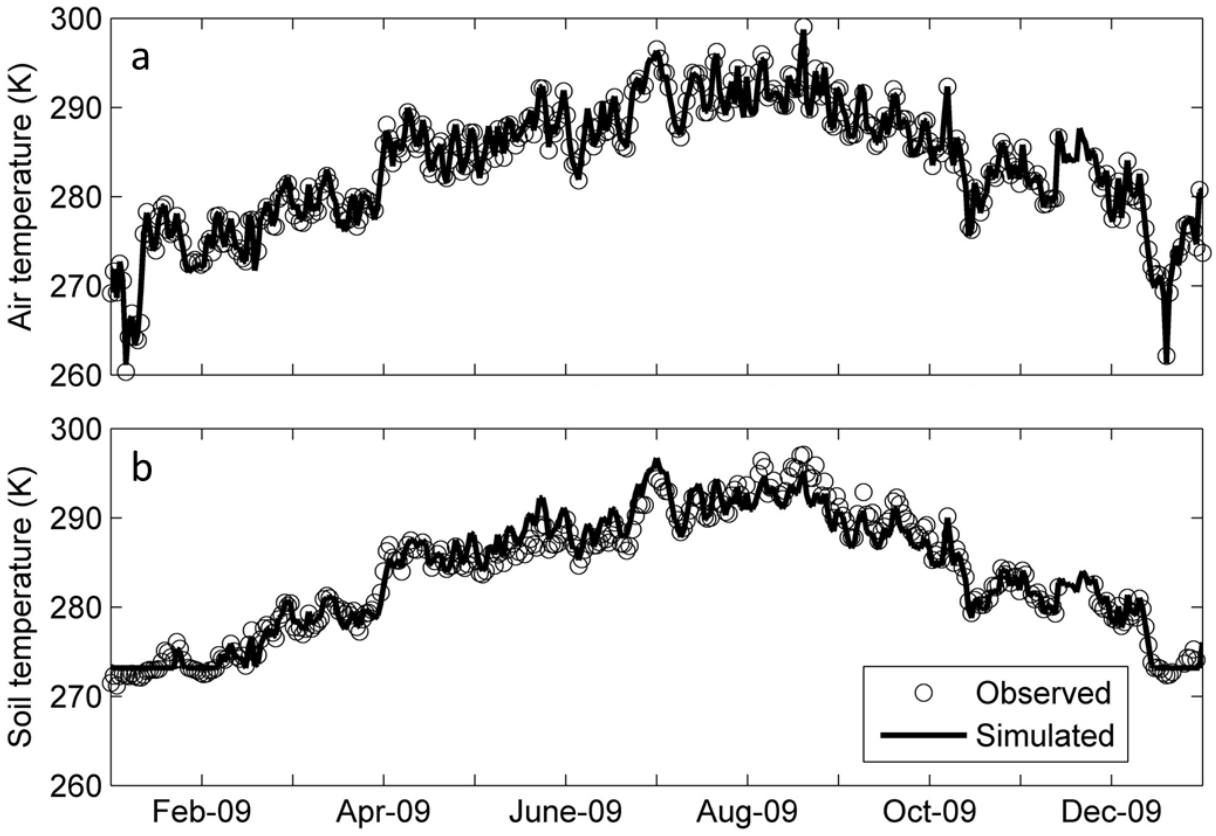

Figure 2.8. Comparison between observed and simulated daily average 2m air temperature (a) and soil temperature (b) from Selhausen site.

Figure 2.10 shows the comparison between observed and simulated *G* at the Selhausen site. The daily variability in the observed flux is captured by the model (Figure 2.10a). Figure 2.10b shows the monthly box plots of daily average observed and simulated *G*. This Figure demonstrates that model is also able to reproduce the seasonal trend in observed *G*, with an exception in January, where the model underestimates the monthly mean value.

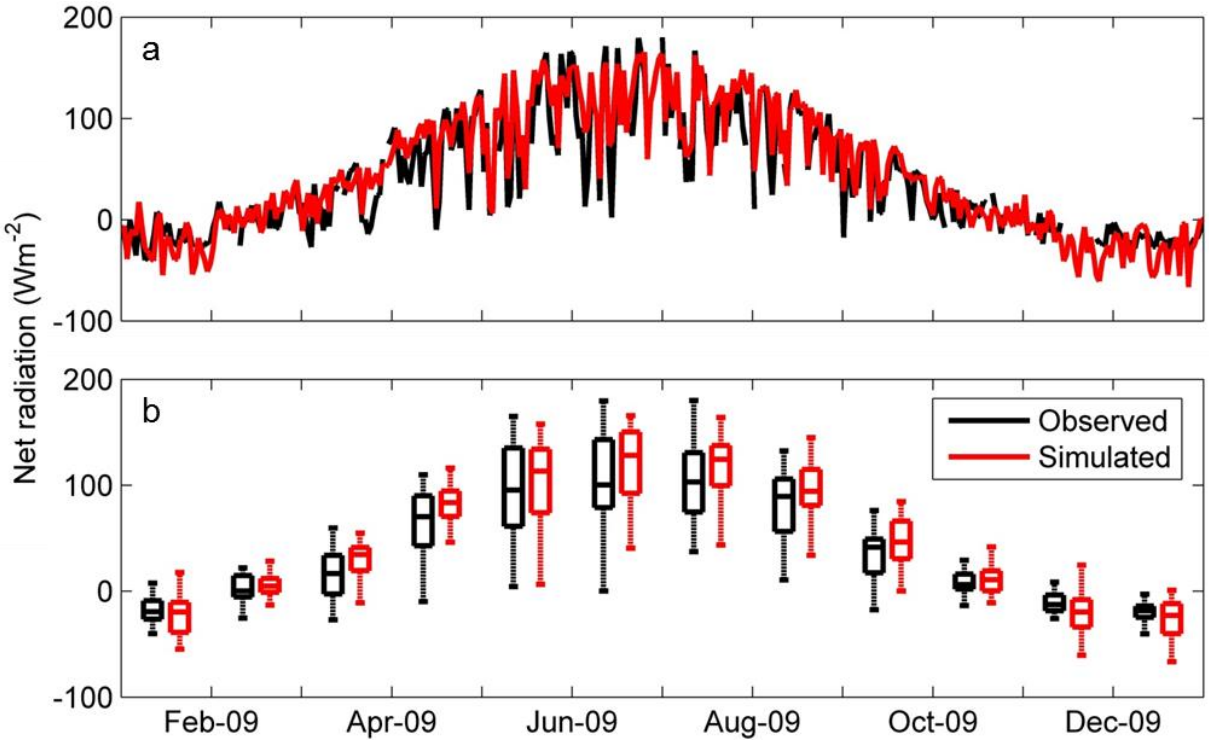

Figure 2.9. Observed and simulated daily average (a) and monthly boxplots (b) of net radiation data from Selhausen site.

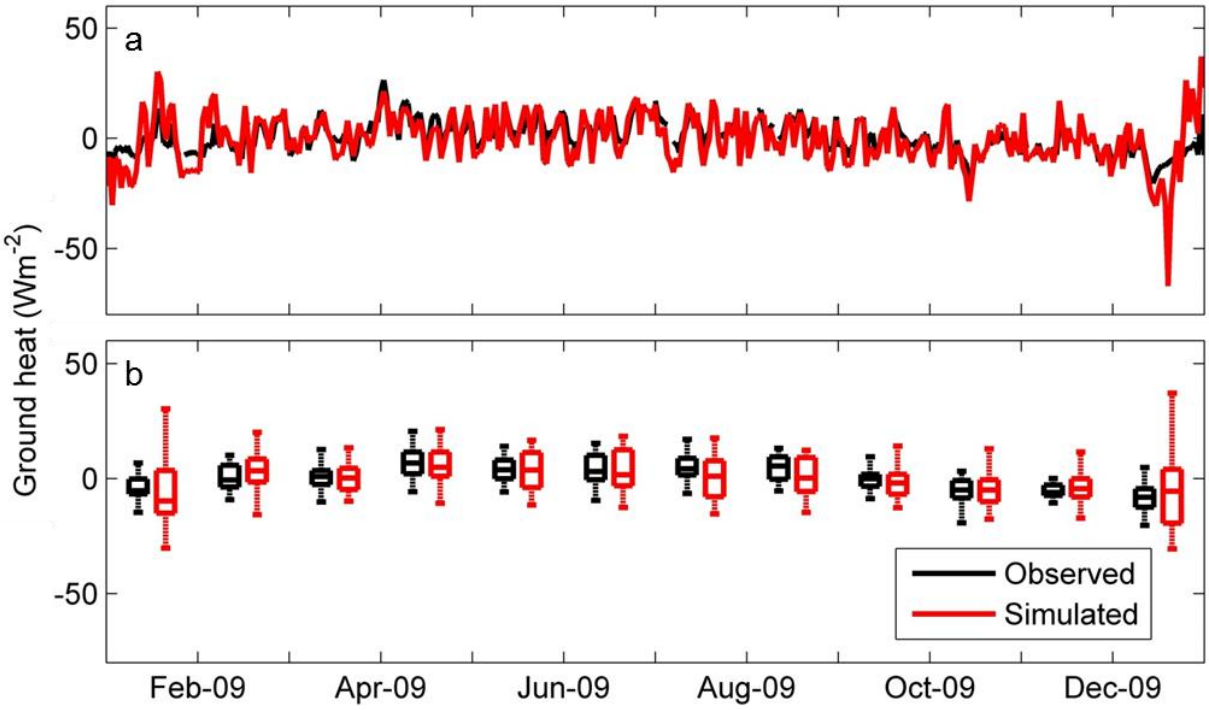

Figure 2.10. Observed and simulated daily average (a) and monthly boxplots (b) of ground heat flux from Selhausen site.

In this section, a comprehensive comparison between observed and simulated mass and energy fluxes of the hydrological cycle is performed. This comparison shows reasonable agreement between simulated and measured variables in terms of dynamics and magnitude. The discrepancies may be attributed to the relatively coarse model grid resolution of 1km, uncertainties in model structure and parameterization, and interpolation of atmospheric forcing data.

2.6 Summary and conclusions

In this chapter, results from the numerical simulation of terrestrial hydrologic cycle over multiple years (2009-2011) were presented. A fully coupled subsurface-land surface model ParFlow.CLM was applied on the Rur catchment, Germany, and the mass and energy fluxes of the coupled water and energy cycles are simulated over three consecutive years. The model results were compared with spatially distributed mass and energy flux observations at various measurement sites over the catchment.

The simulation results for the major fluxes and states in coupled water and energy cycles generally showed good agreement with observed values. The discrepancies between observations and model results may be improved through model tuning or comprehensive model calibration. It should be mentioned that uncertainties in the simulation results may arise from model structure, parameters, and atmospheric forcing data. However, a comprehensive parameter sensitivity and uncertainty analysis in the applied modeling framework would require novel, non-traditional approaches and large computer resources, which is beyond the scope of this thesis.

The comparisons were made between point measurements and cell-centered model grid values based on a one-km resolution, which may also contribute to the discrepancies between observed and simulated fluxes. While the hydrological system is heterogeneous at all scales, it was assumed that cell-centered values are representative of the entire grid cells, which constitutes a major simplifying assumption. This limitation in representing the sub grid spatial heterogeneity in the model parameter values may also contribute to discrepancies between the observed and simulated mass and energy fluxes discussed in this chapter. Note that exact deterministic prediction of observed flux values is not the focus of this thesis. Instead, the objective is to produce reasonable model results to represent the processes in the hydrologic cycle and analyze the space-time variability of these processes. For this purpose, the agreement between observed and simulated fluxes is adequate.

Chapter 3

The concept of dual-boundary forcing in land surface-subsurface interactions of the terrestrial hydrologic and energy cycles*

3.1 Introduction

Atmospheric and subsurface processes show variability at different space-time scales [e.g., *Kumar and Georgiou*, 1993; *Haddad et al.*, 2004; *Gundogdu and Guney*, 2007; *Táany et al.*, 2009; *Beecham and Chowdhury*, 2010]. Land surface connects these two compartments (i.e., atmosphere and subsurface) of the hydrological cycle. Because of the direct interactions, land surface processes (e.g., evapotranspiration, *ET* and sensible heat transfer) are influenced by the variability of atmosphere and subsurface hydrodynamics.

The connection between subsurface hydrodynamics and land surface mass and energy fluxes has been a subject of research for some time [e.g., *Tian et al.*, 2012; *Niu et al.*, 2013]. *Sklash and Farvolden* [1979] discussed the important role of groundwater on surface runoff generation using observations and simulation results. *Liang et al.* [2003] showed the impact of the surface water-groundwater interactions on land surface processes. *Maxwell and Miller* [2005] demonstrated the effect of including detailed subsurface hydrodynamics in a land surface parameterization scheme for simulating the coupled water and energy cycles. *Kollet and Maxwell* [2008] studied the influence of groundwater dynamics on land surface energy fluxes and proposed a critical water table depth (*WTD*) zone where the effect is significant along hillslopes. Similar relationship between *ET* and *WTD* was found by *Szilagyi et al.* [2013], who used observations from Platte river valley, USA. Observations [*Yeh and Eltahir*, 2005] and model results [e.g., *Miguez-Macho and Fan*, 2012a] also reveal the role of groundwater as a modulator of surface runoff. The groundwater control on *ET* through

*Rahman, M., M. Sulis, and S. J. Kollet (2014), The concept of dual-boundary forcing in land surface-subsurface interactions of the terrestrial hydrologic and energy cycles, Water Resour. Res., 50, 8531-8548.

shallow soil moisture has been investigated explicitly in several studies [e.g., *Chen and Hu*, 2004; *Soylu et al.*, 2011]. *Lam et al.* [2011] studied the spatial and temporal connection between groundwater dynamics and *ET* and showed the importance of groundwater contribution towards dry season evaporation. The study by *Miguez-Macho and Fan* [2012b] demonstrated the influence of groundwater on *ET* at a seasonal scale and discussed different mechanisms responsible for this phenomenon. Several studies have demonstrated the scaling properties of groundwater dynamics and showed the connection with surface water system [e.g., *Little and Bloomfield*, 2010; *Schilling and Zhang*, 2012] and energy fluxes [e.g., *Amenu et al.*, 2005].

The interaction between land surface processes and atmospheric variables has also been studied previously [e.g., *Brubaker and Entekhabi*, 1996; *Betts et al.*, 1996; *Porporato et al.*, 2000]. Several studies demonstrated the effect of land surface soil moisture [e.g., *Manabe and Delworth*, 1990; *Rowell and Blondin*, 1990; *Findell and Eltahir*, 1997; *Seuffert et al.*, 2002; *Gedney and Cox*, 2003; *Zhang et al.*, 2008] and groundwater dynamics [e.g., *Maxwell et al.*, 2007; *Yuan et al.*, 2008] on atmospheric processes. The important role of groundwater dynamics on land-atmosphere moisture feedback was discussed by *York et al.* [2002]. *Anyah et al.* [2008] showed the effect of subsurface hydrodynamics on coupled land-atmosphere variability and argued that a shallow groundwater table tends to enhance *ET* in arid regions, which eventually leads to increased precipitation. *Ferguson and Wood* [2011] used global satellite remote sensing data to identify the regions where land-atmosphere coupling persists. *Phillips and Klein* [2014] used the observations from Southern Great Plains, USA, and showed the influence of atmospheric forcing on land surface processes at daily time scale.

The aforementioned studies suggest that interconnections exist between different compartments of the terrestrial hydrological cycle (i.e., subsurface, land surface, and atmosphere). However, quantifying these interconnections between the compartmental mass and energy fluxes is complicated. This is mainly due to the diverse space-time scales associated with the processes that comprise this system, which has been discussed previously in relation to the variability in atmospheric [e.g., *Matsoukas et al.*, 2000; *Hsu and Li*, 2010], land surface [e.g., *Smith et al.*, 1998; *Labat et al.*, 2005; *Ding et al.*, 2013] and subsurface [e.g., *Liang and Zhang*, 2013] processes, as well as land-atmosphere interactions [e.g., *Delworth and Manabe*, 1993; *Wu and Dickinson*, 2004].

In this context, the concept of a *dual-boundary forcing* (DBF) is introduced in this chapter to represent and quantify the interactions between the compartmental mass and energy balance

components at the relevant space and time scales. Observed and simulated mass and energy fluxes of the hydrological cycle are analyzed using spectral and geostatistical techniques. The results illustrate scale-dependent coherence between groundwater dynamics and land surface processes, which substantiate the proposed DBF concept.

3.2 Conceptual approach

The underlying hypothesis of this study is that the land surface processes are influenced by a DBF at different space-time scales. According to this hypothesis, the atmosphere and groundwater act as the upper and the lower boundaries, respectively. The availability of energy and moisture determines which boundary condition dominates the exchange processes. The land surface reacts and interacts at the interface between the free atmosphere and subsurface to adapt or transform the variability of the processes associated with those boundaries. Therefore, the space-time patterns in land surface processes can be in large parts explained by the variability of the dominant boundary condition at the respective space and time scales, when accounting for major non-linear feedbacks.

Figure 3.1 shows a schematic of the proposed DBF concept. Hypothetical time series of atmospheric and land surface (net radiation, R_{net}; latent heat flux, LE; and potential latent heat flux, LE_{pot}), and subsurface (groundwater table depth, WTD) fluxes and states are shown in this figure. Coherence between atmospheric and land surface processes is observed under both energy limited and moisture limited conditions. Under energy limited conditions, LE agrees well with LE_{pot} because moisture is abundant. Under moisture limited conditions, the groundwater contribution becomes essential to meet the daily ET demand. Because of this dependence, the high frequency (daily) variability of land surface energy fluxes is propagated into the subsurface, generating the variability in subsurface hydrodynamics at the respective time scale [e.g., *Gribovszki et al.*, 2010; *Fahle and Dietrich*, 2014]. The subsurface hydrodynamics, in contrast, influence the low frequency variability of the land surface processes under soil moisture limited conditions resulting in the increasing difference between LE_{pot} and LE in Figure 3.1. The controlling effect of the low frequency variability of subsurface hydrodynamics on land surface energy fluxes has been discussed by *Amenu et al.* [2005], who also suggested that this influence may be significant under dry conditions. The proposed concept may be corroborated via the analysis of *in-situ* observations and physics based simulations of moisture and energy states and fluxes. It should be mentioned that the

DBF concept may be simplified compared to the actual non-linear feedbacks between the mass and energy balance components in the hydrological cycles.

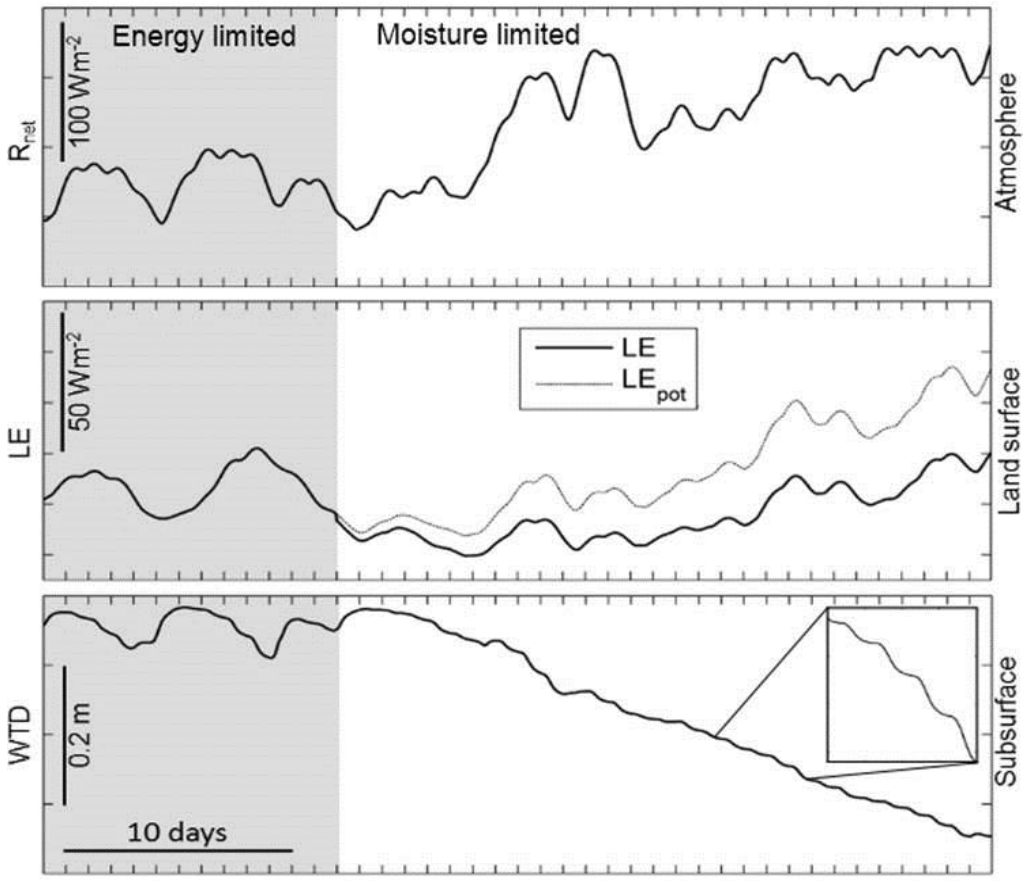

Figure 3.1. Schematic of the proposed *dual boundary forcing* (DBF) concept. Hypothetical time series of atmospheric (R_{net}), land surface (*LE*), and subsurface (*WTD*) processes are partitioned based on the energy and moisture availability. The shaded area in each plot indicates the energy limited period. The inset in *WTD* time series shows the high frequency variability of subsurface hydrodynamics under moisture limited conditions.

In this study, a physics based distributed model is applied, which incorporates mathematical formulations to represent complex processes of the coupled terrestrial hydrological and energy cycles to the best of current knowledge. There is uncertainty with respect to model parameterization and structure, input parameters, and space/time discretization of the governing partial differential equations [e.g., *Vrugt et al.*, 2005]. Accounting for all sources of uncertainty is not feasible in the current modeling framework, because of the limitations of computational resources. However, the capability of the model to reproduce the major states and fluxes was tested by comparing the results with measured data from the experimental catchment in the previous chapter. Additionally, there may be significant feedbacks from the land surface processes and subsurface hydrodynamics to the free atmosphere, which may also

affect the connections between the mass and energy balance components at different space-time scales. These are not considered here, because the model is forced with the atmospheric variables in offline mode.

3.3 Methods

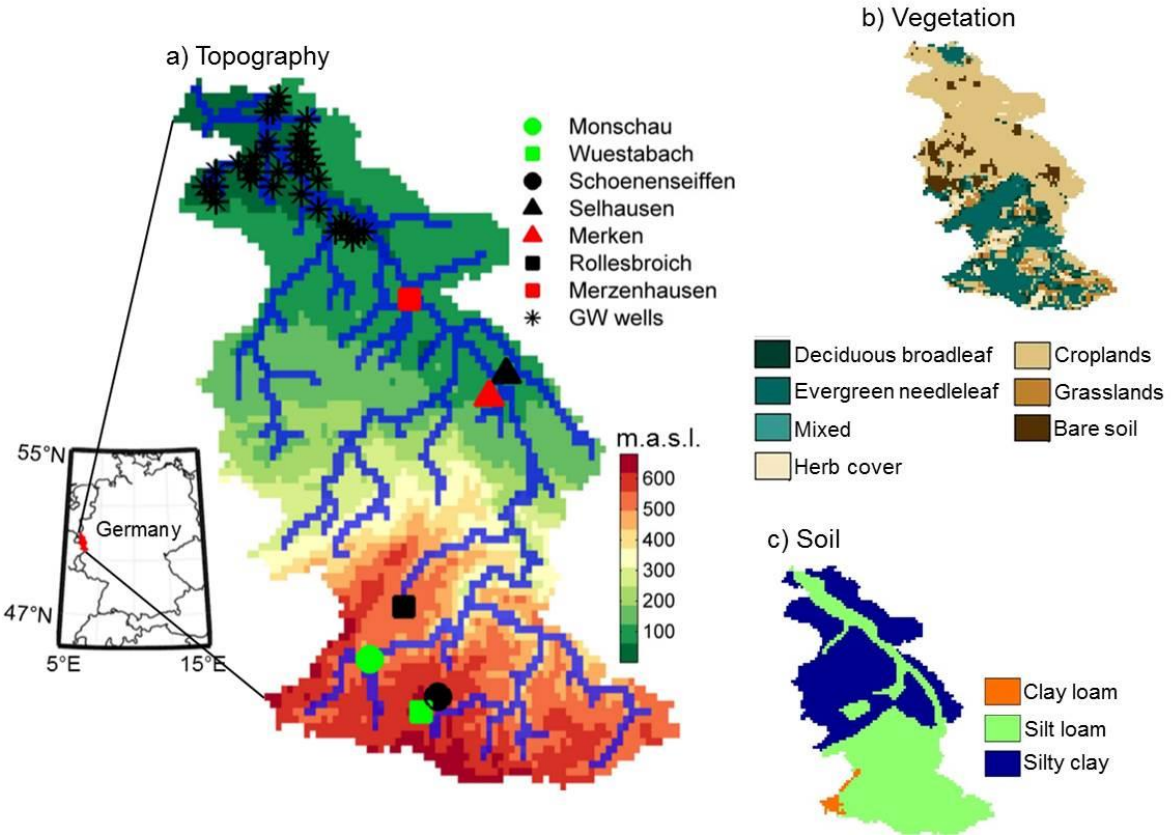

Figure 3.2. Location and topography (a), vegetation cover (b), and soil texture (c) information of the Rur catchment. The blue lines and the legends on the topography show the river network and the locations of the measurement stations, respectively.

3.3.1 The study area: Rur catchment

The study area is the Rur catchment (Figure 3.2a), which is located in western Germany with an area of about 2,400km^2. The Rur River has a length of some 165 km with headwaters located in Belgium and discharge into the Meuse River near Maastricht. The northern part of the catchment is characterized by flat lowland regions, which is a part of the Belgium-Germany loess belt formed by unconsolidated rock deposits. Agriculture is the major land use type in this part of the catchment. This flat region receives an annual precipitation of approximately 600-800mm and contributes to a potential *ET* of approximately 550-600mm/a [*Bogena et al.*, 2005].

The southern part of the catchment is characterized by the mountainous Eifel region, where Palaeozoic and Mesozoic rock outcrops. Compared to the northern lowlands, this mountainous region is characterized by a higher precipitation amount of more than 1200mm/a and a lower potential *ET* amount of approximately 550mm/a [*Bogena et al.*, 2005]. The Eifel is heavily forested with coniferous trees. A distinct difference in the mean annual temperature between the northern (8.5-10.5°C) and the southern (7.0-9.0°C) part of the catchment is observed due a 600m difference in elevation.

3.3.2 The coupled model: ParFlow.CLM

ParFlow is an integrated, parallel, variably saturated groundwater flow model that solves the Richards' equation [*Richards*, 1931] in three spatial dimensions:

$$S_s\theta\frac{\partial\psi}{\partial t}+\phi\frac{\partial\theta(\psi)}{\partial t}=\nabla\cdot\mathbf{q}+S \tag{3.1}$$

$$\mathbf{q}=-k(x)k_r(\psi)\nabla(\psi-z) \tag{3.2}$$

where S_s is specific storage (m^{-1}), θ is soil moisture (-), ψ is pressure head (m), t is time (s), ϕ is porosity (-), $\mathbf{q}$ is water flux (ms^{-1}), S is general source/sink term (s^{-1}), $k(x)$ is saturated hydraulic conductivity (ms^{-1}), $k(r)$ is relative permeability (-), and z is depth below surface (m). ParFlow uses a finite volume scheme with two point flux approximation in space and an implicit backward Euler scheme in time to solve this equation. The surface flow is integrated by applying a free surface overland flow boundary condition at the land surface [*Kollet and Maxwell*, 2006]. The kinematic wave equation is solved maintaining the continuity of pressure and flux at the boundary. A terrain following vertical grid can be used in ParFlow honoring the topographic slopes in an approximate fashion [*Maxwell*, 2013].

The land surface model CLM is coupled with ParFlow to simulate land surface mass and energy balance components [*Maxwell and Miller*, 2005; *Kollet and Maxwell*, 2008]. Vertical mass, energy, and momentum fluxes are described by the Monin-Obukhov similarity principle in CLM. The energy balance equation in CLM can be written as:

$$R_{net}(\theta)=LE(\theta)+H(\theta)+G(\theta) \tag{3.3}$$

where R_{net} is net radiation (Wm^{-2}), LE is latent heat flux (Wm^{-2}), H is sensible heat flux (Wm^{-2}), and G is ground heat flux (Wm^{-2}). This equation is written as a function of θ to demonstrate the connection between land surface energy balance and subsurface

hydrodynamics. The source/sink term *S* in equation (3.1) corresponds to the moisture dependent *LE* in equation (3.3). The surface heat transfer in CLM is simulated by solving the heat diffusion equation. *G* is applied as the top boundary condition to solve this equation at the land surface and obtained as the residual of equation (3.3), which closes the energy balance. It should be mentioned that, CLM considers only conduction process in simulating subsurface energy transport ignoring convection, which eventually decouples the heat transport from the moisture transport in the coupled model [*Kollet et al.*, 2009]. The land surface model CLM is forced with atmospheric variables including precipitation rate, radiation, temperature, barometric pressure, wind speed, and humidity. The off-line coupling scheme considered in this study assumes that, these atmospheric variables do not change due to transient land surface conditions [*Kollet*, 2009]. This assumption may influence the mass and energy fluxes simulated by the model because of the non-linear feedback mechanisms between different compartments mentioned before. *Dai et al.* [2001] describes the parameterizations in CLM in details.

In the coupled modeling framework, ParFlow replaces the simplified hydrological scheme in CLM and simulates subsurface hydrodynamics along with surface runoff. In return, CLM calculates the non-linear source/sink terms of soil moisture (e.g., infiltration from precipitation and *ET*, respectively) for ParFlow. At every 1h time step, the two coupled model components exchange fluxes and shallow soil moisture distributions in an operator splitting approach.

3.3.3 Rur model setup

The ParFlow.CLM model is applied over a model domain encompassing the Rur catchment (Figure 3.2a). A total subsurface depth of 50m is considered in the model, with a variable vertical discretization ranging from 4×10^{-2}m at the land surface to 2×10^{0}m at the bottom of the model domain using the aforementioned terrain following grid implementation. Laterally, the model has a uniform grid resolution ($\Delta x=\Delta y$) of 1km with 168 ×168 cells in x and y dimensions, respectively. No-flow lateral and bottom boundary conditions are applied to the model domain. At the land surface, a free surface overland flow boundary condition is used [*Kollet and Maxwell*, 2006].

Spatially distributed vegetation cover information (Figure 3.2b) for the model domain is obtained from the Global Land Cover 2000 (1km spatial resolution) digital database (GLC2000, European Commission, Joint Research Centre, 2003), with plant parameters

derived following the International Geosphere-Biosphere Program (IGBP) standard. The deeper subsurface in the model is homogeneous with parameter values (Table 2.1) obtained from *Gleeson et al.* [2011]. Digital Soil Map of the World (DSMW) provided by the Food and Agricultural Organization of UNO (FAO) and the Euro-soil database information [e.g., *Dolfing and Scheltens*, 1999] are used to represent the texture of different soil types in the shallow subsurface (Figure 3.2c). The van Genuchten function represents the saturation pressure head relationship for different soil types in the model [*van Genuchten*, 1980], with parameter values (Table 2.2) obtained from *Schaap and Leij* [1998].

The simulation period extends from January 2009 until December 2011 with a time resolution of one hour. Atmospheric variables are obtained from the COSMO-DE re-analysis data set of the German Weather Service (DWD). Linear interpolation technique is applied to downscale these atmospheric variables to the model grid resolution of 1km, because COSMO-DE operates at a lateral grid resolution of 2.8km. A model spin-up is performed to achieve a realistic initial condition. For this purpose, the model is initialized with an arbitrary uniform water table depth of 5m below ground surface. With this setup, repeated model runs are performed using the hourly atmospheric forcing data of 2009 to reach a dynamic equilibrium, which required about 20 years of simulation time.

3.4 Results and discussion

3.4.1 Coherence in observed processes

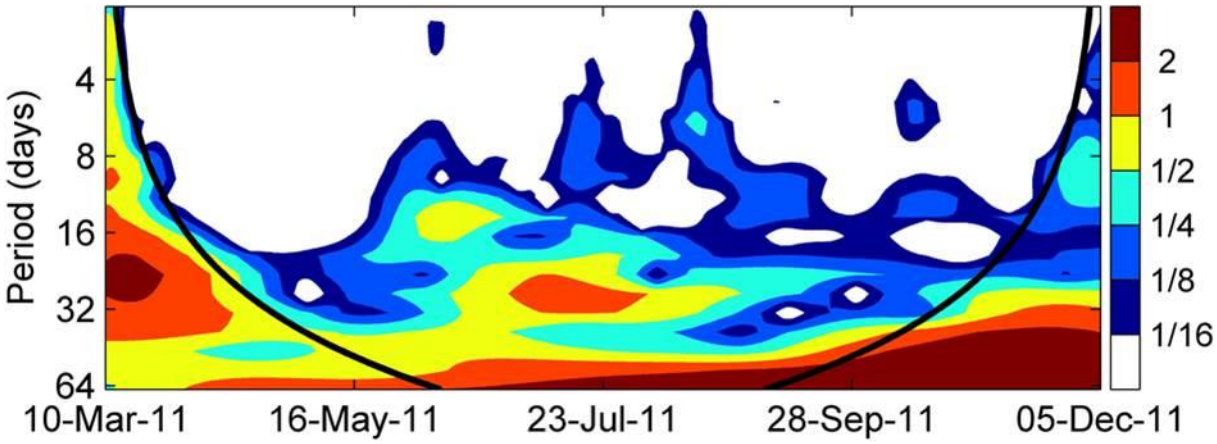

Figure 3.3. Time localized cross-wavelet power of daily average observed latent heat flux, *LE*, and groundwater table depth, *WTD* time series at the Wuestebach test site.

In this section, the time localized coherence between observed *LE* and *WTD* is analyzed using the cross-wavelet transform technique (Appendix B). This analysis is intended to explore the subsurface-land surface connection at different temporal scales in a time localized fashion.

Figure 3.3 shows the time localized cross-wavelet power of daily average measured *LE* and *WTD* time series at the Wuestebach test site. This figure shows cross-wavelet power at a monthly scale (about 32day) in summer (from June 2011 until August 2011). High cross-wavelet power is also observed at about 64day time scale. Figure 3.3 reveals the time localized coherence between observed *LE* and *WTD* at two dominating time scales on the order of months in summer. This result suggests that interconnections exist between subsurface hydrodynamics and land surface processes at different time scales under moisture limited conditions, which motivates the proposed DBF concept. In the following sections this observed coherence patterns in Figure 3.3 will be corroborated with the model results.

3.4.2 Analysis of simulated space-time variability

According to the DBF concept, atmosphere and groundwater act as the upper and the lower boundary conditions, respectively, for the land surface processes. As a first step, the influence of atmospheric variability on simulated land surface processes at different time scales is illustrated. Figure 3.4 shows the time localized wavelet power of simulated R_{net} and *LE* averaged over the catchment. The 1day scale variability in R_{net} spectrum is observed throughout the year, although it is less pronounced in the colder months. Additionally, R_{net} spectrum shows variability at the 32day time scale in summer. Similar to R_{net}, the wavelet power spectrum of *LE* shows temporal variability at 1day scale, indicating the connection between R_{net} and *ET*. At larger time scales, *LE* variability does not directly correlate with R_{net} in summer, although temporal patterns at about 32-64day are observed in the *LE* spectrum.

Figure 3.5 shows time localized wavelet power of catchment-averaged precipitation (*P*), simulated relative surface saturation (S_r), and simulated *WTD*. The *P* and S_r spectra show similar variability at time scales up to 8-16day throughout the year. The variability of *P* is reflected in S_r and WTD spectrum at about 16-32day time scale during February and September, which are the major recharge periods over the catchment. The exception is September 2010, when 16-32day variability is not visible in *WTD* spectrum. It should be mentioned that, 2010 is the driest of the three simulated years. This may be the reason for the discontinuity in the wavelet power spectrum of *WTD*, because simulated groundwater recharge dropped drastically during this time period over the catchment. Additionally,

variability in S_r spectrum at 32-64day time scale is observed in summer. These results agree with the findings of *Lauzon et al*. [2004], who demonstrated that the soil moisture data from the Orgeval watershed in France shows variability at time scales greater than 16day in summer from 1998 until 2001.

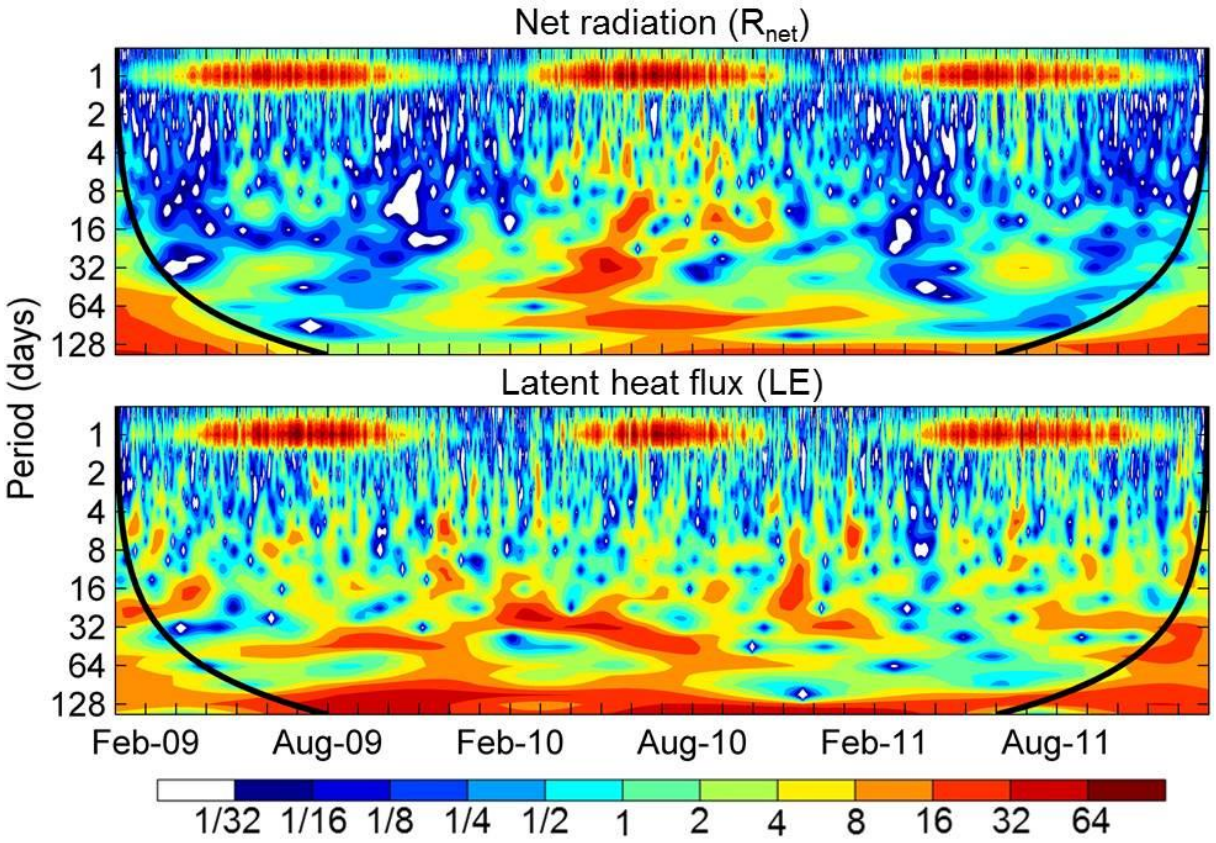

Figure 3.4. Time localized wavelet power of net radiation, R_{net}, and latent heat flux, *LE*.

According to the DBF concept, daily *LE* variability (Figure 3.4) influences groundwater dynamics under moisture limited conditions (Figure3.1, inset in *WTD* plot). The 1day temporal pattern is visible in the *WTD* wavelet power spectrum in Figure 3.5, which is due to the daily groundwater contribution to meet *ET* demand under soil moisture limited conditions [e.g., *Fahle and Dietrich*, 2014]. Therefore, Figure 3.4 and 3.5 connect atmospheric forcing (i.e., R_{net}) and subsurface hydrodynamics to land surface energy fluxes on a 1day time scale.

Figure 3.6a shows the difference between simulated daily average LE_{pot} and *LE* over the simulation period to demonstrate the influence of moisture on *ET*. Significant differences between LE_{pot} and *LE* (LE_{pot} - *LE*) are observed in summer, especially in 2010. As mentioned earlier, 2010 is the driest of the three simulated years, which is the reason for the high LE_{pot} - *LE* observed in this year. According to the DBF concept, groundwater influences *LE* because

of the dependence of *ET* on capillary rise of moisture from the free groundwater table (Figure 3.1).

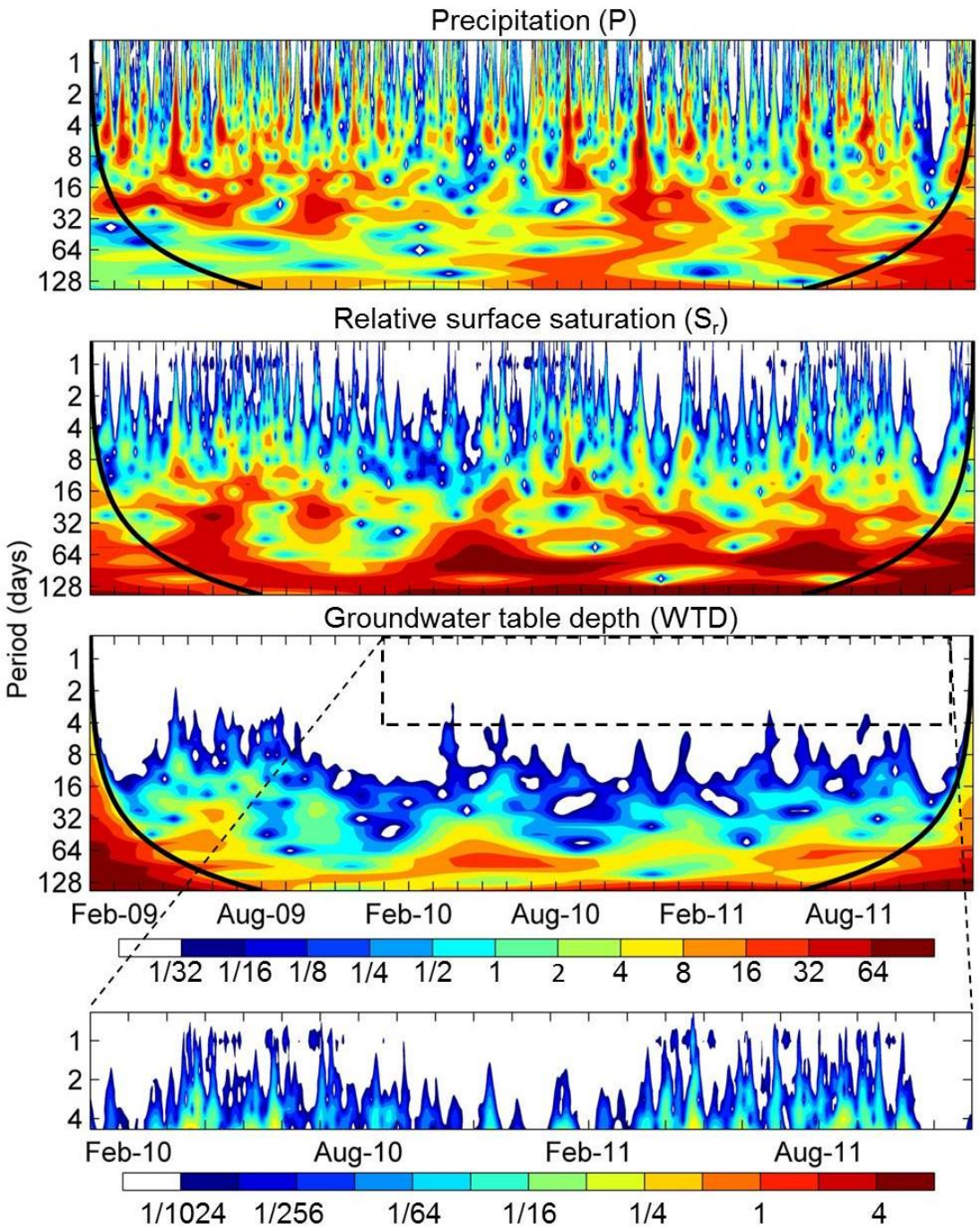

Figure 3.5. Time localized wavelet power of Precipitation, *P*, relative surface saturation, S_r, and groundwater table depth, *WTD*. The enlarged part of *WTD* spectrum (from January 2010 until December 2011) shows the power with small amplitude at 1-4.5day time scale.

Figure 3.6b shows the time localized cross-wavelet power spectrum of LE_{pot} - *LE* and *WTD* to illustrate this connection. This figure shows cross-wavelet power during summer at 1day time scale, while the phase arrows indicate that the two time series generally show an anti-phase

relationship at this time scale. At the 32day time scale, consistent high cross-wavelet power is observed in summer. At this scale, the phase arrows show that the *WTD* time series slightly leads the LE_{pot} - *LE* time series, which demonstrates the feedback of *WTD* variability on summer *ET* at this time scale. In 2010 and 2011, significant wavelet power at the time scales greater than 64day suggests that under dry conditions, coherence between LE_{pot} - *LE* and *WTD* is extended to larger time periods.

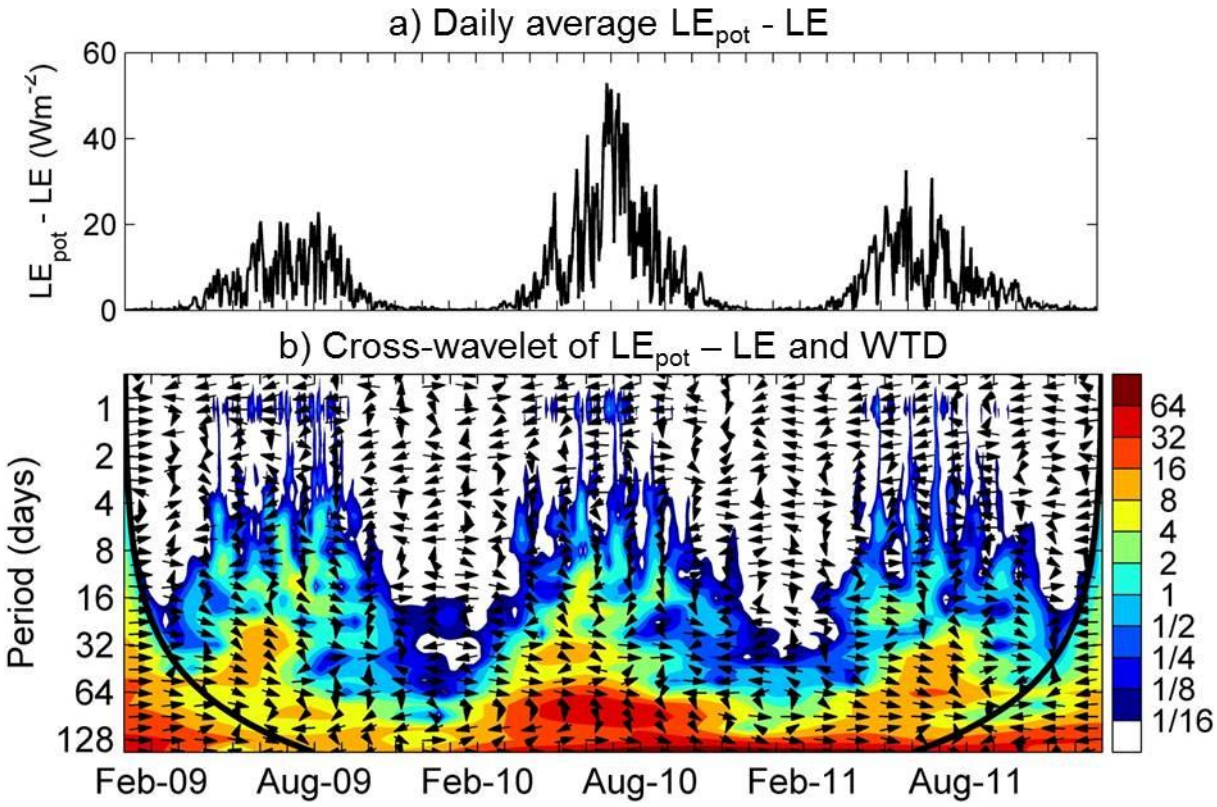

Figure 3.6. Difference between daily average simulated potential and actual latent heat flux, LE_{pot} - *LE* (a), and time localized cross-wavelet power of LE_{pot} - *LE* and water table depth, *WTD*, over the simulation period. The arrows show the phase relationship between the two time series (right arrow: in phase; left arrow: anti-phase; up arrow: LE_{pot} - *LE* is leading by 90°; and down arrow: *WTD* is leading by 90°).

The wavelet transform analysis above correlates the mass and energy balance components across different time scales using the catchment-averaged time series in the context of DBF concept. In order to demonstrate the coherence between the spatial patterns of these processes, log-log unit semivariograms (i.e., power spectra [e.g., *Wen and Sinding-Larsen*, 1997; *Gneiting et al.*, 2012]) of simulated *LE*, *WTD*, and R_{net} in summer and winter over the Rur catchment are presented in Figure 3.7. These semivariograms are based on the average summer and winter time fluxes over the three simulated years (2009-2011).

The unit semivariogram of R_{net} does not exhibit a clear sill within the length scale of the catchment in summer or winter. This indicates that the spatial structure of R_{net} either follows a power law behavior or a large-scale stationary process with a correlation scale larger than the catchment. While the unit semivariogram of *WTD* shows spatial correlation for scales less than 5km throughout the year, the *LE* semivariogram exhibits strong seasonal dependence. In summer, the unit semivariogram of *LE* shows similar spatial pattern to that of *WTD*, with correlation for scales less than 5km. During winter, on the contrary, the semivariogram of *LE* shows similar behavior to that of R_{net} with monotonically increasing semivariance and without a distinct sill within the length scale of the catchment.

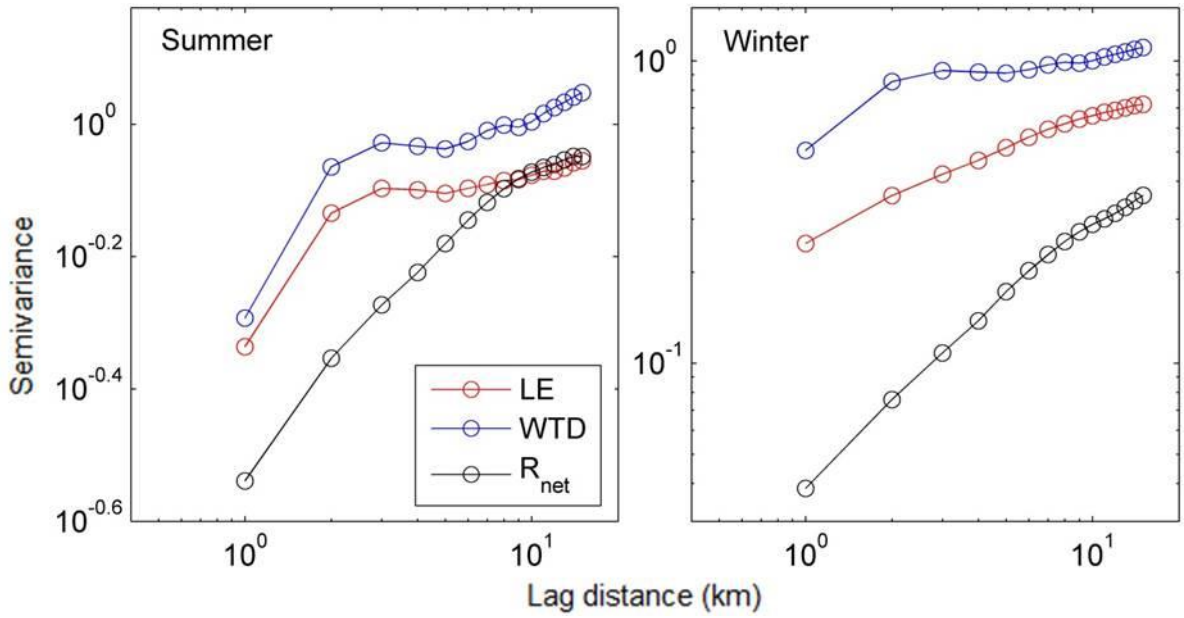

Figure 3.7. Unit semivariograms of latent heat flux, *LE*, groundwater table depth, *WTD*, and net radiation, R_{net} in summer and winter. Note the log-log scale.

The cross-semivariograms in Figure 3.8 demonstrate the spatial coherence between *LE* and *WTD* in summer and winter. Under soil moisture limited conditions (summer), the *LE* and *WTD* are negatively correlated for scales less than 5km, which agrees well with the univariate semivariograms for these variables (Figure 3.7). In winter, on the other hand, *LE* and *WTD* show weaker positive correlation and the cross-semivariogram does not exhibit a clear sill within the length scale of the catchment.

According to the proposed DBF concept, the groundwater influence on *ET* is observed under soil moisture limited conditions. The variogram analysis illustrates groundwater and atmospheric forcing control on the spatial pattern of *LE* in summer and winter, respectively. The negative correlation between *LE* and *WTD* in Figure 3.8 demonstrates the interconnection

between the spatial patterns of groundwater and *ET* under dry conditions. This negative correlation exists due to higher *ET* at locations with shallower groundwater table depth and vice-versa, which suggests the groundwater control on the spatial pattern of summer *ET*. In winter, *LE* semivariogram shows similar behavior to that of R_{net} (Figure 3.7) because of the prevailing energy limited conditions over the catchment during the colder months of the year.

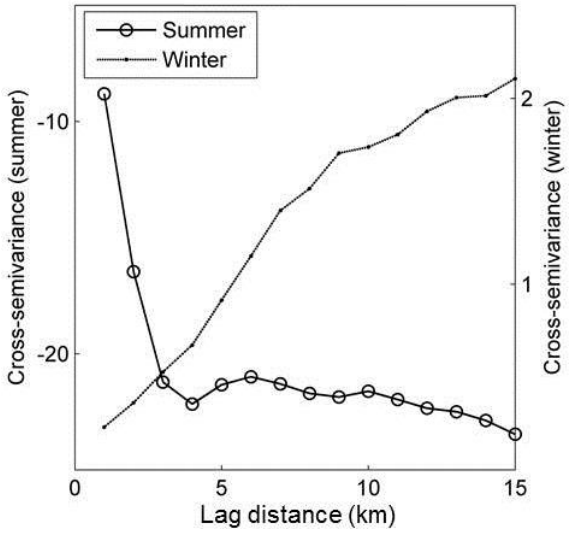

Figure 3.8. Cross-semivariograms of latent heat flux, *LE*, and groundwater table depth, *WTD* in summer and winter. Note the dual y-axis.

3.5 Summary and conclusions

In this chapter, the concept of the *dual-boundary forcing* (DBF) was proposed to describe and quantify the feedback mechanisms between different compartments of the hydrological cycle in space and time. According to the proposed DBF concept, the atmosphere and groundwater act as the upper and lower boundary conditions, respectively, for land surface processes. These boundary conditions influence the land surface at different space-time scales. The availability of energy and moisture determines the dominating boundary condition for the exchange processes.

The coupled subsurface-land surface model ParFlow.CLM was applied on the Rur catchment, Germany, and the space-time patterns of the mass and energy fluxes were analyzed using wavelet transform and variogram techniques to verify this concept. The results suggest that at the daily time scale, *ET* variability is driven by the radiative atmospheric forcing (R_{net}). This variability of *ET* influences the subsurface hydrodynamics and creates the diurnal *WTD* fluctuation through daily water uptake under moisture limited conditions, which is analogous to periodic pumping of groundwater. Groundwater storage, on the other hand, depletes due to

this withdrawal and influences *ET* mainly at the monthly time scale under moisture limited conditions in summer. It was also demonstrated that this influence extends to multi-month time scales in dry periods.

It should be mentioned that the groundwater control on *ET* may be significant at even longer time scales due to the long term memory effect of subsurface hydrodynamics under e.g., prolonged drought conditions. This influence was not considered here due to data limitation, because the simulation was performed and compared to measured data over three years (2009-2011). However, this effect can also be interrogated utilizing the proposed technique with extended time series of fluxes and states, which is planned in future.

The variogram analysis demonstrates the seasonal dependence of spatial variability of *ET*. Under energy limited conditions, the spatial pattern of *ET* is determined by R_{net}. Strong influence of groundwater on the spatial variability of *ET* is observed under moisture limited conditions. These findings suggest that, water table observations are useful in predicting the spatial pattern of *ET* in summer. In winter, however, the spatial pattern of *ET* may be predicted from R_{net} measurements alone (e.g., from remote sensing observations).

It has been discussed earlier that the simulation results may be affected by the coupled model structure, grid resolution, parameterization, and interpolation of atmospheric forcing data. There is a need of a comprehensive sensitivity and uncertainty analysis study to assess the impact of the aforementioned issues on DBF concept, which would require novel, non-traditional approaches and large computer resources. This is beyond the scope of this thesis and should be the subject of future research.

This chapter described the DBF concept that provides a framework to explain the variability of land surface mass and energy balance components with atmospheric and subsurface processes at various space-time scales based on moisture and energy availability. In the next chapter, this concept is evaluated considering different lower boundary conditions based on groundwater dynamics in ParFlow.CLM.

Chapter 4

Evaluating the dual-boundary forcing concept in subsurface-land surface interactions of the hydrological cycle*

4.1 Introduction

The mass and energy balance components in different compartments of the hydrological cycle (e.g., subsurface, land surface, and atmosphere) interact with each other via complex non-linear feedback mechanisms. Studying these feedbacks between compartmental processes is important to understand the overall mechanisms of the hydrological cycle and in water resources assessments [e.g., *Bonan and Stillwell-Soller*, 1998]. Interconnections between the mass and energy fluxes of the hydrological cycle are difficult to examine using observations, because continuous, spatially distributed measurements covering all the compartments of the hydrological cycle (e.g., subsurface, land surface, and atmosphere) over the same region over extended time periods is required for this purpose, which are not generally available [e.g., *Seneviratne and Stöckli*, 2008; *Fernández-Prieto et al.*, 2013]. In order to fill this gap, physically-based distributed models may be used to study fluxes and states continuously in both the space and time domains. Coupled simulation platforms consisting of subsurface, land surface, and atmospheric models can be constructed to study interactions between different compartments of the hydrological cycle, where direct observations are missing. In these models, groundwater may be explicitly modeled based on Darcy's law or conceptualized as a lower boundary condition (LBC) for closure of the hydrological cycle in these models [e.g., *Campoy et al.*, 2013].

Interactions of groundwater dynamics with land surface and atmospheric processes have been the subject of research for some time [e.g., *Sklash and Farvolden* 1979; *York et al.*, 2002;

*Rahman, M., M. Sulis, and S. J. Kollet (2015), Evaluating the dual-boundary forcing concept in subsurface-land surface interactions of the hydrological cycle, Hydrol. Porcess. (submitted).

Maxwell et al., 2007]. Several previous studies demonstrated the impact of groundwater table depth (*WTD*) on land surface soil moisture and runoff [e.g., *Yeh and Eltahir*, 2005; *Miguez-Macho and Fan*, 2012]. The space-time connection between groundwater dynamics and evapotranspiration (*ET*) was discussed by *Lam et al.* [2011]. *Miguez-Macho and Fan* [2012] examined the influence of *WTD* on *ET* at a seasonal time scale over the Amazon region and discussed various mechanisms responsible for such interactions. Because of this influence of the moving free groundwater table on *ET* via shallow soil moisture [e.g., *Chen et al.*, 2004; *Niu et al.*, 2007; *Soylu et al.*, 2011], interactions between *WTD* and atmospheric processes, e.g., precipitation, may also exist [e.g., *Anyah et al.*, 2008; *Leung et al.*, 2011].

The important role of groundwater dynamics has motivated studies to examine the specific space-time scales of the correlation between *WTD* and land surface processes. *Kollet and Maxwell* [2008] described a method to examine the spatial correlation between *WTD* and land surface energy fluxes at the watershed scale. *Lo and Famiglietti* [2010] studied the role of groundwater on land surface hydrologic memory and demonstrated that *WTD* influences the temporal variability of surface soil moisture. *Schilling and Zhang* [2012] studied the temporal scaling of *WTD* and stream discharge in order to identify surface water – groundwater interactions. *Fahle and Dietrich* [2014] showed the connection between diurnal *WTD* fluctuations and *ET*. The outcomes of these studies indicate that the interconnections exist between groundwater dynamics and land surface processes at various space-time scales. However, the quantification of the space-time scales remains largely unresolved despite the aforementioned efforts.

In order to explain and quantify the scale-dependent coherence of land surface mass and energy fluxes with groundwater dynamics and atmospheric processes at different space-time scales, a new hypothesis, namely, the *dual-boundary forcing* (DBF) concept was presented in *Rahman et al.* [2014]. According to the DBF concept, the atmosphere and the free groundwater table act as the upper and lower boundary conditions, respectively, influencing and forcing land surface processes at different frequencies. Atmospheric forcing influences the variability of the land surface processes at small time scales leading to coherence in variability of atmospheric forcing and e.g., *ET* at periods of days. Groundwater dynamics, on the other hand, affect land surface processes mainly at longer time scales (e.g., monthly to multi-month periods) under soil moisture limited conditions.

In this chapter, the aforementioned DBF concept [*Rahman et al.*, 2014] is assessed considering different LBCs. The hypothesis is that a parameterization of groundwater

dynamics via simple constant head or free drainage boundary conditions may lead to an alteration of variance in land surface fluxes, which may ultimately reduce the model's prognostic capabilities. The coupled model used here (ParFlow.CLM [e.g., *Maxwell and Miller*, 2005; *Kollet and Maxwell*, 2008]) is consistent with *Rahman et al.* [2014]. In order to evaluate the DBF concept, simulations are performed considering three different LBC configurations, namely, dynamic, constant, and free-drainage lower boundary conditions (DBC, CBC, and FD, respectively). The dynamic lower boundary condition (DBC) allows the temporal evolution of the LBC, while constant lower boundary condition (CBC) maintains a temporally constant *WTD* throughout the simulation period. The free drainage (FD) configuration, on the other hand, mimics the classical description of soil water flow in land surface models at the bottom of the model domain. The results from the three model configurations are analyzed using the continuous wavelet transform technique (Appendix B) ensuing the model runs and are discussed in the context of the DBF concept.

4.2 Methods

4.2.1 Study area

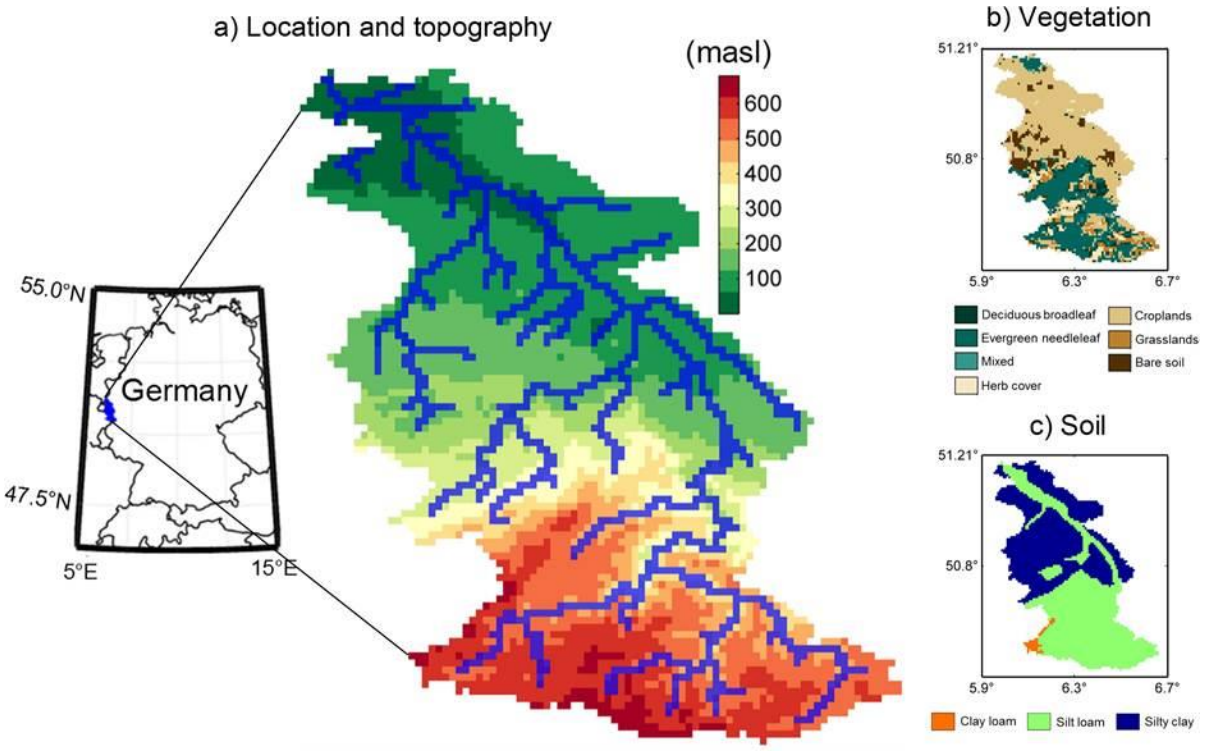

Figure 4.1. Location and topography (a), vegetation cover (b), and soil texture (c) information of the Rur catchment. The blue lines on the topography show the river network.

The study area is the Rur catchment [*Bogena et al.*, 2006; *Vereecken et al.*, 2010; *Simmer et al.*, 2015] located in Western Germany with an area of about 2,400km^2 (Figure 4.1a). The Rur River is approximately 165 km in length with headwaters in Belgium discharging into the Meuse River near Maastricht. The northern part of the catchment is characterized by flat lowland regions. This flat part of the Rur catchment receives an annual precipitation amount of about 550-600 mm/a and contributes to a potential *ET* of approximately 550-600 mm/a [*Bogena et al.*, 2005]. Agriculture is the major land use type with cereals (e.g., winter wheat) and sugar beet being the dominant crops in the northern part of the catchment.

In contrast to the northern flat lands, the southern part of the catchment is the mountainous Eifel region and is characterized by higher annual precipitation amount (~1200 mm) and lower potential *ET* (550 mm/a) [*Bogena et al.*, 2005]. The Eifel is mostly forested with coniferous trees. Because of a distinct 600m elevation difference, there exists a difference in the mean annual temperature between the northern (8.5-10.5 °C) and the southern (7.0-9.0 °C) part of the catchment.

4.2.2 Coupled Model

The coupled subsurface-land surface model ParFlow.CLM has been described in detail in several previous studies [e.g., *Maxwell and Miller*, 2005; *Kollet and Maxwell*, 2008; *Maxwell and Kollet*, 2008]. This coupled model consists of a groundwater flow model ParFlow and a land surface model CLM. ParFlow, an integrated, parallel, variably saturated groundwater flow model solves the Richards' equation in three spatial dimensions using a finite volume scheme with two point flux approximation in space and an implicit backward Euler scheme in time. ParFlow integrates surface flow by applying a free surface overland flow boundary condition at the land surface [*Kollet and Maxwell*, 2006]. In this study, a terrain following vertical grid along with a variable vertical spatial discretization is used honoring the topographic slopes in an approximate fashion for ParFlow [*Maxwell*, 2013].

The Common Land Model (CLM) simulates the mass and energy fluxes at the land surface. It needs precipitation rate, radiation, atmospheric temperature, pressure, wind, and water vapor data as atmospheric forcing input. In the coupled modeling framework, ParFlow is coupled to CLM over the first ten downward vertical model layers starting at the land surface. ParFlow, which replaces the simplified soil moisture and runoff formulations in CLM, simulates the distribution of soil moisture in the subsurface and sends this information to CLM. In return, CLM calculates the source/sink of soil moisture (e.g., infiltration from precipitation, soil

evaporation, and plant transpiration) for ParFlow. The two coupled model components communicate at every time step based on an operator splitting approach for the exchange of fluxes and the shallow soil moisture distribution.

4.2.3 Rur model setup

The coupled subsurface-land surface model ParFlow.CLM is applied over a model domain encompassing the Rur catchment. A uniform lateral grid resolution ($\Delta x=\Delta y$) of 1 km is considered with 168 ×168 cells in x and y dimensions, respectively. A total subsurface depth of 50 m is discretized ranging from 4×10^{-2}m at the land surface to 2×10^{0}m at the bottom of the model domain using the aforementioned terrain following grid implementation. A free surface overland flow boundary condition is applied at the land surface following *Kollet and Maxwell* [2006].

Global Land Cover 2000 digital database (GLC2000, European Commission, Joint Research Centre, 2003) is used to represent the spatially distributed vegetation cover (Figure 1b) over the model domain. The plant parameters are derived following the International Geosphere-Biosphere Program (IGBP) standard. The soil texture information of the shallow subsurface (Figure 4.1c) is derived from the Digital Soil Map of the World (DSMW) provided by the Food and Agricultural Organization of UNO (FAO) and the Euro-soil database information [e.g., *Dolfing and Scheltens*, 1999]. Considering spatial homogeneity, soil hydraulic parameters for the deeper subsurface are adapted from *Gleeson et al.* [2011]. Saturation pressure head relationship for different soil types are represented using van Genuchten function [*van Genuchten*, 1980], with parameter values following *Schaap and Leij* [1998].

A simulation period of three years (2009-2011) with a time resolution of one hour is considered in this study. COSMO-DE re-analysis data set provided by the German Weather Service is used to obtain the atmospheric variables (e.g., precipitation rate, radiation, temperature, barometric pressure, wind speed, and humidity) to force ParFlow.CLM. Because COSMO-DE operates at a lateral grid resolution of 2.8 km, downscaling of the atmospheric variables to the model grid resolution of 1 km is performed applying linear interpolation. In order to achieve a realistic initial condition, a model spin-up was performed by forcing ParFlow.CLM repeatedly with the hourly atmospheric information over 2009 until a dynamic equilibrium was achieved. A detailed description of model setup, input data, and spin-up process can be found in *Rahman et al.* [2014]

4.2.4 Experimental setup

In the experimental setup, three different model configurations, namely, dynamic, constant, and free drainage boundary condition were considered to identify the influence of the LBC on the variability of land surface mass and energy fluxes in the framework of DBF concept. Note, except for the treatment of the LBC, these model configurations are identical in terms of model inputs, initial and boundary conditions. In the dynamic boundary condition (DBC) configuration, *WTD* is allowed to evolve freely through time. In contrast, the constant boundary condition (CBC) configuration maintains the initial *WTD* at individual horizontal model grid cells throughout the simulation period. In the free drainage boundary condition (FD) configuration, gravity drainage is implemented at the bottom of the model domain that allows moisture to drain gravitationally through the lower boundary. Model runs are performed for three consecutive years (2009-2011) considering each of the aforementioned configurations and the mass and energy fluxes of the coupled water and energy cycles are simulated. Differences in simulation results are analyzed using continuous wavelet transform (Appendix B) techniques ensuing the model runs and discussed in context of DBF concept.

4.3 Results and discussion

According to the DBF concept, atmosphere and groundwater act as the upper and lower boundaries, respectively, for the land surface processes. The boundary condition that dominates the exchange processes and induces variability in the land surface energy fluxes is determined by the time and space localized availability of soil moisture and energy. At small time scales (e.g., daily), variability of land surface processes is generally governed by atmospheric forcing. This high frequency variability of the land surface processes influences *WTD* under soil moisture limited conditions because of groundwater contribution towards daily *ET* [e.g., *Gribovszki et al.*, 2010; *Fahle and Dietrich*, 2014], which is analogous to periodic pumping. A the large time scales, the influence of this depletion of groundwater storage can be observed on land surface processes at monthly to multi-month time scales governed by groundwater table dynamics [*Rahman et al.*, 2014].

In this section, the proposed DBF concept is tested by analyzing the differences in model results from the three aforementioned configurations. Temporal dynamics of fluxes and states from the three model configurations are analyzed applying continuous wavelet transform technique (Appendix B). Because DBC, CBC, and FD configurations are identical except for

the LBCs, differences in the variability of the fluxes from these configurations can be attributed directly to groundwater dynamics.

4.3.1 Differences in groundwater table depth

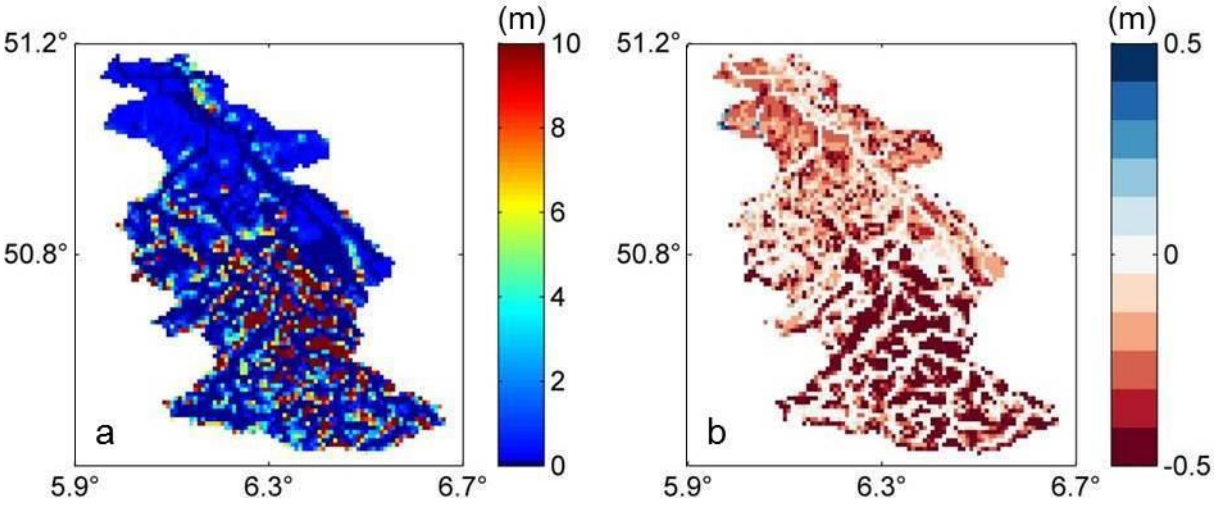

Figure 4.2. Average groundwater table depth (*WTD*) from DBC configuration (a), and difference between average groundwater table depth between DBC and CBC configurations (b) over the simulation period.

Figure 4.2a shows the temporally averaged *WTD* from DBC model configuration over the entire simulation period. This figure illustrates that groundwater table is deeper in the mountainous southern part of the catchment compared to the northern lowlands, which indicates the correlation of *WTD* with topography. Figure 4.2b illustrates the difference in average *WTD* from DBC and CBC model configurations (WTD_{DBC} - WTD_{CBC}) over the simulation period. This figure shows that both model configurations maintain a shallow groundwater table along the river valleys as expected. The reason for this is the lateral redistribution of water in the model that ensures the convergence of moisture in the valleys [e.g., *Maxwell and Kollet*, 2008]. Figure 4.2b shows that the DBC configuration is characterized by a deeper temporally averaged *WTD* compared to CBC over the catchment, because CBC configuration maintains the initial *WTD* at every horizontal model grid throughout the simulation period.

Closer inspection of Figure 4.2b also reveals that the differences between temporally averaged WTD_{DBC} and WTD_{CBC} are higher in the mountainous part of the study area. As aforementioned, the FD configuration considers a free drainage boundary condition at the bottom of the model domain. Therefore, this configuration does not maintain a physically consistent groundwater table, because moisture is able to leave the model domain through the

bottom boundary via gravity drainage unaffected by topography and groundwater convergence along river corridors.

4.3.2 LBC influence on soil moisture and evapotranspiration

In this section, the differences in land surface mass and energy fluxes from DBC, CBC, and FD configurations are examined in order to test the DBF concept. As mentioned earlier, the only difference between the three configurations is the groundwater dynamics, which, in this study, is explicitly simulated as the LBC of the model. Therefore, the differences in land surface processes presented in this section can be attributed directly to the differences in groundwater dynamics in the simulations.

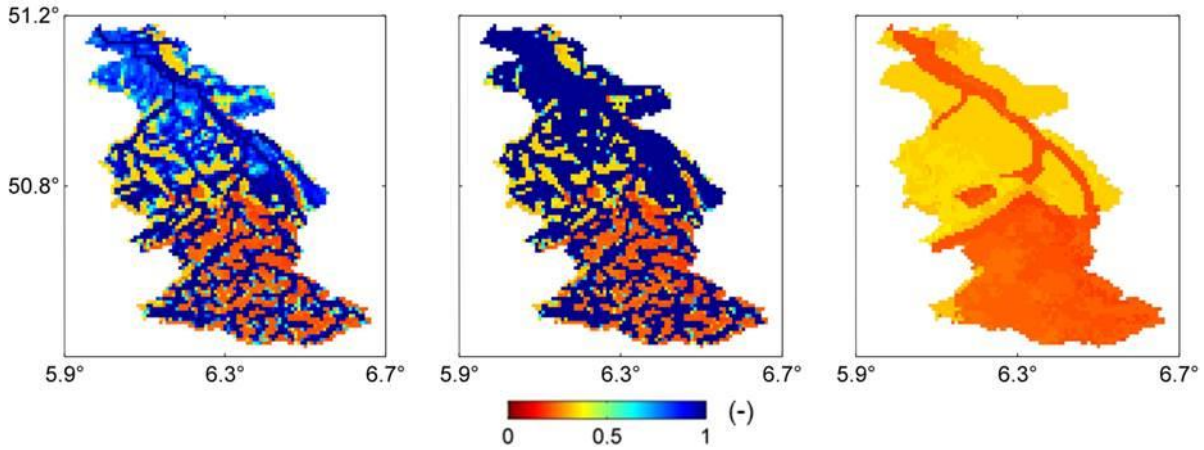

Figure 4.3. Temporally averaged (over the entire simulation period) relative surface saturation (S_r) from DBC (left), CBC (middle), and FD (right) model configurations.

Figure 4.3 shows temporally averaged relative surface saturation (S_r, soil moisture normalized by porosity) over the Rur catchment from the three model configurations. This figure demonstrates the role of soil texture (Figure 4.1c) and *WTD* (Figure 4.2) on spatial distribution of S_r. DBC and CBC show the signature of the river network, with higher S_r along the river valleys and drier conditions in the uplands. Both configurations show lower S_r in the mountainous southern part of the catchment that is characterized by deeper groundwater table (Figure 4.2a). Figure 4.3 also reveals that CBC generally simulates higher S_r over the catchment compared to DBC, which is consistent with the shallower *WTD* in CBC (Figure 4.2b). The S_r distribution from FD, in contrast, shows strong dependence only on soil texture distribution over the catchment. This configuration is characterized by less spatial variability of S_r compared to DBC and CBC. Because FD is not able to maintain a consistent

groundwater table throughout the simulation period, the S_r distribution does not show additional variability resulting from spatial distribution of *WTD*.

Figure 4.4 shows catchment averaged daily precipitation (P) and S_r time series from DBC, CBC, and FD model configurations. This figure illustrates that there are significant differences between S_r from the three model configurations, which is intuitive. Discrepancies in S_r from DBC and CBC are pronounced during the warmer months of the year, where CBC shows higher S_r. The largest difference between S_r from these two configurations is observed in summer 2010, because this is the driest of the three simulated years. FD, on the other hand, shows significantly lower soil moisture compared to DBC and CBC throughout the simulation period.

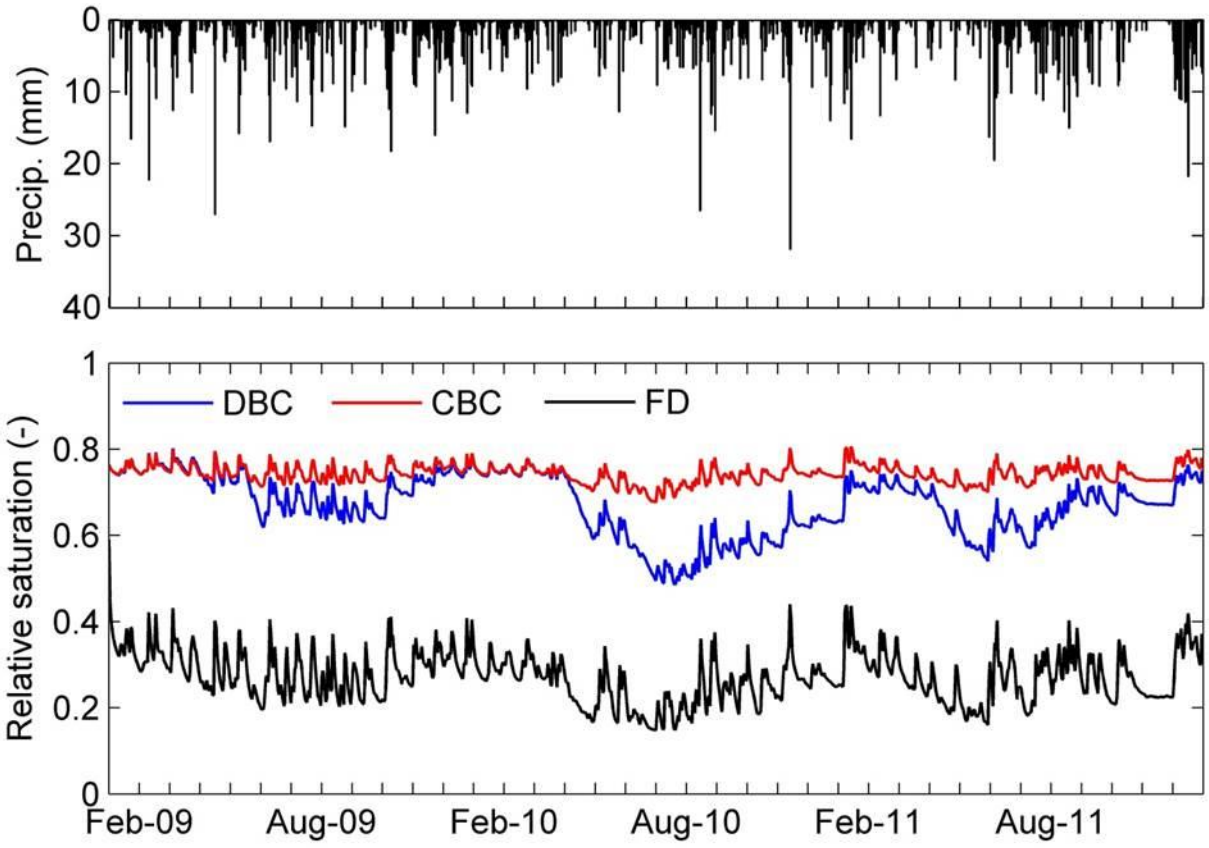

Figure 4.4. Catchment average daily mean precipitation (top) and relative surface saturation (S_r) from the three model configuration (bottom) over the simulation period.

The study by *Maxwell and Miller* [2005] illustrated the differences between land surface processes from ParFlow.CLM (with a dynamic groundwater table) and CLM (with a free drainage boundary condition at the bottom), which suggests that groundwater dynamics affect shallow soil moisture. However, *Maxwell and Miller* [2005] considered different soil

hydraulic parameters for ParFlow.CLM and CLM models. In this study, DBC, CBC, and FD configurations are identical in terms of hydraulic parameters, initial and boundary conditions except for the LBC. Therefore, the discrepancies in S_r (Figure 4.3 and 4.4) can be attributed explicitly to the differences in groundwater dynamics in the simulations.

Because *LE* is dependent on soil moisture [e.g., *Wetzel and Chang*, 1987], discrepancies in simulated *LE* from the three model configurations are expected due to the differences in S_r. Figure 4.5 plots the time series of differences in *LE* from DBC, CBC, and FD configurations. Difference between *LE* from DBC and CBC (LE_{DBC} - LE_{CBC}) shows that especially in the warmer months of the year, LE_{CBC} is higher compared to LE_{DBC}. Figure 4.3 shows that the CBC configuration simulates higher S_r compared to DBC and the differences are pronounced during summer months. Therefore, the discrepancies between LE_{DBC} - LE_{CBC} can be explained by the S_r differences. In contrast, the FD configuration shows lower *LE* (LE_{FD}) compared to DBC, which is again consistent with S_r differences between these configurations (Figure 4.3).

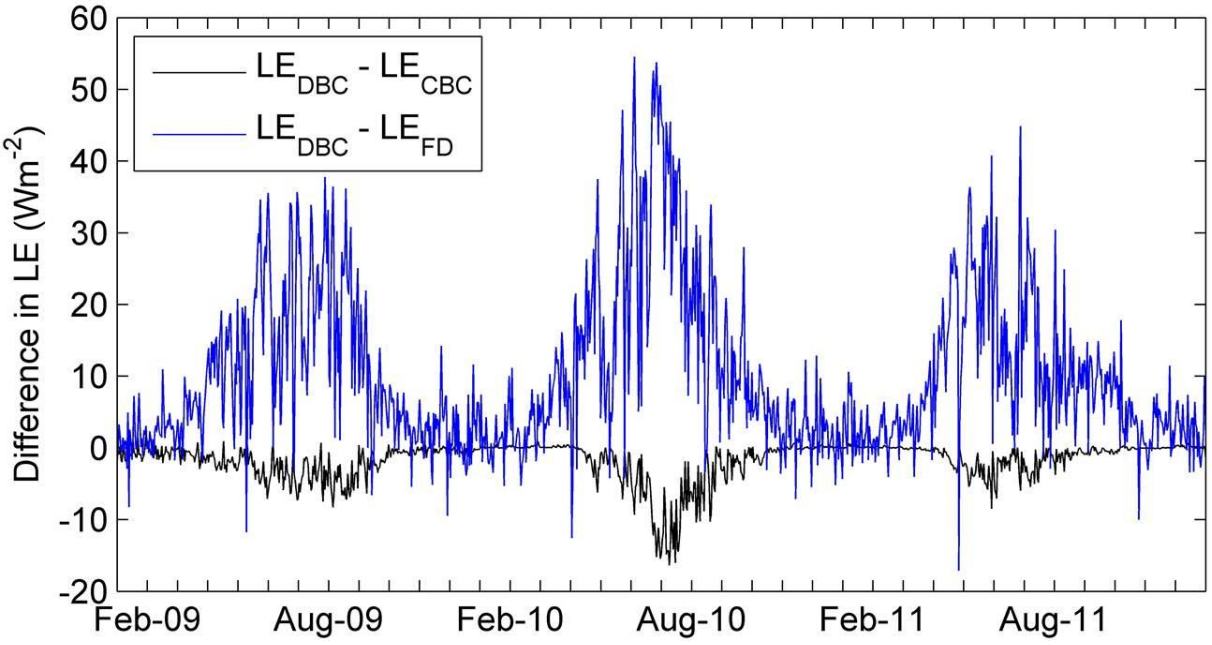

Figure 4.5. Difference between catchment average daily mean latent heat fluxes (*LE*) from the three model configurations.

The study by *Chen et al.* [2004] demonstrated that groundwater influences *LE* by modifying shallow soil moisture. *WTD* affects the water availability for *LE* because capillary rise may be a significant source of moisture to the root zone [e.g., *Soylu et al.*, 2011]. The results from DBC, CBC, and FD configurations are consistent with the findings of the aforementioned

studies. Therefore, the results corroborate that different LBCs based on groundwater dynamics in the coupled model affect absolute values of *LE* via shallow soil moisture.

According to the DBF concept, the influence of groundwater dynamics on land surface processes is observed under soil moisture limited conditions, i.e., in summer. Figure 4.5 demonstrates that the warmer months of the year are characterized by high differences between LE_{DBC} and LE_{CBC}. In contrast, differences between *LE* from DBC and CBC become insignificant in colder periods. Differences between monthly mean *WTD* time series from DBC and CBC configurations is shown in Figure 4.6. This figure depicts that CBC configuration generally simulates shallower *WTD* compared to DBC, which is consistent with Figure 4.3. Figure 4.5 and 4.6 shows that although there are differences between WTD_{DBC} and WTD_{CBC} throughout the simulation period, significant differences between LE_{DBC} and LE_{CBC} are observed only in summer months. Therefore, it appears that the influence of groundwater dynamics based LBCs on *LE* is observed mainly under soil moisture limited conditions, which supports the DBF concept. Under energy limited conditions, LE_{DBC} - LE_{CBC} is insignificant due to the abundance of soil moisture that can be observed from the increased S_r during the colder months in Figure 4.4.

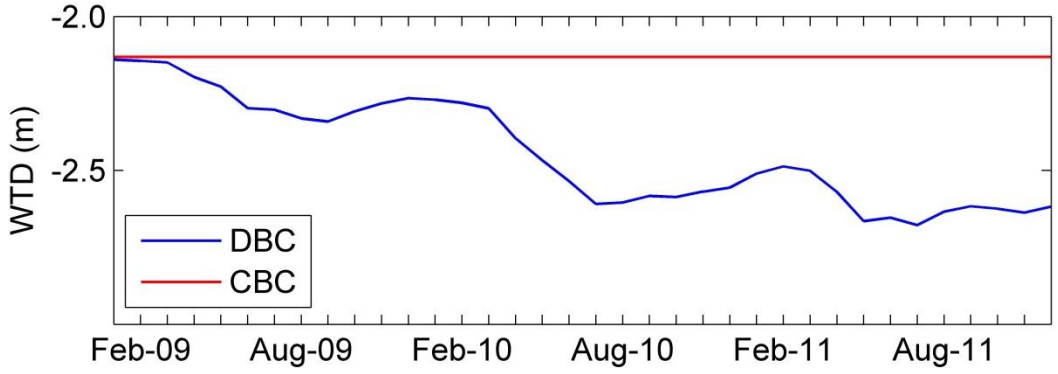

Figure 4.6. Catchment average monthly mean groundwater table depth (*WTD*) from DBC and CBC configurations.

In Figure 4.5, LE_{DBC} - LE_{FD} is higher compared to LE_{DBC} - LE_{CBC}, which can be explained by the dry condition simulated by the FD configuration (Figure 4.4). Although LE_{DBC} - LE_{FD} is higher in summer, significant differences are also observed during the colder months. In Figure 4.4 note that S_r from FD is much lower compared to both DBC and CBC even in the colder periods, which may explain the differences between LE_{DBC} and LE_{FD} under energy limited conditions. The results suggest that the FD configuration, which does not maintain a

physically consistent representation of *WTD* in the model, simulates significantly lower *LE* compared to DBC and CBC even during colder months of the year.

4.3.3 LBC influence on temporal dynamics of land surface processes

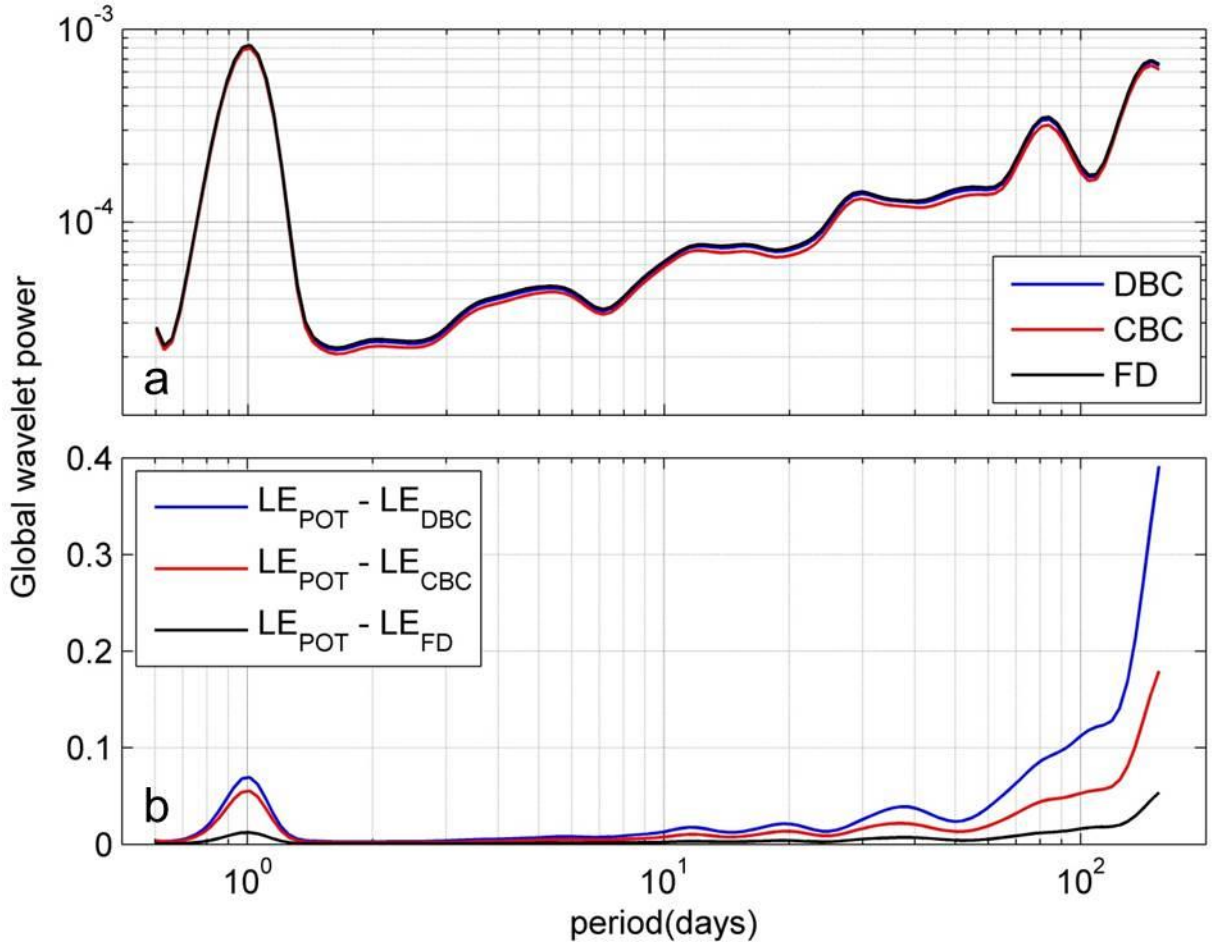

Figure 4.7. Global wavelet power of catchment average (a) net radiation (R_{net}) and (b) difference between potential and actual latent heat flux (LE_{POT} - LE) from the three model configurations.

Continuous wavelet transform analysis (Appendix B) was performed to analyze the temporal variability of land surface processes simulated by the three model configurations and to study the impact of simplified groundwater table parameterizations on variances in land surface energy fluxes. The DBF concept states that land surface processes are affected by atmospheric forcing and groundwater dynamics at different time scales. Figure 4.7a plots global wavelet power spectra of catchment averaged net radiation (R_{net}) from DBC, CBC, and FD, revealing the scale dependent variability of atmospheric radiative forcing. In this figure, a distinct peak at 1 day period is observed in all three spectra, which is due to the diurnal cycle of solar radiation. Additionally, the three spectra exhibit almost identical power at all periods, which indicates that R_{net} is not influenced by the LBCs considered in these model configurations.

This is important to show in order to exclude any potential impact of changes of R_{net} variability due to differences in soil moisture from the three configurations on the variability of land surface energy fluxes.

Figure 4.7b compares global wavelet power spectra of the difference between potential latent heat flux (LE_{POT}, *Rahman et al.*, 2014) and *LE* (LE_{POT} - *LE*) from DBC, CBC, and FD model configurations (LE_{POT} - LE_{DBC}, LE_{POT} - LE_{CBC}, and LE_{POT} - LE_{FD}, respectively). Similar to R_{net}, LE_{POT} - *LE* spectra from all three configurations show a peak at 1 day period, which demonstrate the effect of atmospheric radiative forcing (i.e., R_{net}) on *LE* variability at the daily time scale. These results substantiate the statement of the DBF concept that at the daily time scale, land surface processes are dominated by atmospheric forcing. Figure 4.7b also reveals that there are differences in variability of LE_{POT} - LE_{DBC}, LE_{POT} - LE_{CBC}, and LE_{POT} - LE_{FD} at 1 day period in spite of identical R_{net} variability (Figure 4.7a).

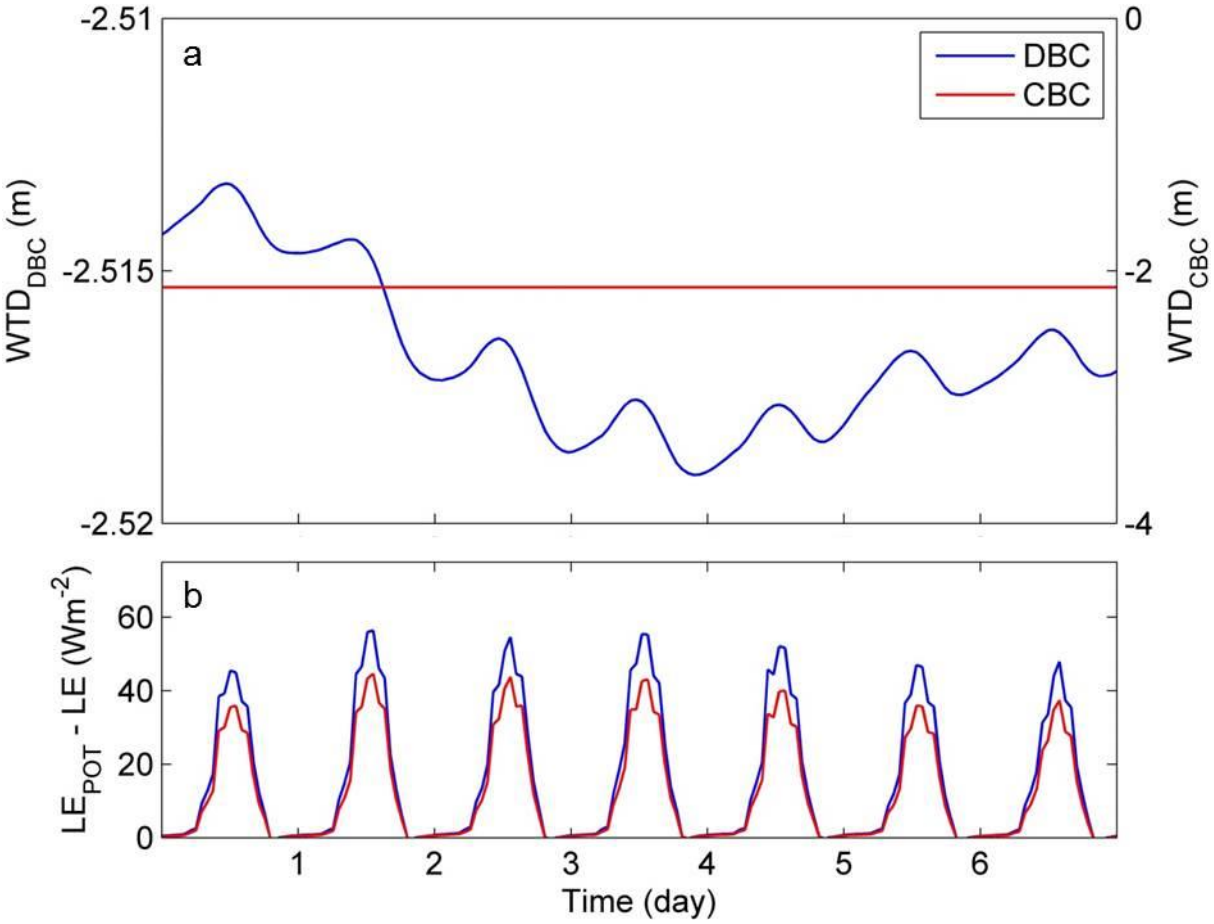

Figure 4.8. Average weekly composites of (a) hourly groundwater table depth (*WTD*) and (b) differences between potential and actual latent heat flux (LE_{POT} - *LE*) from DBC and CBC in summer of the three simulated years.

Figure 4.8a shows average weekly composites of hourly *WTD* from DBC and CBC configurations in summer (June-September) over the three simulated years. This figure clearly depicts WTD_{DBC} fluctuation at 1 day time scale under soil moisture limited condition, which is due to groundwater contribution to daily evapotranspiration similar to periodic pumping [e.g., *Fahle and Dietrich*, 2014; *Mazur et al.*, 2014]. Of course, daily variability of groundwater table is not observed in CBC (but shown for completeness), because this configuration maintains a constant *WTD* throughout the simulation period. Figure 4.8b plots average weekly composites of hourly LE_{POT} - *LE* form DBC and CBC configurations in summer (June-September) over the three simulated years. The daily variability of LE_{POT} - *LE* observed in this figure is due to atmospheric radiative forcing, which has been discussed earlier (Figure 4.7a). The differences in LE_{POT} - *LE* from DBC and CBC observed in Figure 4.8b is due to the difference in groundwater contribution to daily evapotranspiration (Figure 4.8a), which may explain the small difference in LE_{POT} - *LE* variability at the daily time scale from DBC and CBC configurations in Figure 4.7b. Figure 4.7b also illustrates differences between LE_{POT} - LE_{DBC} and LE_{POT} - LE_{CBC} wavelet power at about 30-50 day, which increases at longer periods. On the other hand, LE_{POT} - LE_{FD} shows lower power compared to LE_{POT} - LE_{DBC} and LE_{POT} - LE_{CBC} at all periods in this figure. As mentioned earlier, the FD configuration does not maintain a physically consistent groundwater table, because of the gravitational drainage at the bottom of the model domain, which may be the reason of low LE_{POT} - LE_{FD} wavelet power in Figure 4.7b.

According to the DBF concept, atmospheric forcing generally dominates the variability of land surface processes at the daily time scale. The peaks of wavelet power spectra in Figure 4.7a and b show the influence of atmospheric forcing (i.e., R_{net}) on *LE* variability at 1 day period, which supports the proposed concept. In Figure 4.7a, the FD configuration shows significantly lower power compared to DBC and CBC at 1 day period. Groundwater does not contribute to daily *LE* in FD, because this configuration does not maintain a physically consistent *WTD* in the model, which may explain low LE_{POT} - LE_{FD} variability at the daily time scale. The DBF concept also states that groundwater dynamics affect the variability of land surface processes at longer (e.g., monthly to multi-month) time scales [*Rahman et al.*, 2014]. Figure 4.7a and b show that there are significant differences in wavelet power of LE_{POT} - LE_{DBC}, LE_{POT} - LE_{CBC}, and LE_{POT} - LE_{FD} especially at periods larger than 30 days, which is considered to be the time scale at which groundwater dynamics start to impact land surface energy flux variability. In the simulations, these differences can be directly attributed to groundwater dynamics, because LBC is the only modification between the model

configurations and Figure 4.7a shows identical R_{net} variability precluding changes in e.g., albedo as a factor. These results therefore corroborate that groundwater indeed influences *LE* variability at monthly to multi-month time scales, which again substantiates the proposed DBF concept. In addition, the hypothesis is confirmed that simplified groundwater table parameterizations may significantly modify/reduce land surface energy flux variability at monthly time scales.

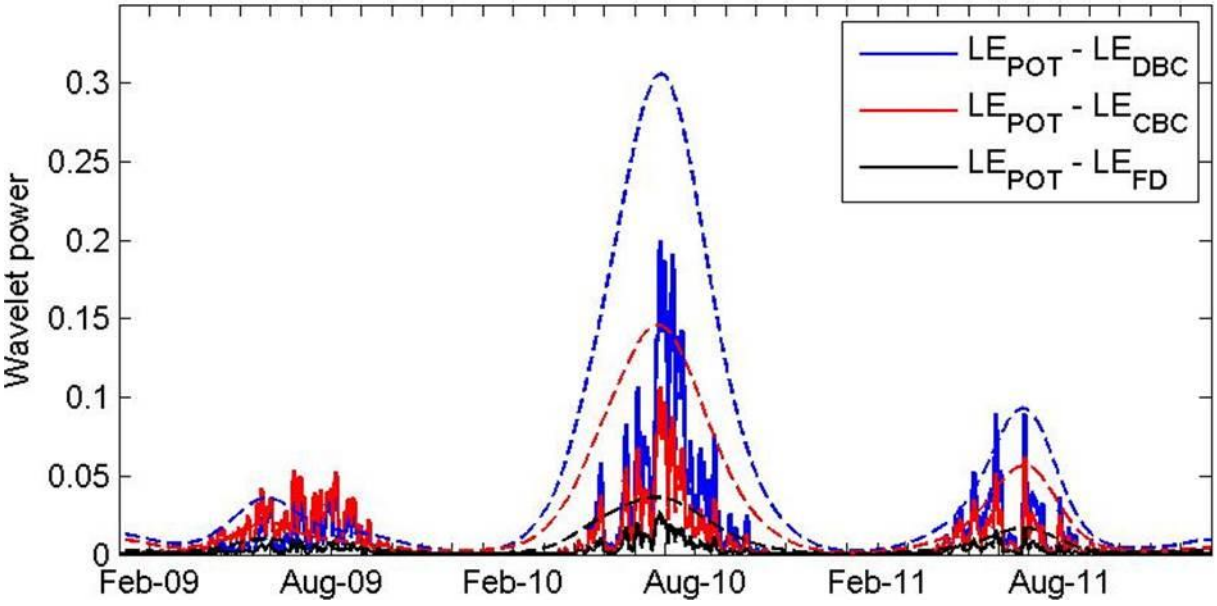

Figure 4.9. Time localized wavelet power of potential and actual latent heat flux (LE_{POT} - *LE*) from the three configurations averaged over two periods (soil line: ~1-3 day; dashed line: ~32-91 day).

In order to further substantiate the latter, time localized powers of LE_{POT} - *LE* from the three configurations averaged over two periods (~1-3 day and ~32-91 day) are shown in figure 4.9. At the ~1-3 day time scale, LE_{POT} - LE_{DBC} and LE_{POT} - LE_{CBC} generally show similar power, although differences are observed especially in summer 2010, where LE_{POT} - LE_{DBC} show somewhat higher power. At ~32-91 day period, significant differences between wavelet powers of LE_{POT} - LE_{DBC} and LE_{POT} - LE_{CBC} are observed in summer, which is consistent over the three simulated years. The highest difference in wavelet power at ~32-91 day period is found again in summer 2010. The high differences between wavelet powers in 2010 may be attributed to the prevailing dry condition during this year. The LE_{POT} - LE_{FD} time series, on the other hand, shows lower power compared to LE_{POT} - LE_{DBC} and LE_{POT} - LE_{CBC} at both periods (~1-3 day and ~32-91 day) due to the absence of a physically consistent *WTD* in FD configuration due to the free drainage boundary condition. Figure 4.9 confirms that the

groundwater dynamics and its simplification significantly affect *ET* variability at monthly to multi-month time scales in summer, which supports the proposed DBF concept.

The DBF concept states that groundwater dynamics affect time scale dependent variability of S_r and *ET*, which was tested considering different LBCs in the coupled subsurface-land surface model ParFlow.CLM in this section. Several previous studies have discussed land surface-atmosphere interactions and demonstrated that variability of land surface soil moisture and energy fluxes affects atmospheric processes, e.g., convective precipitation [e.g., *Schär et al.*, 1999; *Hohenegger et al.*, 2009; *Froidevaux et al.*, 2014]. *Bierkens and van den Hurk* [2007] demonstrated the role of groundwater convergence on the persistence in rainfall via shallow soil moisture and *ET*. Therefore, the influence of groundwater dynamics on the time scale dependent variability of land surface processes discussed in presented study may be important to consider in atmospheric simulations, which will be addressed in the next chapter.

Temporal dynamics of the fluxes and states of hydrological cycle are important for various water management practices. For instance, several previous studies have discussed the importance of near surface soil moisture variability on drought prediction [e.g., *Oglesby and Erickson*, 1989; *Sheffield and Wood*, 2008]. *Wu and Kinter* [2009] discussed the role of local soil moisture on drought variability at different time scales. *Schubert et al.* [2007] argued that drought prediction requires knowledge of the mechanisms that control land surface processes at various time scales. The results presented here demonstrated that the variability of land surface processes at relatively long time scales (e.g., monthly to multi-month) is affected by the representation of groundwater dynamics in a model, which may be important to consider in water resources assessments, and e.g., drought prediction and mitigation.

It is important to note that differences in wavelet powers from the three model configurations may be even more pronounced at longer time scales (e.g., seasonal and annual), because of the low frequency variability of *WTD* [e.g., *Li and Zhang*, 2007; *Little and Bloomfield*, 2010]. However, variability of the fluxes and states at these time scales is not analyzed here, because of data limitation as the simulations were performed over 3 consecutive years (2009-2011) in this study. In future, mass and energy fluxes for simulations over decadal time scales may provide insight into additional time scales of coherence between groundwater dynamics and land surface processes.

4.4 Summary and conclusions

In this study, the *dual-boundary forcing* (DBF) concept [*Rahman et al.*, 2014] was evaluated considering different lower boundary conditions (LBCs) based on groundwater dynamics in a coupled subsurface-land surface model. The underlying hypothesis was that a simple groundwater dynamics parameterization via constant head or free drainage boundary condition may lead to an alteration of variance in land surface fluxes in a numerical simulation platform. In order to substantiate this hypothesis, the coupled model ParFlow.CLM was applied on a study area encompassing the Rur catchment, Germany. Three different model configurations that are dynamic boundary condition (DBC), constant boundary condition (CBC), and free drainage boundary condition (FD) were considered to assess the influence of groundwater dynamics on simulated land surface processes. DBC allows groundwater table (*WTD*) to evolve freely through time. In contrast, CBC maintains a constant *WTD* at each model grid throughout the simulation period. In case of FD, a gravity drainage boundary is implemented at the bottom of the model domain. The three configurations were identical in terms of input, initial, and boundary conditions except for the LBCs. With the aforementioned model configurations, simulations were performed for three consecutive years (2009-2011) using atmospheric forcing variables obtained from the German Weather Service to force the model. In ensuing steps, simulation results were analyzed and the differences in land surface processes from the three model configurations were discussed in order to evaluate the DBF concept and test the hypothesis.

The results showed clear differences in spatial and temporal patterns of relative saturation (S_r) and latent heat flux (*LE*) from the three model configurations, which is intuitive because of the previously established connection of groundwater dynamics and land surface energy fluxes [e.g., *Chen et al.*, 2004; *Yeh and Eltahir*, 2005; *Soylu et al.*, 2011]. While DBC and CBC showed pronounced influence of *WTD* on S_r, surface saturation from FD configuration was found to be strongly dependent on soil texture. Significant differences in S_r and *LE* time series from the three configurations were noticed especially in summer, which demonstrates the connection between shallow soil moisture and evapotranspiration (*ET*) in the warmer months of the year.

In order to analyze the variability of land surface mass and energy balance components, the continuous wavelet transform technique was applied on the simulated time series of net radiation (R_{net}) and difference between potential latent heat flux and *LE* (LE_{POT} - *LE*) from

DBC, CBC, and FD model configurations. This analysis showed almost identical global wavelet power of net radiation (R_{net}) from DBC, CBC, and FD configurations at all periods. At 1 day period, LE_{POT} - LE and R_{net} from all three configurations showed a distinct peak in global wavelet power spectra, indicating the connection between atmospheric radiative forcing and *ET* at the daily time scale. On the other hand, significant differences in time localized wavelet power of LE_{POT} - LE from DBC and CBC are observed at longer periods (~32-91 day) in the summer months, which was consistent over the three simulated years. These results support the statement of the DBF concept that groundwater dynamics influences the variability of the land surface processes under soil moisture limited conditions at monthly to multi-month time scales. The FD configuration, in contrast, showed significantly lower wavelet power compared to DBC and CBC at both daily and monthly periods. As aforementioned, this configuration does not maintain a physically consistent groundwater table in the simulation, because moisture is able to leave the model domain through the bottom boundary via gravity drainage. Therefore, it appears from the results that *ET* variability is affected even at smaller time scales (~1-3 days) in case of a free drainage LBC in the model.

This study demonstrated the importance of representing groundwater dynamics in a coupled land surface-subsurface model. The results indicate that variability of land surface processes is affected without a physically consistent representation of groundwater dynamics in simulations starting at monthly to multi-month time scales. This effect of groundwater dynamics on time scale-dependent variability of land surface processes may thus have a significant effect on the predictability of hydrologic droughts, which is important in water resources assessments and management.

Chapter 5

The subsurface-land surface-atmosphere connection under convective conditions*

5.1 Introduction

In the terrestrial hydrological cycle, subsurface, land surface, and atmospheric processes are related via complex feedback mechanisms, which have been subject of research for some time [e.g., *Manabe*, 1969; *Chang and Wetzel*, 1991; *Betts at al.*, 1996; *Santanello et al.*, 2009; *Ferguson and Wood*, 2011]. Several previous studies have shown that the land-atmosphere interaction is significantly influenced by the heterogeneity of land surface processes [e.g., *Zeng et al.*, 2003; *Patton et al.*, 2005; *Adler et al.*, 2011]. An important aspect of heterogeneity in land surface processes is the variability of shallow soil moisture [e.g., *Orth and Seneviratne*, 2013]. The impact of land surface soil moisture variability on the atmosphere has been shown previously using observations [e.g., *Findell and Eltahir*, 1997; *Koster et al.*, 2003; *Taylor and Ellis*, 2006] and model results [e.g., *Schär et al.*, 1999; *Seuffert et al.*, 2002; *Koster et al.*, 2004; *Kim and Wang*, 2007; *Su et al.*, 2014]. Variability in land surface soil moisture influences surface energy partitioning, which eventually affects atmospheric processes, such as, convective precipitation [e.g., *Clark and Arritt*, 1995; *Taylor et al.*, 2012; *Khodayar et al.*, 2013; *Collow et al.*, 2014]. *Hohenegger et al.* [2009] studied soil moisture-precipitation feedback mechanisms over Alpine regions and showed that the variability in shallow soil moisture creates significant differences in simulated convective precipitation. *Hauck et al.* [2011] showed the influence of land surface soil moisture on convective processes over complex terrains and discussed the importance of realistic soil moisture initialization for weather prediction models. *Juang et al.* [2007] studied the triggering mechanisms of summertime convective precipitation and suggested that a negative

*Rahman, M., M. Sulis, and S. J. Kollet (2015), The subsurface-land surface-atmosphere connection under convective conditions, Adv. Water Resour. (under review).

feedback between land surface soil moisture state and convection exists, i.e., convective precipitation may be triggered over dry regions. *Froidevaux et al.* [2014] also demonstrated a negative soil moisture-convection feedback in idealized simulations and discussed the influence of background wind on this mechanism. These studies suggest that there exists a strong link between land surface hydrology and atmospheric processes especially under convective conditions.

In order to illustrate land-atmosphere connection, the aforementioned studies generated heterogeneity in land surface soil moisture via arbitrary or statistical perturbation. However, soil moisture heterogeneity as a result of physical processes (e.g., groundwater dynamics) may also affect atmospheric processes, which is not yet well-understood. In the coupled water and energy cycles of the terrestrial system, the groundwater table acts as the lower boundary condition (LBC) that influences land surface mass and energy balance components [e.g., *Fan et al.*, 2007; *Kollet and Maxwell*, 2008; *Tian et al.*, 2012; *Rahman et al.*, 2014]. Demonstrating the interactions between this LBC and the land surface mass and energy fluxes has been the focus of several previous studies [e.g., *Sklash and Farvolden*, 1979; *Liang et al.*, 2003; *Maxwell et al.*, 2005]. The effect of groundwater table depth (*WTD*) on surface runoff [e.g., *Yeh and Eltahir*, 2005; *Miguez-Macho and Fan*, 2012a] and evapotranspiration [*Lam et al.*, 2011; *Soylu et al.*, 2011] is well-established. *Chen and Hu* [2004] showed that the influence of subsurface hydrodynamics on root zone soil moisture depends on *WTD*. *Miguez-Macho and Fan* [2012b] demonstrated the effect of groundwater dynamics on seasonal soil moisture over the Amazon region. The subsurface-land surface connection with respect to the scaling properties of groundwater dynamics has also been discussed previously in several studies [e.g., *Amenu and Kumar*, 2005; *Little and Bloomfield*, 2010; *Schilling and Zhang*, 2012]. From these studies this is evident that *WTD* influences land surface mass and energy balance components including soil moisture.

While the aforementioned studies show the interconnections between various compartmental processes of the hydrological cycle, the influence of LBC dynamics (i.e. water table dynamics) on atmospheric simulations via land surface mass and energy fluxes remains largely unresolved. As aforementioned, studies discussing the influence of land surface soil moisture on atmospheric processes generally perturb the soil moisture state arbitrarily in the simulations and demonstrate the influence on simulated mass and energy balance components [e.g., *Hohenegger et al.*, 2009; *Hauck et al.*, 2011]. However, as discussed earlier, the LBC dynamics affect land surface soil moisture, which may eventually affect the atmospheric

processes. Few studies have discussed the relationship between groundwater dynamics and atmosphere via land surface processes previously. *Quinn et al.* [1995] coupled the hydrologic TOPMODEL with a single-column boundary layer model (SLAB) and discussed groundwater- atmospheric boundary layer connection via land surface energy fluxes. *Maxwell et al.* [2007] showed the correlation between *WTD* and several atmospheric variables, e.g., atmospheric potential temperature and boundary layer height. *Anyah et al.* [2008] demonstrated that especially over convection-dominated regimes, groundwater influences precipitation by modifying evapotranspiration. *Campoy et al.* [2013] studied the effect of hydrological bottom boundary condition of land surface models on shallow soil moisture and argued that this subsurface-land surface connection may affect atmospheric processes, e.g., precipitation. Despite the aforementioned studies suggest that the LBC dynamics influence atmospheric processes, the impact of groundwater dynamics on atmosphere in a fully coupled model that simulates subsurface, land surface, and atmospheric processes consistently is not yet well-discussed.

This chapter examines the sensitivity of simulated atmospheric processes to *WTD* induced modifications in land surface mass and energy balance components under convective conditions. It is hypothesized that groundwater dynamics influence convective initiation through the coupling with atmosphere via soil moisture and land surface energy fluxes, and, thus, may introduce systematic uncertainties, if groundwater dynamics are neglected. The coupled simulation platform TerrSysMP [*Shrestha, et al.*, 2014] is applied to a regional scale catchment (on the order of 10^4 km^2) in Western Germany and the mass and energy balance components of the hydrological cycle are simulated from groundwater across the land surface into the atmosphere.

In order to identify the influence of LBC on the mass and energy balance components, simulations are performed considering two different *WTD* configurations, namely, dynamic and constant lower boundary conditions (DBC and CBC, respectively). The dynamic lower boundary condition (DBC) configuration allows the temporal evolution of groundwater, while constant lower boundary condition (CBC) configuration maintains a temporally constant *WTD* throughout the simulation period. Ensemble simulations are performed by perturbing the initial conditions to deal with the internal variability in atmospheric simulations. As a first step, the differences in atmospheric processes (e.g., precipitation, atmospheric boundary layer height, and convective available potential energy) between DBC and CBC model configurations are shown. Finally, the interactions between the compartmental processes in

the simulation results are interpreted as a possible reason of the sensitivity of atmospheric processes to LBC.

5.2 Methods

5.2.1 Study area

The model domain (Figure 5.1) is located in the Western Germany with an area of 2.25×10^4 km^2 encompassing the Rur catchment [*Bogena et al.*, 2006; *Vereecken et al.*, 2010; *Simmer et al.*, 2015]. The southern part of the model domain is characterized by the mountainous Eifel region, which is forested with mainly coniferous trees. This mountainous region receives an annual precipitation of about 1000-1200mm. In contrast, the northern part of the study area is characterized by flat lowland regions with an annual precipitation amount of about 550-600mm/a. In this part of the area, agriculture is the major land use type with cereals (e.g., winter wheat) and sugar beet as the dominant crops. Difference in the mean annual temperature between the northern (8.5-10.5°C) and the southern (7.0-9.0°C) part of the study area exists because of a distinct 600m elevation difference.

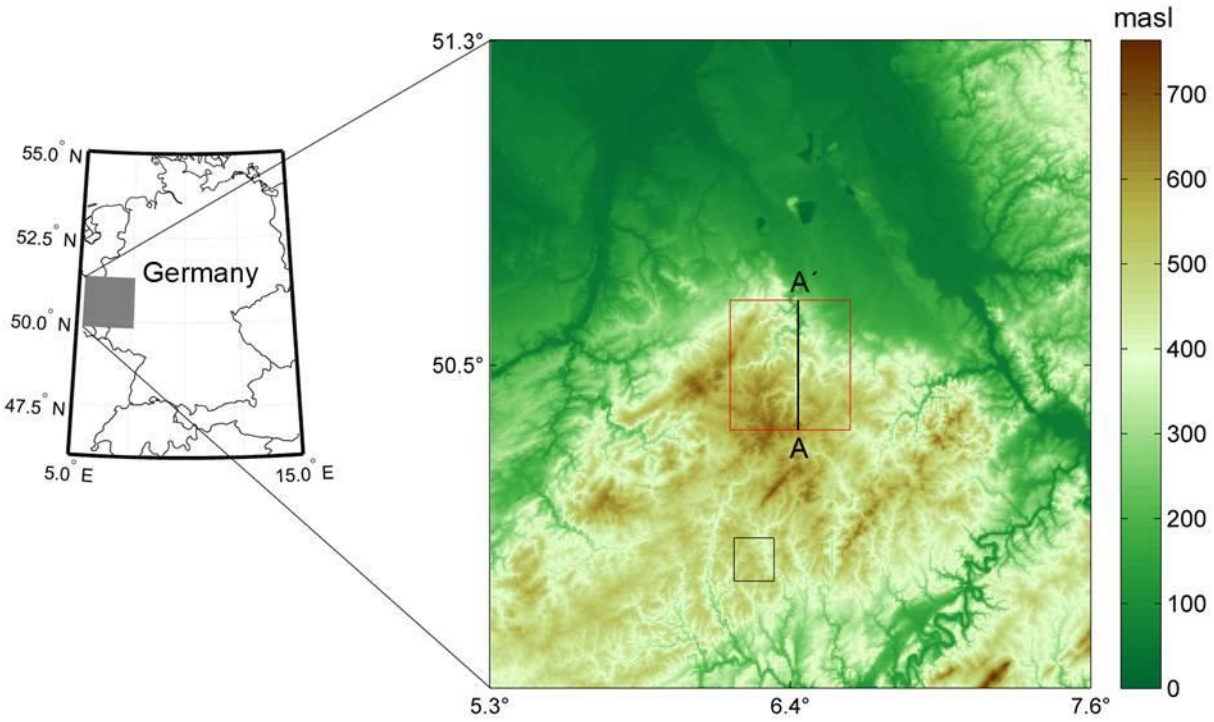

Figure 5.1. Location (left) and topography (right) of the study area. The red box (30km x 30km) shows the area used for spatial averaging in Figure 5.3a, 5.4a, and 5.5. The black box (10km x 10km) bounds the area used for spatial averaging in Figure 5.3b and 5.4b. AA´ shows the cross-section used in Figure 5.6.

5.2.2 The coupled simulation platform: TerrSysMP

The highly modular scale-consistent Terrestrial System Modeling Platform (TerrSysMP) has been introduced in *Shrestha et al.* [2014]. This simulation platform consists of an atmospheric model (COSMO-DE), a land surface model (CLM3.5), and a three-dimensional variably saturated groundwater flow model (ParFlow). An external coupler (OASIS3-MCT [e.g., *Valcke*, 2013; *Gasper et al.*, 2014]) is used to couple the three models employing a multiple-executable-multiple-data approach. In TerrSysMP, the model components are able to exchange fluxes at different spatial and temporal resolutions using time integration/averaging and spatial interpolation operators based on the downscaling algorithms developed by *Schomburg et al.* [2010, 2012].

Soil Texture	Saturated hydraulic conductivity, k_{sat} (ms^{-1})	Van Genuchten parameter, α [m^{-1}]	Van Genuchten parameter, n [-]	Porosity, ϕ [-]
Clay	$1.7x10^{-6}$	2.1	2.0	0.4701
Clay loam	$9.4x10^{-7}$	2.1	2.0	0.4449
Sand	$1.4x10^{-6}$	2.0	2.0	0.4386
Sandy loam	$4.4x10^{-6}$	2.7	2.0	0.4071

Table 5.1. Soil hydraulic parameters of top 10 model layers

The atmospheric model COSMO is used as the numerical weather prediction system by the German Weather Service (DWD). In this study, the convection permitting configuration of COSMO (referred to as COSMO-DE) is used [e.g., *Baldauf et al.*, 2011]. This model uses the split-explicit time-stepping method [e.g., *Wicker and Skamarock*, 2002] in order to solve the nonhydrostatic compressible atmospheric equations. The parameterization in COSMO-DE includes a surface transfer scheme to calculate heat and momentum transfer coefficients [e.g., *Raschendorfer*, 2001], a radiation scheme after *Ritter and Geleyn* [1992], a single-momentum cloud microphysics scheme [e.g., *Lin et al.*, 1983; *Reinhardt and Seifert*, 2006], a level-2.5 turbulence parameterization after *Mellor and Yamada* [1982], and a shallow convection scheme after *Tiedtke* [1982].

The parameterization of the land surface model (CLM3.5) is described in detail in *Oleson et al.* [2008]. The energy balance equation in this model can be written as:

$$R_{net} = LE + H + G \tag{5.1}$$

where R_{net} is net radiation (Wm^{-2}), LE is latent heat flux (Wm^{-2}), H is sensible heat flux (Wm^{-2}), and G is ground heat flux (Wm^{-2}). In order to close the energy balance, G is applied as the top boundary condition to solve this equation at the land surface and obtained as the residual

of equation (1). The vertical mass, energy, and momentum fluxes are described by the Monin-Obukhov similarity principle in CLM3.5. The surface heat transfer is simulated by solving the heat diffusion equation.

In TerrSysMP, the atmospheric model (COSMO-DE) and the land surface model (CLM3.5) exchange atmospheric forcing terms and land surface fluxes in a sequential manner via the external coupler OASIS3-MCT. The atmospheric variables (i.e., air temperature, pressure, wind speed, specific humidity, incoming short and long wave radiation, precipitation, and measurement height) at the lowest COSMO-DE layer is used to drive CLM3.5 at the current time step and the land surface mass and energy balance components are calculated. The land surface energy and momentum fluxes along with albedo and outgoing long wave radiation are then sent back to COSMO-DE in an operator splitting approach. The dimensionless surface transfer coefficients of COSMO-DE are subsequently updated based on these fluxes. The vertical gradients at the lowest level are calculated based on the surface temperature from the previous time step.

The integrated, parallel, variably saturated groundwater flow model ParFlow [*Ashby and Falgout*, 1996; *Jones and Woodward*, 2001; *Kollet and Maxwell*, 2006] solves the Richards' equation [*Richards*, 1931] in three spatial dimensions:

$$S_s\theta\frac{\partial\psi}{\partial t}+\phi\frac{\partial\theta(\psi)}{\partial t}=\nabla\cdot\mathbf{q}+S \tag{5.2}$$

$$\mathbf{q}=-k(x)k_r(\psi)\nabla(\psi-z) \tag{5.3}$$

where S_s is specific storage (m^{-1}), θ is soil moisture (-), ψ is pressure head (m), t is time (s), ϕ is porosity (-), $\mathbf{q}$ is water flux (ms^{-1}), S is general source/sink term (s^{-1}), $k(x)$ is saturated hydraulic conductivity (ms^{-1}), $k(r)$ is relative permeability (-), and z is depth below surface (m). A finite volume scheme with two point flux approximation in space and an implicit backward Euler scheme in time are used to solve this equation. A free surface overland flow boundary condition is applied at the land surface to integrate the surface flow [*Kollet and Maxwell*, 2006]. At the boundary, the kinematic wave equation is solved maintaining the continuity of pressure and flux. A terrain following grid with a variable vertical discretization can be used in ParFlow [*Maxwell*, 2013].

In the coupled modeling framework of TerrSysMP, ParFlow is coupled to CLM3.5 via the external OASIS3-MCT coupler. Through this coupling, ParFlow replaces the simplified

hydrological scheme in CLM3.5 and simulates subsurface hydrodynamics and surface runoff. The two coupled model components exchange fluxes and shallow soil moisture distributions following a sequential information exchange procedure.

5.2.3 Model configurations and input data

The atmospheric model (COSMO-DE) is configured with 1 km horizontal grid resolution and 50 vertical levels with variable discretization using an Arakawa C-grid. Laterally, both the land surface model (CLM3.5) and hydrological model (ParFlow) have a uniform grid resolution of $\Delta x = \Delta y = 500$ m. ParFlow considers a total subsurface depth of 30 m, which is discretized using a terrain following grid implementation [*Maxwell*, 2013] and variable vertical discretization ranging from $2x10^{-2}$ at the land surface to $1.35x10^{0}$ m at the bottom of the domain. The temporal resolution of COSMO-DE, CLM3.5, and ParFlow are 9 seconds, 90 seconds, and 90 seconds, respectively. Both subsurface-land surface and land surface-atmosphere coupling frequencies are set to 90 seconds in the simulations. The atmospheric variables from COSMO-DE are interpolated to the grid resolution of CLM3.5 by OASIS3-MCT.

The MODIS land cover type for plant functional type (PFT) classification (Type 5) is used to represent the spatially distributed vegetation cover information in the model. Monthly leaf area index values for each PFT were obtained from a phenology study using MODIS (MCD15A2 product) 8 day composite from Aqua and Terra satellite from 2002-2011 [*Shrestha et al.*, 2014]. Digital Soil Map of the World (DSMW) provided by the Food and Agricultural Organization of UNO (FAO) is used to represent the texture of different soil types for top 10 soil layers in the model (Table 5.1). The soil hydraulic parameters for the deeper subsurface are adapted from *Gleeson et al.* [2011].

Period	**Model initialization time (YYYY:MM:DD:HH)**				
	Ensemble 1	Ensemble 2	Ensemble 3	Ensemble 4	Ensemble 5
4-7 June 2011	2011:06:03:22	2011:06:03:23	2011:06:04:00	2011:06:04:01	2011:06:04:02
21-22 July 2012	2012:07:21:00	2012:07:21:01	2012:07:21:02	2012:07:21:03	2012:07:21:04

Table 5.2. Initialization of the ensemble members for the two events

The initial and boundary conditions for COSMO-DE are obtained from the re-analysis dataset of the German Weather Service (DWD), with COSMO-DE updating the boundary condition every 1 hour. An off-line model spinup was performed to obtain realistic initial conditions for ParFlow and CLM3.5. For this purpose, the coupled ParFlow-CLM3.5 model was forced by

hourly atmospheric forcing obtained from COSMO-DE re-analysis dataset and repeated simulations were performed over 2011 and 2012 to reach a dynamic equilibrium.

5.2.4 Experimental Setup

Simulations are performed using TerrSysMP for two different precipitation events. The first event extends from 4 - 7 June 2011, and the second event extends from 21 - 22 July, 2012. Two separate model configurations, dynamic and constant boundary condition with respect to the free water table, are considered to generate heterogeneity in land surface soil moisture by modifying groundwater dynamics in the simulations. The dynamic boundary condition (DBC) configuration allows *WTD* to evolve through time, while the constant boundary condition (CBC) maintains the initial *WTD* at every horizontal model grid throughout the simulation period. Note, except for the treatment of the *WTD* boundary condition, these two model configurations are identical in terms of model inputs, initial and boundary conditions. Thus, differences in the results between the two configurations may be directly attributed to the impact of the lower boundary condition i.e. the free water table. Ensemble simulations are performed by perturbing the initial conditions in order to account for the inherent model variability and intrinsic chaos of the atmosphere. For this purpose, the time of model initialization is varied following the established approach by the German Weather Service [*Bouallègue et al.*, 2013]. Table 5.2 describes the ensemble members for the two events.

5.3 Results and discussion

In this section, the simulation and analyses results from the two model configurations are provided and discussed. In the first step, the differences in atmospheric processes between DBC and CBC ensembles are provided, which are analyzed in ensuing steps. The objective of this analysis is to demonstrate the sensitivity of convective initiation and precipitation rate on *WTD* induced changes in land surface processes.

5.3.1 Differences in atmospheric processes

Figure 5.2 shows the difference between ensemble mean cumulative precipitation from DBC and CBC configurations over 5 June 2011 (E1) and 21 July 2012 (E2). For E1, the highest difference between DBC and CBC precipitation is observed at the center of the model domain, where DBC configuration predominantly shows more precipitation (5-10 mm) compared to CBC. In the northern flat and southern mountainous part of the domain, no significant precipitation difference between the two configurations is observed. E2, on the

other hand, shows precipitation differences in the southern mountainous part of the domain. However, these differences between DBC and CBC precipitation for E2 (~1 mm) are small compared to E1. It should be mentioned that, E1 presents a much stronger convective precipitation case compared to E2. This may be the reason of the low precipitation difference from the two configurations in case of E2.

Figure 5.3 compares spatially averaged time series of precipitation from the two model configurations for E1 and E2. The areas considered for spatial averaging for the two events are shown in Figure 1. For E1, in the morning hours (until 1200 LST) the two model configurations yield identical precipitation. However, difference between DBC and CBC precipitation time series is observed in the afternoon (1600-1900 LST). During this period, the DBC configuration shows significantly higher (e.g., ~2 mmh^{-1} at 1800 LST) precipitation compared to CBC. E2 shows similar results in terms of precipitation difference, with identical spatially averaged precipitation during morning hours. In the afternoon (1200-1400 LST), CBC configuration yields lower precipitation than DBC (~0.5 mmh^{-1} at 1300 LST), which is not significant.

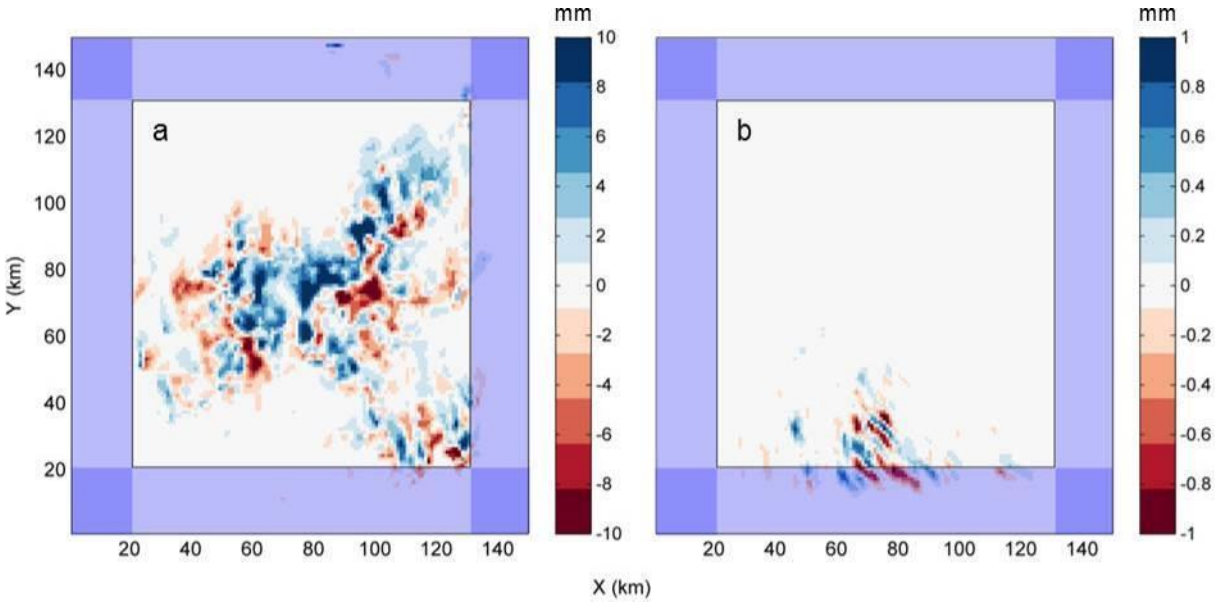

Figure 5.2. Ensemble mean difference between precipitation (mm) from the two model configurations (DBC - CBC) for E1 (a) and E2 (b). The shaded areas exclude a buffer zone of 20 km where the influence of atmospheric boundary condition may be very high.

Figure 5.2 and 5.3 show spatial and temporal precipitation differences from the two model configurations, respectively. Figure 5.3 shows that the significant precipitation differences from the two model configurations are observed in the afternoon hours for both events. Previous studies showed that soil moisture influence on convective precipitation via land

surface processes is observed predominantly during afternoon hours [e.g., *Hohenegger et al.*, 2009; *Froidevaux et al.*, 2014]. *Taylor et al.* [2012] argued that afternoon moist convection may be intensified due to enhanced sensible heat flux over drier soils. As aforementioned, the only difference between DBC and CBC model configurations in this study is the treatment of the LBC. Therefore, the differences between the afternoon precipitation amounts from DBC and CBC configurations may be attributed to the LBC induced differences in land surface processes also considering the ensemble approach.

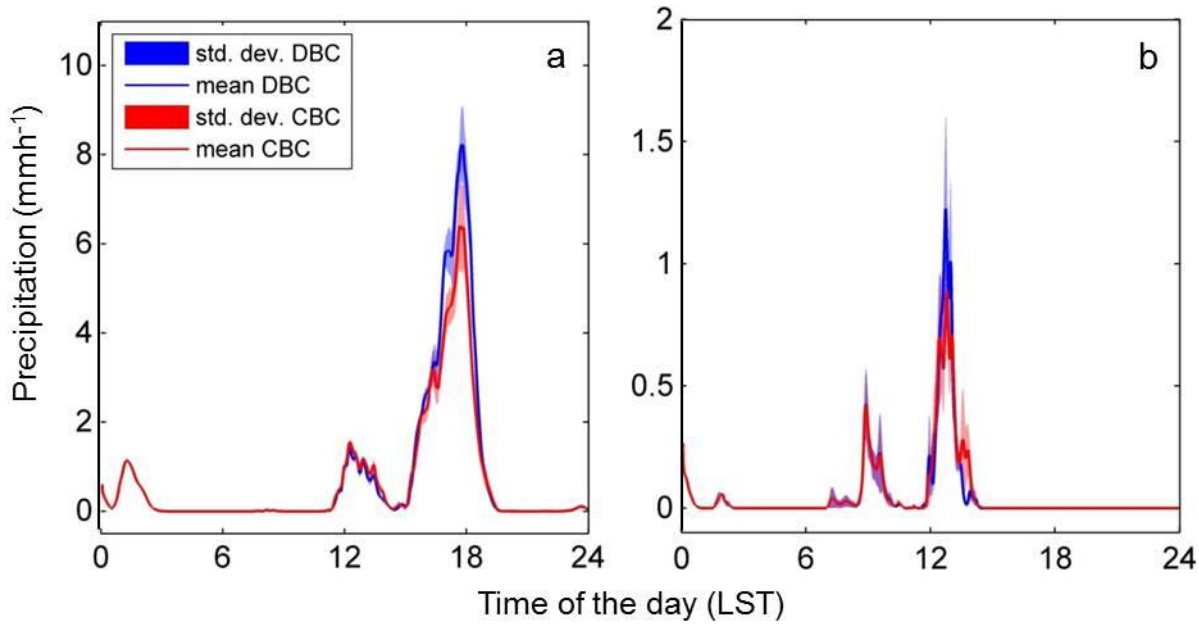

Figure 5.3. Spatially averaged precipitation time series for E1 (a) and E2 (b).

Figure 5.4 shows cloud liquid water content evolution for the two configurations over the two events. In case of E1 (Figure 5.4a), identical clouds are observed around 1200 LST. However, clear differences in clouds from the two configurations are observed around 1700 LST with DBC showing deeper and denser clouds compared to CBC. This higher cloud cover supports the fact that DBC configuration yields more precipitation compared to CBC around 1700 LST (Figure 5.3). Figure 5.4b shows liquid cloud water content evolution for E2. Compared to E1, E2 does not show significant differences in clouds. However, the small difference in cloud depth observed at around 1300 LST is consistent with the time of precipitation difference between DBC and CBC for E2 (Figure 5.3b).

Figure 5.5 shows the difference in atmospheric boundary layer height (ABLH) and convective available potential energy (CAPE) between the two model configurations for E1. A brief description of ABLH and CAPE along with mathematical formulations is provided in

appendices. It is remarkable that no difference in ABLH between the two configurations is observed in the morning hours (until 1200 LST), when the ABLH is increasing. After 1200 LST, differences in ABLH from DBC and CBC configurations are observed. Prior to the precipitation event, the DBC configuration shows significantly higher ABLH (~50 m) compared to CBC. Similar results are obtained for the differences in CAPE. Until 1200 LST, DBC and CBC configurations show identical CAPE. However, in the afternoon, DBC configuration shows higher CAPE (~30 Jkg^{-1}) prior to the precipitation event.

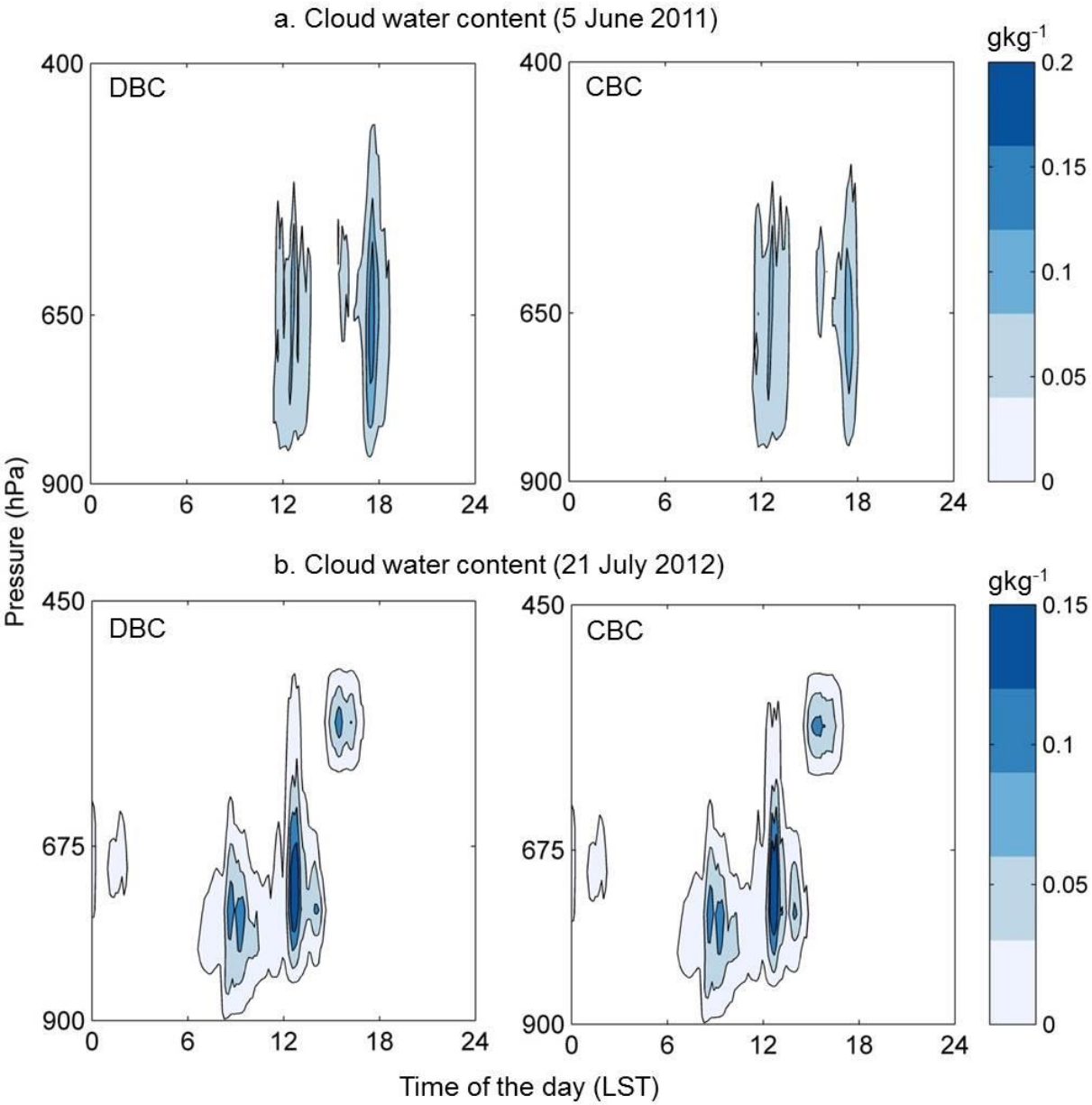

Figure 5.4. Liquid cloud water content from the two model configurations for E1 (a) and E2 (b).

The role of the ABLH on atmospheric simulations was discussed by *Shin and Ha* [2007], who demonstrated the sensitivity of precipitation to spatial and temporal variation of ABLH.

Again, CAPE is important in describing the atmospheric conditions of local convection [*Eltahir*, 1998]. In general, higher CAPE values indicate the potential for stronger convection [e.g., *Barthlott and Kalthoff*, 2011]. *Schär et al.*, [1999] argued that higher CAPE values ensure enhanced convective instability. The relationship between CAPE and precipitation was discussed by *Khodayar et al*. [2013], who showed that there exists a positive correlation between CAPE and ensuing rainfall. Therefore, the differences in ABLH and CAPE in Figure 5.5 may explain the higher precipitation from DBC configuration compared to CBC in E1. Note that for E2, such consistent differences between ABLH and CAPE were not observed clearly (not shown), which may be because of the weaker convection compared to E1.

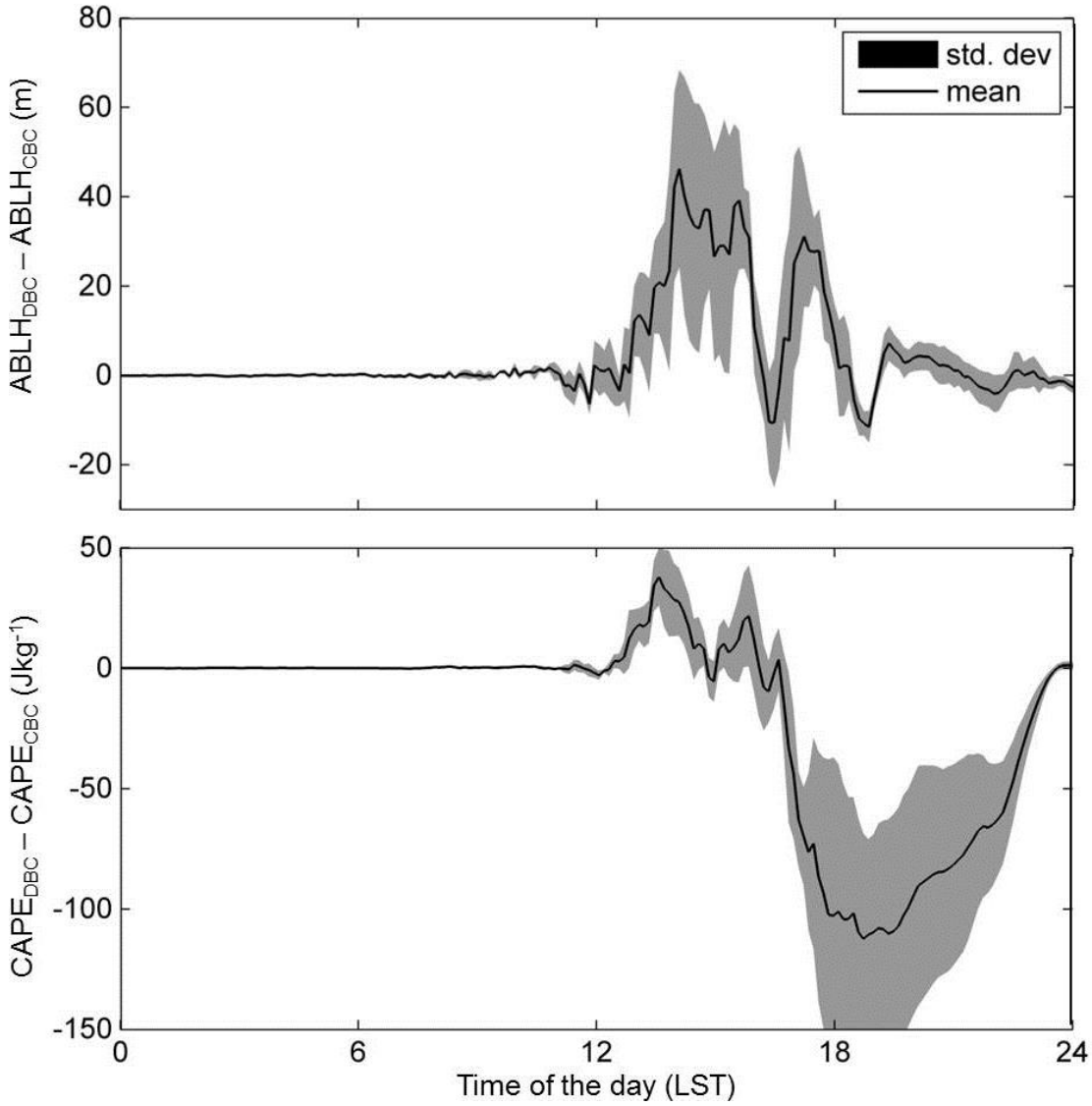

Figure 5.5. Spatially averaged time series of Atmospheric boundary layer height (ABLH, top) and Convective Available Potential Energy (CAPE, bottom) for E1. The shaded area and solid line show ensemble standard deviation and mean, respectively.

Differences in various atmospheric processes from DBC and CBC configurations for two convective precipitation events (E1 and E2) are presented and analyzed in this section. Because LBC is the only physical difference between these two configurations in the ensemble simulations, it appears that the representation of groundwater dynamics generates *systematic* uncertainties in atmospheric simulations in TerrSysMP, especially under strong convective conditions. Note that demonstrating a direct link between groundwater dynamics and convective precipitation would require longer simulation periods and application of sophisticated statistical analysis methods. This is out of the scope of this study because the simulation periods considered here are relatively short.

5.3.2 Interactions in simulated compartmental processes

In the previous section, the differences in atmospheric processes from DBC and CBC model configurations were discussed. The results showed that consistent differences exist in various atmospheric processes for E1. In this section, the interconnections between the compartmental processes for this event are examined.

Figure 5.6 shows the cross-sections (along AA´ line in Figure 5.1) of ensemble mean θ, *LE*, *H*, and vertical wind velocity (*w*) difference between DBC and CBC model configurations at 1430 LST for E1. Figure 5.6a shows the difference in θ along the cross-section. This figure illustrates that along Y = 20-30 km, DBC configuration shows lower near surface soil moisture compared to CBC. Figure 5.6b shows the difference between *LE* from DBC and CBC model configurations (LE_{DBC} and LE_{CBC}, respectively) along AA´. In this figure, the highest difference in *LE* is observed along Y = 20-30 km, where DBC shows lower *LE* compared to CBC. Consequently, the difference between *H* from DBC and CBC model configurations (H_{DBC} and H_{CBC}, respectively) in Figure 5.6c shows that along Y = 20-30 km, DBC results in higher sensible heat flux compared to CBC. Figure 5.6d shows the difference in *w* from DBC and CBC configurations at different altitudes. Note that Y = 25-30 km is characterized by higher *w* from DBC configuration, which is consistent with the lower θ, lower *LE*, and higher *H* at Y = 20-30 km.

In Figure 5.6a, the DBC model configuration shows drier condition compared to CBC along Y = 20-30 km due to θ difference between the two model configurations. Figure 5.6b and c clearly shows that this discrepancy in θ affects land surface energy fluxes. Because θ is lower, the DBC model configuration shows lower *LE* and higher *H* over this patch. Figure 5.6d reveals the interesting fact that this modification in land surface energy fluxes influences the

atmosphere. This figure shows higher *w* for DBC configuration over the drier part of the cross-section, which is consistent with lower *LE* and higher *H*.

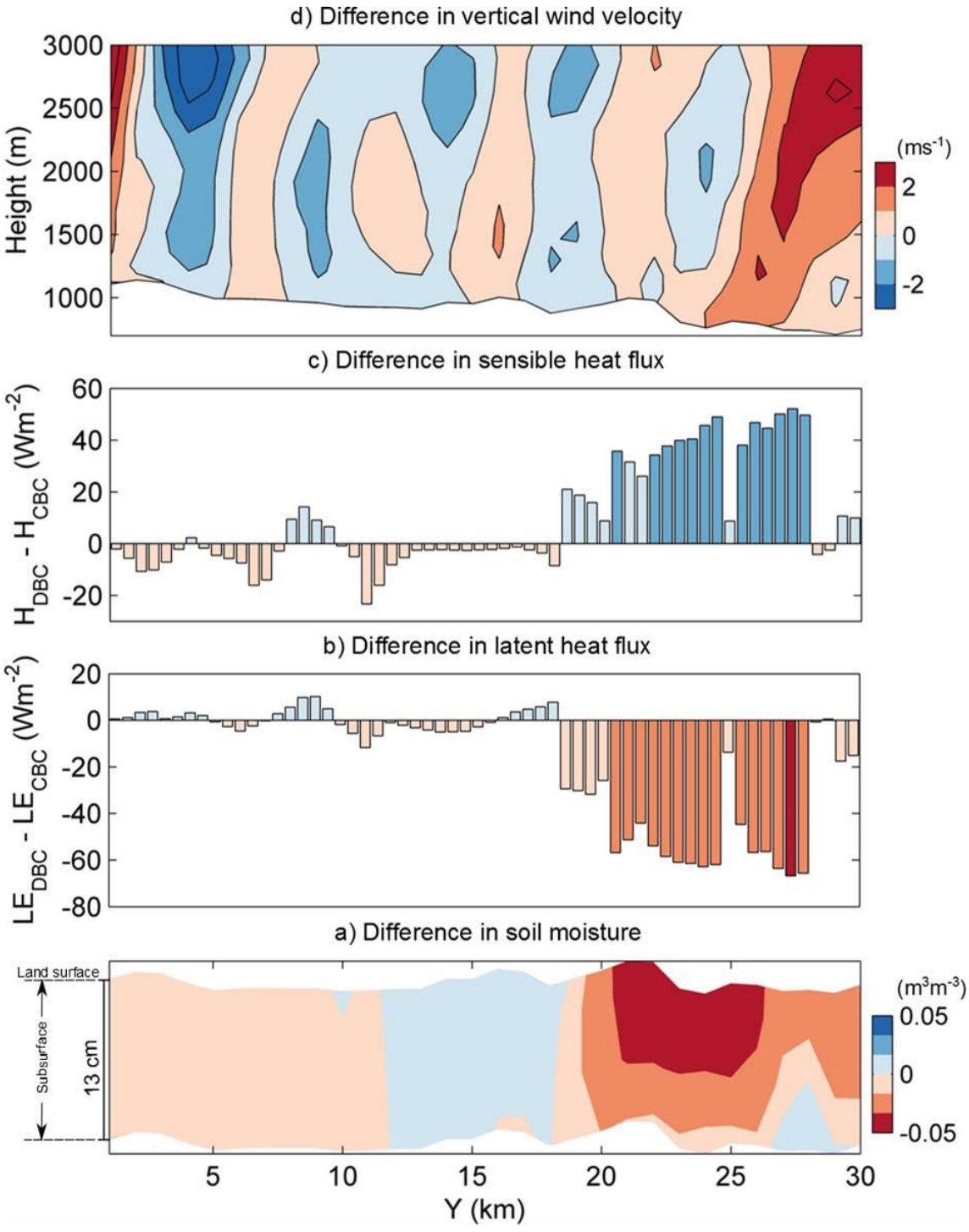

Figure 5.6. Differences in soil moisture, θ (from land surface to 13 cm below land surface) (a), latent heat flux, *LE* (b), sensible heat flux, *H* (c), and vertical wind velocity, *w* (d) from the two model configurations along AA´ cross-section (Figure 5.1) at 1430 LST. Note that topography is detrended in Figure 5. 6a.

Similar results were found by *Patton et al.* [2005], who showed that vertical wind velocity becomes higher over dry soil patches because of the more vigorous thermals. *Hohenegger et*

al. [2009] demonstrated that lower *LE* (and subsequently higher *H*) over dry soil generates stronger thermals, which eventually facilitate the formation of deep convection in the afternoon hours. The study by *Cook et al.* [2006] suggested that dry areas with lower *LE* enhance atmospheric instability and, thus, precipitation formation. The θ differences observed in Figure 5.6a can, according to *Emori* [1998], aid the initiation of afternoon convection. The *LE* and *H* difference observed in Figure 5.6 due to the θ contrast may affect the thermally induced local circulation. *Emori* [1998] argued that the upward motion of such local circulation initiates afternoon convection.Figure 5.6 demonstrates a potential mechanism of subsurface-land surface-atmosphere interaction prior to a convective precipitation event. This figure indicates that the discrepancy in *LE* and *H* from the two model configurations due to θ difference affects *w*. As aforementioned, the only difference between DBC and CBC model configurations is the treatment of the LBC. The discrepancy in θ from the two configurations can thus be attributed to the difference in representing groundwater dynamics in the ensemble framework, which is conceptualized as the LBC in this study. Figure 5.6 therefore shows that differences in groundwater dynamics influences land surface soil moisture and energy balance components, which eventually affect atmospheric processes (Figures 5.2 to 5.5). The differences in atmospheric processes including CAPE, ALBH, and precipitation observed in the previous section may be attributed to such local interactions between *WTD* and atmosphere via land surface processes.

5.4 Summary and Conclusions

In this study, groundwater dynamics was explicitly simulated as the lower boundary condition (LBC) of the terrestrial hydrological cycle and the sensitivity of land surface and atmospheric processes to this LBC was examined. A fully coupled simulation platform (TerrSysMP) was applied on a 150km x 150km area located in Western Germany to simulate the mass and energy fluxes from subsurface across land surface into the atmosphere. In order to assess the effect of groundwater dynamics on atmospheric simulations, two model configurations, namely, dynamic boundary condition (DBC) and constant boundary condition (CBC) were considered. While DBC allowed the groundwater to evolve through time, CBC maintained a constant groundwater table depth (*WTD*) over the simulation period at each horizontal model grid. All other model inputs, initial and boundary conditions were identical for the two configurations. With the aforementioned model configurations, simulations were performed for two convective precipitation events (E1 and E2). In order to acknowledge the intrinsic atmospheric variability, ensemble simulations were performed by varying the model initial

conditions following the prescribed ensemble generation method by the German Weather Service.

The two model configurations showed differences in spatial pattern and temporal dynamics of afternoon convective precipitation for both E1 and E2. These differences were pronounced for E1 because it represents a much stronger convective precipitation case compared to E2. Discrepancies in liquid cloud water content were also observed for the two events that were consistent with the precipitation differences. However, E2 showed minor differences in liquid cloud water content compared to E1, which was again consistent with the relative strength of the two convective precipitation events.

The differences in atmospheric boundary layer height (ABLH) and convective available potential energy (CAPE) from DBC and CBC configurations were also studied for E1. The results showed that in the morning hours, the two model configurations reproduce identical ABLH. However, prior to the precipitation event, DBC configuration simulated higher ABLH compared to CBC. The evolution of CAPE from the two configurations showed similar trends. Although DBC and CBC simulated identical CAPE in the morning hours, DBC showed higher CAPE prior to the precipitation event, which is consistent with the precipitation differences between the two configurations. It is important to emphasize that the two model configurations are consistent in terms of model inputs, initial and boundary conditions except for the LBC. Therefore, the results indicate that the representation of groundwater dynamics in a fully-coupled model systematically influences simulated atmospheric processes in general and convective initiation.

In order to illustrate the subsurface-land surface-atmosphere interaction in the simulations, cross-sections of soil moisture (θ), latent heat flux (LE), sensible heat flux (H), and vertical wind velocity (w) were examined. The cross-sections showed differences in LE and H due to the discrepancies in θ from the two configurations. Furthermore, it was demonstrated that the differences in land surface energy fluxes create discrepancies in w from DBC and CBC model configurations, which can be conceptualized as a potential mechanism of the interactions between the compartmental processes.

The results suggest that the representation of groundwater dynamics in a fully-coupled model may generate *systematic* uncertainties in atmospheric simulations. A mechanism of subsurface-land surface-atmosphere interaction was also discussed, which can be interpreted as the potential reason of sensitivity of atmospheric processes to groundwater dynamics.

Following the proposed approach, it is possible to reveal a direct connection between subsurface hydrodynamics and convective precipitation via land surface soil moisture, which may be important to incorporate in atmospheric simulations.

Chapter 6

Summary, conclusions, and recommendations

6.1 Summary and conclusions

In this thesis, processes in subsurface, land surface, and atmosphere compartments of the terrestrial hydrological cycle, such as, groundwater flow, evapotranspiration, precipitation, were studied to explain and quantify the interconnections between compartmental mass and energy fluxes at various space-time scales. In the first step, the coupled subsurface-land surface model ParFlow.CLM forced by hourly atmospheric variables obtained from the German Weather Service (DWD) was applied over a study area encompassing the Rur catchment, Germany, and the fluxes and states of subsurface and land surface compartments of the hydrological cycle were simulated. Note that ParFlow.CLM ensures closure of the mass and energy balances, resulting in an internally consistent description of the relevant processes, system dynamics and feedbacks. Ensuing the model runs, a comprehensive comparison between model results and *in-situ* measurements was performed. This comparison showed that ParFlow.CLM was able to reproduce magnitude and dynamics of various mass and energy balance components (e.g., shallow soil moisture, groundwater table depth, latent heat flux, sensible heat flux, near-surface temperature) reasonably well without model calibration, which lends confidence in the model. The comparison showed some discrepancies between observations and model results, which may be attributed to the uncertainties arising from model structure, parameters, grid resolution, and spatial interpolation of atmospheric forcing. The comparisons were made between point measurements and cell-centered model grid values based on a one-km resolution, which constitutes a major simplifying assumption that the cell-centered values are representative of the entire grid cells. The results indicate that physics based models may be used for water resources management, e.g., predicting fluxes in ungauged basins.

In the second step, the aforementioned simulation results and observations were used to substantiate a new concept, namely, the *dual-boundary forcing* (DBF) concept. The DBF concept connects the variability of land surface mass and energy fluxes to subsurface and atmospheric processes at different space-time scales. This concept describes atmosphere and groundwater as the upper and lower boundary conditions, respectively, for land surface processes. According to this concept, the dominant boundary condition for the exchange processes is determined by space-time localized availability of energy and moisture. The land surface reacts and interacts at the interface between these two boundaries to adapt or transform the variability of the associated processes. Using geostatistical and spectral analysis techniques it was demonstrated that atmospheric radiative forcing generally drives the variability of the land surface processes at the daily time scale. In contrast, groundwater dynamics drives the variability of land surface mass and energy fluxes starting at monthly to multi-month time scales under soil moisture limited conditions. Variogram analysis demonstrated that under energy limited conditions, spatial variability of latent heat flux can be predicted from atmospheric radiative forcing alone (e.g., remote sensing measurements of net radiation). Under soil moisture limited conditions, on the other hand, the influence of groundwater table depth was clearly observed on the spatial variability of latent heat flux.

The DBF concept establishes the groundwater table as the lower boundary condition (LBC) of the coupled water energy cycles, which was evaluated in the third step. The hypothesis was that a simplified parameterization of groundwater dynamics may modify the variance in land surface processes, which may reduce the model's prognostic capabilities. In order to substantiate this hypothesis, simulations were performed using ParFlow.CLM considering three different LBCs, namely, dynamic, constant, and free-drainage lower boundary conditions. While the dynamic lower boundary condition (DBC) allowed the temporal evolution of the LBC, constant lower boundary condition (CBC) maintained a temporally constant *WTD* throughout the simulation period. In contrast, the free drainage (FD) configuration mimicked the classical description of soil water flow in land surface models and allowed moisture to leave through the bottom of the model domain via gravity drainage. The model results showed reduced temporal variance of latent heat flux simulated by CBC and FD configurations compared to DBC especially at ~32-91 day period in summer. This finding indicates that variability of land surface processes is indeed modified without a physically consistent representation of groundwater dynamics in simulations starting at monthly to multi-month time scales, which substantiates the aforementioned DBF concept.

Finally, a coupled Terrestrial System Modeling Platform (TerrSysMP) was applied on the extended Rur catchment and the mass and energy fluxes were simulated considering DBC and CBC model configurations over two convective precipitation events to study the influence of groundwater dynamics on atmospheric processes. Using ensemble simulations it was demonstrated that the representation of groundwater dynamics in a fully coupled model introduces systematic uncertainties to simulated atmospheric boundary layer height (ABLH), convective available potential energy (CAPE), and convective precipitation rate. A mechanism of subsurface-land surface-atmosphere interaction in the simulation results was illustrated, which showed that local vertical wind velocity may be affected by the representation of groundwater dynamics in the model via the coupling with land surface soil moisture and energy fluxes. This mechanism was interpreted as the potential reason of sensitivity of atmospheric variables to groundwater dynamics.

This thesis showed the influence of groundwater dynamics on land surface processes (e.g., soil moisture, evapotranspiration) at different space and time scales in the framework of the DBF concept. While the results demonstrated that groundwater starts affecting evapotranspiration at monthly to multi-month time scales, as aforementioned, there may be significant coherence between groundwater dynamics and land surface processes at longer (e.g., seasonal, yearly) time scales. The results indicate that the wavelet transform analysis can be used as a tool for inverse prediction, which may be important in water resources assessments, e.g., hydrological drought prediction and mitigation.

The interactions between subsurface, land surface, and subsurface compartments of the hydrological cycle were also discussed in this thesis. The results depicted that groundwater dynamics may introduce systematic uncertainties to the atmospheric variables in a numerical simulation platform. Therefore, a realistic representation of groundwater dynamics may be important to consider in local weather prediction models.

Studying the interactions between the compartmental mass and energy fluxes is important to understand the overall mechanisms of the hydrological cycle. As aforementioned, quantifying the interconnections between the compartmental processes of the coupled water and energy cycles can facilitate various water resources assessments. With the objective of revealing the coherence between the compartmental processes, this thesis formulated a concept (i.e., the DBF concept) that is a novel way to explain and quantify the groundwater-land surface-atmosphere connection at various space-time scales and corroborated this concept using model results and observations. The approach described here can be used to interrogate

various mechanisms in the hydrological cycle governed by the interconnections between compartmental processes. For example, the direct influence of subsurface-land surface interactions on atmospheric processes (e.g., precipitation) can be examined by applying the DBF concept on the compartmental mass and energy fluxes over decadal period.

6.2 Recommendations for future work

- The influence of groundwater dynamics on the temporal variability of land surface mass and energy fluxes was discussed from daily to multi-month time scales in the context of the DBF concept. However, there may be significant interactions between groundwater dynamics and land surface processes at longer time scales (e.g., seasonal and yearly). These time scales were not considered here due to data limitation, because the simulations were performed and compared with observations over three consecutive years (2009-2011). These interactions should be interrogated in future utilizing the proposed techniques considering extended time series of fluxes and states.
- Continuous wavelet transform technique, which may be used for inverse forecasting, was used in this thesis to analyze the inherent variability of the processes in hydrological cycle. The results may be re-corroborated using other analysis methods (e.g., principal component analysis and Fourier transform technique), which should be subject of future research.
- The simulation results may be influenced by the uncertainties due to model structure, grid resolution, and parameterization. A comprehensive sensitivity and uncertainty analysis should be subject of future work to assess the influence of the aforementioned issues on the proposed DBF concept, which will require novel approaches and large computer resources.
- Using a fully-coupled simulation platform, this thesis demonstrated that groundwater may introduce systematic uncertainties in atmospheric simulations. Future works should focus on demonstrating a direct link between groundwater dynamics and atmospheric processes considering longer simulation periods and advanced statistical analysis techniques.

Bibliography

Abramopoulos, F., C. Rosenzweig, and B. Choudhury (1988), Improved ground hydrology calculation for Global Climate Models (GCMs): Soil water movement and evapotranspiration, J. Climate, 1, 921-941.

Adler, B., N. kalthoff, and L. Gantner (2011), The impact of soil moisture inhomogeneities on the modification of a mesoscale convective system: An idealized model study, Atmos. Res., 101, 354-372.

Amenu, G. G., and P. Kumar (2005), Interannual variability of deep-layer hydrologic memory and mechanisms of its influence on surface energy fluxes, J. Climate, 18, 5024-5040.

Andreo, B., P. Jimenez, J. J. Duran, F. Carrasco, I. Vadillo, and A. Mangin (2006), Climatic and hydrological variations during the last 117–166 years in the south of the Iberian Peninsula, from spectral and correlation analyses and continuous wavelet analyses, J. Hydrol., 324, 24-39.

Anyah, R. O., C. P. Weaver, G. Miguez-Macho, Y. Fan, and A. Robock (2008), Incorporating water table dynamics in climate modeling; 3. Simulated groundwater influence on coupled land-atmosphere variability, J. Geophys. Res., 113, D07103, doi:10.1029/2007JD009087.

Ashby, S. F., and R. D. Falgout (1996), A parallel multigrid preconditioned conjugate gradient algorithm for groundwater flow simulations, Nucl. Sci. Eng., 124(1), 145– 159.

Baker, I., A. S. Denning, N. Hanan, L. Prihodko, M. Uliasz, P.-L. Vidale, K. Davis, and P. Bakwin (2003), Simulated and observed fluxes of sensible and latent heat and CO2 at the WLEF-TV tower using SiB2.5, Glob. Change Biol., 9, 1262–1277.

Baldauf, M., A. Seifert, J. Förstner, D. Majewski, M. Raschendorfer, and T. Reinhardt (2011) Operational convective-scale numerical weather prediction with the COSMO model: Description and sensitivities, Mon. Wea. Rev., 139, 3887–3905, doi:10.1175/MWR-D-10-05013.1.

Balnchard, D. O. (1998), Assessing the vertical distribution of convective available potential energy, Wea. Forecasting, 13, 870-877.

Barthlott, C., and N. Kalthoff (2011), A numerical sensitivity study on the impact of soil moisture on convective-related parameters and convective precipitation over complex terrain, J. Atmos. Sci., 68, 2971-2987.

Beecham, S., and R. K. Chowdhury (2010), Temporal characteristics and variability of point rainfall: a statistical and wavelet analysis, Int. J. Climatol., 30, 458–473.

Betts, A. K., J. H. Ball, A. C. M. Beljaars, M. J. Miller, and P. A. Viterbo (1996), The land-atmosphere interaction: A review based on observational and global modeling perspectives, J. Geophys. Res., 101(D3), 7209-7225.

Beven, K., and A. Binley (1992), The future of distributed models: Model calibration and uncertainty prediction, Hydrol. Process., 6, 279-298.

Bierkens, M. F. P., and B. J. J. M. van den Hurk (2007), Groundwater convergence as a possible mechanism for multi-year persistence in rainfall, Geophys. Res. Lett., 34.

Blöschl,G, and M. Sivapalan (1995), Scale issues in hydrological modelling: A review, Hydrol. Process, 9, 251-290.

Bogena, H. R., K. Schulz, and H. Vereecken (2006), Towards a network of observatories in terrestrial environmental research, Adv. Geosci., 9, 109-114.

Bogena, H. R., M. Herbst, J. A. Huisman, U. Rosenbaum, A. Weuthen, and H. Vereecken (2010), Potential of wireless sensor networks for measuring soil water content variability, Vadise Zone J., 9, 1002-1013.

Bogena, H., M. Herbst, J.-F. Hake, R. Kunkel, C. Montzka, Th. Puetz, H. Vereecken, and F. Wendland (2005), "MOSYRUR - Water balance analysis in the Rur basin," Forschungszentrum Juelich, ISBN 3-89336-385-8.

Bonan, G. G., and L. M. Stillwell-Soller (1998), Soil water and the persistence of floods and droughts in the Mississippi River Basin, Water Resour. Res., 34(10), 2693-2701.

Bonetti, S., G. manoli, J.-C. Domec, M. Putti, M. Marani, and G. G. Katul (2015), The influence of water table depth and the free atmospheric state on convective rainfall predisposition, Water Resour. Res., accepted.

Bouallègue, Z. B., S. E. Theis, and C. Gebhardt (2013), Enhancing COSMO-DE ensemble forecasts by inexpensive techniques, Meteorol. Z., 22, 49-59.

Brubaker, K. L., and D. Entekhabi (1996), Analysis of feedback mechanisms in land-atmosphere interaction, Water Resour. Res., 32, 1343-1357.

Campoy, A., A. Ducharne, F. Cheruy, F. Hourdin, J. Polcher, and J. C. Dupont (2013), Response of land surface fluxes and precipitation to different soil bottom hydrological conditions in a general circulation model, J. Geophys. Res. Atmos., 118, 10,725–10,739, doi:10.1002/jgrd.50627.

Chang, J.-T., and P. J. Wetzel (1991), Effects of spatial variations of soil moisture and vegetation on the evolution of a prestorm environment: A numerical case study, Mon. Wea. Rev., 119, 1368-1390.

Chen, X., and Q. Hu (2004), Groundwater influences on soil moisture and surface evapotration, J. Hydrol., 297, 285-300.

Clark, C. A., and R. W. Arritt (1995), Numerical simulations of the effect of soil moisture and vegetation cover on the development of deep convection, J. Appl. Meteorol., 34, 2029-2045.

Collow, T. W., A. Robock, and W. Wu (2014), Influence of soil moisture and vegetation on convective precipitation forecasts over the United States Great Plains, J. Geophys. Res., 119, doi:10.1002/2014JD021454.

Cook, B. I., G. B. Bonan, and S. Levis (2006), Soil moisture feedbacks to precipitation in Southern Africa, J. Clim., 19, 4198-4206.

Dai, X. P., X. Zeng, and C. D. Dickinson (2001), The Common Land Model (CLM): Technical documentation and user's guide.

Dai, Y. J., et al. (2003), The Common Land Model, Bull. Am. Meteorol. Soc., 84(8), 1013–1023.

Decharme, B., A. Alkama, H. Houdville, M. Becker, and A. Cazenave (2010), Global evaluation of the ISBA-TRIP continental hydrological system. Part II: Uncertainties in river routing simulation related to flow velocity and groundwater storage, J. Hydrometeorol., 11, 601-617.

Delworth, T., and S. Manabe (1988), Climate variability and land-surface processes, Adv. Water Resour., 1, 523-547.

Ding, R., S. Kang, R. Vargas, Y. Zhang, X. Hao (2013), Multiscale spectral analysis of temporal variability in evapotranspiration over irrigated croplands in arid region, Agric. Water Manage., 130, 79-89.

Dolfing, J., and S. D. Scheltens (1999), Facilitated transport in European soils from the Euro-soil project, Env. Toxicol. Chem., 18(7), 1417-1420.

Doswell, C. A., and E. N. Rasmussen (1994), The effect of neglecting the virtual temperature on CAPE calculation, Wea. Forecasting, 9, 625-629.

Eltahir, E. A. B. (1998), A soil moisture-rainfall feedback mechanism 1. Theory and observations, Water Resour. Res., 34, 765-776.

Emori, S. (1998), The interaction of cumulus convection with soil moisture distribution: An idealized simulation, J. Geophys. Res., 103, 8873-8884.

Fahle, M., and O. Dietrich (2014), Estimation of evapotranspiration using diurnal groundwater level fluctuation: Comparison of different approaches with groundwater lysimeter data, Water Resour. Res., 50, 273-286, doi:10.1002/2013WR014472.

Fan, Y., and G. Miguez-Macho (2010), Potential groundwater contribution to Amazon evapotranspiration, Hydrol. Earth Syst. Sci., 14, 2039–2056, doi:10.5194/hess-14-2039-2010.

Fan, Y., G. Miguez-Macho, C. P. Weaver, R. Walko, and A. Robock (2007), Incorporating water table dynamics in climate modeling: 1. Water table observations and equilibrium water table simulations, J. Geophys. Res., 112, doi:10.1029/2006JD008111.

Ferguson, C. R., and E. F. Wood (2011), Observed land-atmospheric coupling from satellite remote sensing and reanalysis, J. Hydrometeorol., 12, 1221-1254, doi: 10.1175/2011JHM1380.1.

Fernández-Prieto, D., J. Kesselmeier, M. Marconcini, A. Reissell, and T. Suni (2013), Earth observation for land-atmosphere interaction science, Biogeosciences, 10, 261–266.

Findell, K. L., and E. A. B. Eltahir (1997), An analysis of the soil moisture-rainfall feedback, based on direct observations from Illinois, Water Resour. Res., 33(4), 725-735.

Froidevaux, P., L. Schmidli, W. Langhans, and C. Schär (2014), Influence of background wind on the local soil moisture-precipitation feedback, J. Atmos. Sci., 71, 782-799.

Gasper, F., Goergen, K., Kollet, S., Shrestha, P., Sulis, M., Rihani, J., and Geimer, M.: Implementation and scaling of the fully coupled Terrestrial Systems Modeling Platform (TerrSysMP) in a massively parallel supercomputing environment – a case study on JUQUEEN (IBM Blue Gene/Q) (2014), Geosci. Model Dev. Discuss., 7, 3545-3573, doi:10.5194/gmdd-7-3545-2014.

Gedney, N., and P. M. Cox (2003), The sensitivity of global climate model simulations to the representation of soil moisture heterogeneity, J. Hydrometeorol., 4, 1265-1275.

Gleeson, T., L. Smith, N. Moosdorf, J. Hartmann, H. H. Duerr, A. H. Manning, L. P. H. van Beek, and A. M. Jellinek (2011), Mapping permeability over the surface of the Earth, Geophys. Res. Let., 38, L02401, doi:10.1029/2010GL045565.

Gneiting, T., H. Ševčiková, and D. B. Percival, Estimators of fractal dimension: Assessing the roughness of time series and spatial data, Statis. Sci., 27(2), 247-277, doi: 10.1214/11-STS370.

Goderniaux, P., S. Brouyère, H. J. Fowler, S. Blenkinsop, R. Therrien, P. Orban, and Alain Dassargues (2009), Large scale surface-subsurface hydrological model to assess climate change impacts on groundwater reserves, J. Hydrol., 373, 122-138.

Goovaerts, P., (1997) Geostatistics for natural resources evaluation, Oxford University Press New York, 496pp.

Graf, A., D. Schüttemeyer, H. Geiß, A. Knaps, M. Möllmann-Coers, J. H. Schween, S. Kollet, B. Neininger, M. Herbst, H. Vereecken (2010), Boundedness of turbulent temperature probability distributions and their relation to the vertical profile in the convective boundary layer, Bound. Layer Meteorol., 134, 459–486.

Gribovszki, Z., J. Szilágye, and P. Kalicz (2010), Diurnal fluctuations in shallow groundwater levels and streamflow rates and their interpretation – A review, J. Hydrol., 385, 371-383.

Grinsted, A., J. C. Moore, and S. Jevrejeva (2004), Application of the cross wavelet transform and wavelet coherence to geophysical time series, Nonlin. Process. Geophys., 11, 561-566.

Gundogdu, K. S., and I. Guney (2007), Spatial analysis of groundwater levels using universal kriging, J. Earth Syst. Sci., 116(1), 49-55.

Haddad, Z. S., J. P. Meagher, R. F. Adler, E. A. Smith, E. Im, and S. L. Durden (2004), Global variability of precipitation according to the tropical rainfall measuring mission, J. Geophys. Res., 109, doi:10.1029/2004JD004607.

Hauck, C., C. Barthlott, L. Krauss, and N. Kalthoff (2011), Soil moisture variability and ist influence on convective precipitation over complex terrain, Q. J. R. Meteorol. Soc., 137, 42-56.

Hohenegger, C., P. Brockhaus, C. S. Bretherton, and C. Schär (2009), The soil moisture-precipitation feedback in simulations with explicit and parameterized convection, J. Clim., 22, 5003-5020.

Hsu, K.-C., and S.-T. Li (2010), Clustering spatial-temporal precipitation data using wavelet transform and self-organizing map neural network, Adv. Water Resour., 33, 190-200.

Jones, J. E., and C. S. Woodward (2001), Newton-Krylov-multigrid solvers for large-scale, highly heterogeneous, variably saturated flow problems, Adv. Water Resour., 24(7), 763– 774.

Juang, J.-Y, A. Porporato, P. C. Stoy, M. S. Sequeira, A. C. Oishi, M. Detto, H.-S. Kim, and G. G. Katul (2007), Hydrologic and atmospheric controls on initiation of convective precipitation events, Water Resour. Res., 43, doi:10.1029/2006WR004945.

Kessomkiat, W., H.-J. Franssen, A. Graf, and H. Vereecken (2013), Estimating random errors of eddy covariance data: An extended two-tower approach, Agric. Forest Meteorol., 171-172, 203-219.

Khodayar, S., N. Kalthoff, and G. Schädler (2013), The impact of soil moisture on seasonal convective precipitation simulations. Part I: validation, feedbacks, and realistic initialization, Meteorol. Z., 22, 489-505.

Kim, Y., and G. Wang (2007), Impact of initial soil moisture anomalies on subsequent precipitation over North America in the coupled land-atmosphere model CAM3-CLM3, J. Hydrometeorol., 8, 513-533.

Kollet, S. J. (2009), Influence of soil heterogeneity on evapotranspiration under shallow water table conditions: transitent, stochastic simulations, Environ. Res. Lett., 4, doi:10.1088/1748-9326/4/3/035007.

Kollet, S. J., and R. M. Maxwell (2006), Integrated surface-groundwater flow modeling: A free-surface overland flow boundary condition in a parallel groundwater flow model, Adv. Water Resour., 29(7), 945– 958.

Kollet, S. J., and R. M. Maxwell (2008), Capturing the influence of groundwater dynamics on land surface processes using an integrated, distributed watershed model, Water Resour. Res., 44, W02402, doi:10.1029/2007WR006004.

Kollet, S. J., I. Cvijanovic, D, Schüttermeyer, R. M. Maxwell, A. F. Moene, and P. Bayer (2009), The influence of rain sensible heat and subsurface energy transport on the energy balance at the land surface, Vadose Zone J., 8, 846-857, doi:10.2136/vzj2009.0005.

Koster, R. D., M. J. Suarez, R. W. Higgins, and H. M. van den Dool (2003), Observational evidence that soil moisture variations affect precipitation, Geophys. Res. Lett., 30, doi: 10.1029/2002GL016571.

Koster, R., D., et al. (2004), Regions of strong coupling between soil moisture and precipitation, Science, 305, 1138-1140.

Kumar, P., and E. F. Georgiou (1993), A multicomponent decomposition of spatial rainfall fields 1. Segregation of large- and small-scale features using wavelet transforms, Water Resour. Res., 29(8), 2515-2532.

Kuo W.-L., T. S. Steenhuis, C. E. McCulloch, C. L. Mohler, D. A. Weinstein, S. D. DeGloria, and D. P. Swaney (1999), Effect of grid size on runoff and soil moisture for a variable-source-area hydrology model. Water Resour. Res., 35(11), 3419–3428.

Labat, D., J. Ronchail, and J. L. Guyot (2005), Recent advances in wavelet analyses: Part2-Amazon, Parana, Orinoco and Congo discharges time scale variability, J. Hydrol., 314, 289-311.

Lam, A., D. Karssenberg, B. J. J. M. van den Hurk, and M. F. P. Bierkens (2011), Spatial and temporal connections in groundwater contribution to evaporation, Hydrol. Earth Syst. Sci., 15, 2621–2630.

Lauzon, N., F. Anctil, and J. Petrinovic (2004), Characterization of soil moisture conditions at temporal scales from a few days to annual, Hydrol. Process., 18, 3235-3254, doi: 10.1002/hyp.5656.

Leung, L. R., M. Huang, Y. Qian, and X. Liang (2011), Climate-soil-vegetation control on groundwater table dynamics and its feedback in a climate model, 36, 57-81.

Li, Z., and Y.-K. Zhang (2007), Quantifying fractal dynamics of groundwater systems with detrended fluctuation analysis, J. Hydrol., 336, 139-146.

Liang, X., and Y.-K. Zhang (2013), Temporal and spatial variation and scaling of groundwater levels in a bounded unconfined aquifer, J. Hydrol., 479, 139-145.

Liang, X., Z. Xie, and M. Huang (2003), A new parameterization for surface and groundwater interactions and its impact on water budgets with the variable infiltration capacity (VIC) land surface model, J. Geophys. Res., 108(D16), doi:10.1029/2002JD003090.

Lin, Y.-L., R. D. Farley, and H. Orville (1983), Bulk parameterization of the snow field in a cloud model, J. Climate Appl. Meteor., 22, 1065–1092, doi:10.1175/1520-0450.

Little, M. A., and J. P. Bloomfield (2010), Robust evidence for random fractal scaling of groundwater levels in unconfined aquifers, J. Hydrol., 393, 362-369.

Liu, H.-L., A.-M. Bao, X. Chen, L. Wang, and X.-L. Pan (2011), Response analysis of rainfall–runoff processes using wavelet transform: a case study of the alpine meadow belt, Hydrol. Process., 25, 2179-2187.

Liu. Y., and H. V. Gupta (2007), Uncertainty in hydrologic modeling: Towards an integrated data assimilation framework, Water Resour. Res., 43, W07401, doi:10.1029/2006WR005756.

Lo, M.-H., and J. S. Famiglietti (2010), Effect of water table dynamics on land surface hydrologic memory, J. Geophys. Res, 115, doi:10.1029/2010JD014191.

Manabe, S. (1969), Climate and the ocean circulation, Mon. Wea. Rev., 97, 739-774.

Manabe, S., and T. Delworth (1990), The temporal variability of soil wetness and its impact on climate, *Climate Change*, *16*, 185-192.

Matsoukas, C., S. Islam, and I. Rodriguez-Iturbe (2000), Detrended fluctuation analysis of rainfall and streamflow time series, J. Geophys. Res., 105, D23, 29165-29172.

Maxwell, R. M. (2013), A terrain-following grid transform and preconditioner for parallel, large-scale integrated hydrologic modeling, Adv. Water Resour., 53, 109-117.

Maxwell, R. M., and N. L. Miller (2005), Development of a coupled land surface and groundwater model, J. Hydrometeorol., 6, 233-247.

Maxwell, R. M., and S. J. Kollet (2008), Interdependence of groundwater dynamics and land-energy feedbacks under climate change, Nat. Geosci., 1, 665-669.

Maxwell, R. M., F. K. Chow, and S. J. Kollet (2007), The groundwater-land-surface-atmosphere connection; Soil moisture effects on the atmospheric boundary layer in fully-coupled simulations, Adv. Water Resour., 30, 2447-2466.

Mellor, G. L., and T. Yamada (1982), Development of a turbulence closure model for geophysical fluid problems, Rev. Geophys. Space Phys., 20, 851–875, doi:10.1029/RG020i004p00851.

Miguez-Macho, G., and Y. Fan (2012a), The role of groundwater in the Amazon water cycle: 1. Influence on seasonal streamflow, flooding and wetlands, J. Geophys. Res., 117, D15113, doi:10.1029/2012JD017539.

Miguez-Macho, G., and Y. Fan (2012b), The role of groundwater in the Amazon water cycle: 2. Influence on seasonal soil moisture and evapotranspiration, J. Geophys. Res., 117, D15114, doi:10.1029/2012JD017540.

Moradkhani, H., K.-L. Hsu, H. Gupta, and S. Sorooshian (2005), Uncertainty assessment of hydrologic model states and parameters: Sequential data assimilation using the particle filter, Water Resour. Res., 41, W05012.

Nash, J. E., and J. V. Sutcliffe (1970), River flow forecasting through conceptual models Part I – A discussion of principles, J. Hydrol., 10, 282-290.

Niu, G.-Y., C. Paniconi, P. A. Troch, R. L. Scott, M. Durcik, X. Zeng, T. Huxman, and D. C. Goodrich (2013), An integrated modelling framework of catchment-scale ecohydrological processes: 1. Model description and tests over an energy-limited watershed, Ecohydrol., doi: 10.1002/eco.1362.

Niu, G.-Y., Z.-L. Yang, R. E. Dickinson, L. E. Gulden, and H. Su (2007), Development of a simple groundwater model for use in climate models and evaluation with Gravity Recovery and Climate Experiment data, J. Geophys. Res., 112, doi:10.1029/2006JD007522.

Oglesby, R. J., and D. J. Erickson (1989), Soil moisture and the persistence of North American drought, J. Climate, 2, 1362-1380.

Oleson, K. W., et al. (2004), Technical Description of the Community Land Model (CLM). NCAR Tech. Note NCAR/TN-461+STR, 257 pp., doi:10.5065/D6N877R0.

Orth, R., and S. I. Seneviratne (2013), Predictability of soil moisture and streamflow on subseasonal timescales: A case study, J. Geophys. Res., 118, 10963-10979.

Parajka, J., R. Merz, and G. Blöschl (2005), A comparison of regionalisation methods for catchment model parameters, Hydrol. Earth Syst. Sci., 9, 157-171.

Patton, E. G., P. P. Sullivan, and C.-H. Moeng (2005), The influence of idealized heterogeneity on wet and dry planetary boundary layers coupled to the land surface, 62, 2078-2097.

Perez-Valdivia, C., D. Sauchyn, and J. Vanstone (2012), Groundwater levels and teleconnection patterns in the Canadian Prairies, Water Resour. Res., 48, W07516, doi:10.1029/2011WR010930.

Phillips, T. J., and S. A. Klein (2014), Land atmosphere coupling manifested in warm-season observations on the U.S. southern great plains, J. Geophys. Res. Atmos., 119, 509–528, doi:10.1002/2013JD020492.

Porporato, A., P. D'Odorico, L. Ridolfi, and I. Rodriguez-Iturbe (2000), A spatial model for soil-atmosphere interaction: Model construction and linear stability analysis, Am. Met. Soc., 1, 61-74.

Quinn, P., K. Beven, A. Culf (1995), The introduction of macroscale hydrological complexity into land surface-atmosphere transfer models and the effect on planetary boundary layer development, J. Hydrol., 166, 421-444.

Rahman, M., M. Sulis, and S. J. Kollet (2014), The concept of dual-boundary forcing in land surface-subsurface interactions of the terrestrial hydrologic and energy cycles, Water Resour. Res., 50, 8531-8548.

Rahman, M., M. Sulis, and S. J. Kollet (2015a), Evaluating the dual-boundary forcing concept in subsurface-land surface interactions of the hydrological cycle, Hydrol. Porcess. (submitted).

Rahman, M., M. Sulis, and S. J. Kollet (2015b), The subsurface-land surface-atmosphere connection under convective conditions, Adv. Water Resour. (under review).

Raschendorfer, M. (2001), The new turbulence parameterization of LM, COSMO Newsletter, Vol.1, Consortium for Small-Scale Modeling, 89–97.

Reinhardt, T., and A. Seifert (2006), A three-category ice scheme for LMK, COSMO Newsletter, Vol. 6, Consortium for Small-Scale Modeling, 115–120.

Richards, L. A. (1931), Capillary conduction of liquids through porous mediums, Physics 1, 318, doi: 10.1063/1.1745010.

Ritter, B., and J. F. Geleyn (1992), A comprehensive radiation scheme for numerical weather prediction models with potential applications in climate simulations, Mon. Wea. Rev., 120, 303–325.

Rodell, M., P. R. Houser, U. Jambor, J. Gottschalck, K. Mitchell, C. -J. Meng, K. Arsenault, B. Cosgrove, J. Radakovich, M. Bosilovich, J.K. Entin, J.P. Walker, D. Lohmann, and D. Toll (2004), The Global Land Data Assimilation System, Bull. Amer. Meteor. Soc., 85(3), 381-394.

Rosenbaum, U., H. R. Bogena, M. Herbst, J. A. Huisman, T. J. Peterson, A. Weuthen, A. W. Western, and H. Vereecken (2012), Seasonal and event dynamics of spatial soil moisture patterns at the small catchment scale, Water Resour. Res., 48, W10544, doi:10.1029/2011WR011518.

Rowell, D. P., and C. Blondin (1990), The influence of soil wetness distribution on short-range rainfall forcasting in the West African Sahel, Q. J. R. Meteorol. Soc, 116, 1471-1485.

Samaniego, L., R. Kumar, and S. Attinger (2010), Multiscale parameter regionalization of a grid-based hydrologic model at the mesoscale, Water Resour. Res., 46, W05523, doi:10.1029/2008WR007327.

Santanello, J. A., C. D. Peters-Lidard, S. V. Kumar, C. Alonge, and W.-K. Tao (2009), A modeling and observational framework for diagnosing local land-atmosphere coupling on diurnal time scales, J. Hydrometeorol., 10, 577-599.

Schaap, M. G., and F. J. Leij (1998), Database-related accuracy and uncertainty of pedotransfer functions, Soil Sci., 163(10), 765–779.

Schär, C., D. Lüthi, U. Beyerle, and E. Heise (1999), A soil-precipitation feedback: A process study with a regional climate model, J. Clim., 12, 722-741.

Schilling, K. E., and Y.-K. Zhang (2012), Temporal scaling of groundwater level fluctuations near a stream, Ground Water, 50(1), 59-67.

Schomburg, A., V. Venema, R. Lindau, F. Ament, and C. Simmer (2010), A downscaling scheme for atmospheric variables to drive soil-vegetation-atmosphere transfer models, Tellus, 62B, 242–258, doi:10.1111/j.1600-0889.2010.00466.x.

Schomburg, A., V. Venema, R. Lindau, F. Ament, and C. Simmer (2012), Disaggregation of screen-level variables in a numerical weather prediction model with an explicit simulation of subgrid scale land-surface heterogeneity, Meteor. Atmos. Phys., 116, 81–94, doi:10.1007/s00703-012-0183-y.

Schubert, S., R. Koster, M. Hoerling, R. Seager, D. Lettermaier, A. Kumar, and D. Gutzler (2007), Predicting drought on seasonal-to-decadal time scales, Bul. Am. Met. Soc., 1625-1630.

Seneviratne, S.I., and R. Stöckli (2008), in: Bronnimann, S., J. Luterbacher, T. Ewen, H.F. Diaz, R.S. Stolarski, U. Neu (Eds.), Climate Variability and Extremes during the Past 100 Years, Series: Adv. Global Change Research, vol. 33, Springer, Dordrecht, pp. 179–193.

Seuffert, G., P. Gross, and C. Simmer (2002), The influence of hydrologic modeling on the predicted local weather: Two-way coupling of a mesoscale weather prediction model and a land surface hydrologic model, J. Hydrometeorol., 3, 505-523.

Sheffield, J., and E. F. Wood (2008), Global trends and variability in soil moisture and drought characteristics, 1950-2000, from observation-driven simulations of the terrestrial hydrological cyle, J. Climate, 21, 432-458.

Shen, C., J. Niu, and M. S. Phanikumar (2013), Evaluating controls on coupled hydrologic and vegetation dynamics in a humid continental climate watershed using a subsurface-land surface processes model, Water Resour. Res., 49, doi:10.1002/wrcr.20189.

Shin, S.-H, and K.-J. Ha (2007), Effects of spatial and temporal variations in PBL depth on a GCM, J. Clim, 20, 4717-4732.

Shrestha, P., M. Sulis, M. Masbou, S. Kollet, and C. Simmer (2014) A Scale-Consistent Terrestrial Systems Modeling Platform Based on COSMO, CLM, and ParFlow, Mon. Wea. Rev., 142, 3466–3483.

Shukla, J., and Y. Mintz (1982), Influence of land-surface evapotranspiration on the earth's climate, Science, 215, 1498–1501.

Simmer, C., et al. (2015), Monitoring and Modeling the Terrestrial System from Pores to Catchments - the Transregional Collaborative Research Center on Patterns in the Soil-Vegetation-Atmosphere System, Bul. Am. Met. Soc., doi: 10.1175/BAMS-D-13-00134, in press.

Sklash, M. G., and R. N. Farvolden (1979), The role of groundwater in storm runoff, J. Hydrol., 43, 45-65.

Smith, L. C., D. L. Turcotte, and B. L. Isacks (1998), Stream flow characterization and feature detection using a discrete wavelet transform, Hydrol. Process., 12, 233-249.

Soylu, M. E., E. Istanbulluoglu, J. D. Lenters, and T. Wang (2011), Quantifying the impact of groundwater depth on evapotranspiration in a semi-arid grassland region, Hydrol. Earth Syst. Sci., 15, 787–806.

Stull, R. B. (1988), An Introduction To Boundary Layer Meteorology, Dordrecht: Kluwer Academic Publishers, 2pp.

Su, H., Z.-L. Yang, R. E. Dickinson, and J. Wei (2014), Spring soil moisture-precipitation feedback in the Southern Great Plains: How is it related to large-scale atmospheric conditions?, Geophys. Res. Lett., 41, 1283-1289.

Sulis, M., C. Paniconi, and M. Camporese (2011), Impact of grid resolution on the integrated and distributed response of a coupled surface–subsurface hydrological model for the des Anglais catchment, Quebec, Hydrol. Proc., 25, 1853-1865.

Szilagyi, J., V. A. Zlotnik, and J. Jozsa (2013), Net recharge vs. depth to groundwater relationship in the platte river valley of Nebraska, United States, Groundwater, 51(6), 945-951.

Táany, R. A., A. B. Tahboub, and G. A. Saffarini (2009), Geostatistical analysis of spatiotemporal variability of groundwater level fluctuations in Amman-Zarqa basin, Jordan: a case study, Environ. Geol., 57, 525-535.

Taylor, C. A., R. A. M. de Jeu, F. Guichard, P. P. Harris, and A. Dorigo (2012), Afternoon rain more likely over drier soils, Nature, 489, 423-426.

Tian, W., X. Li, G.-D. Cheng, X.-S. Wang, and B. X. Hu (2012), Coupling a groundwater model with a land surface model to improve water and energy cycle simulation, Hydrol. Earth Syst. Sci., 16, 4707–4723, doi:10.5194/hess-16-4707-2012.

Tiedtke, M. (1989), A comprehensive mass flux scheme for cumulus parameterization in large-scale models, Mon. Wea. Rev., 117, 1779-1800.

Torrence, C., and G. P. Compo (1997), A practical guide to wavelet analysis, Bul. Am. Met. Soc., 79(1), 61-78.

Valcke, S., T. Craig, and L. Coquart, Eds. (2013), OASIS3-MCT user guide: OASIS3-MCT 2.0, CERFACS Tech. Rep. TR/CMGC/13/17, CERFACS/CNRS SUC URA 1875, 50 pp.

van de Boer, A., A.F. Moene, D. Schüttemeyer, A. Graf (2013), Sensitivity and uncertainty of analytical footprint models according to a combined natural tracer and ensemble approach, Agric. For. Meteorol., 169, 1–11.

van Genuchten, M. Th. (1980), A closed-form equation for predicting the hydraulic conductivity of unsaturated soils, Soil Sci. Soc. Am. J., 44,892-898.

Vereecken, H., S. Kollet, and C. Simmer (2010), Patterns in Soil–Vegetation–Atmosphere systems: Monitoring, modeling, and data assimilation, Vadose Zone J., 9, 821-827.

Vrugt, J. A., C. G. H. Diks, H. V. Gupta, W. Bouten, and J. M. Verstraten (2005), Improved treatment of uncertainty in hydrologic modeling: Combining the strengths of global optimization and data assimilation, Water Resour. Res., 41, W01017, doi:10.1029/2004WR003059.

Wen, R., and R. Sinding-Larsen (1997), Uncertainty in fractal dimension estimated from power spectra and variograms, Math. Geol., 29(6), 727-753.

Wetzel, P. J. (1982), Toward parameterization of the stable boundary layer, J. Appl. Meteorol., 21, 7-13.

Wetzel, P. J., and J.-T. Chang (1987), Concerning the relationship between evapotranspiration and soil moisture, J. Clim. Appl. Meteorol., 26, 18-27.

Wicker, L. J., and W. C. Skamarock (2002), Time-splitting methods for elastic models using forward time schemes, Mon. Wea. Rev., 130, 2088–2097.

Williams, J. L., and R. M. Maxwell (2011), Propagating subsurface uncertainty to the atmosphere using fully coupled stochastic simulations, J. Hydrometeorol., 12, 690-701.

Wu, R., and J. L. Kinter (2009), Analysis of the relationship of U.S. drought with SST and soil moisture: Distinguishing the time scale of droughts, J. Climate, 22, 4520-4538.

Wu, W., and R. E. Dickinson (2004), Time scales of layered soil moisture memory in the context of land-atmosphere interaction, J. Climate, 17, 2752-2764.

Yeh, P. J.-F, and E. A. B. Eltahir (2005), Representation of water table dynamics in a land surface scheme. Part I: model development, J. Climate, 18, 1861-1880.

York, J. P., M. Person, W. J. Gutowski, and T. C. Winter (2002), Putting aquifers into atmospheric simulation models: An example from the Mill Creek Watershed, northeastern Kansas, Adv. Water Resour., 25(2), 221– 238.

Yuan, X., Z. Xie, J. Zheng, X. Tian, and Z. Yang (2008), Effects of water table dynamics on regional climate: A case study over east Asian monsoon area, J. Geophys. Res., 113, D21112, doi:10.1029/2008JD010180.

Zeng, X.-M., M. Zhao, B.-K. Su, J.-P. Tang, Y.-Q. Zheng, and J. Chen (2003), Effects of the land-surface heterogeneities in temperature and moisture from the “combined approach” on regional climate: a sensitivity study, Glob. Planet. Change, 37, 247-263.

Zhang W., and D. R. Montgomery (1994), Digital elevation model grid size, landscape representation, and hydrologic simulation, Water Resour. Res., 30(4), 1019–1028.

Zhang, J., W.-C. Wang, and J. Wei (2008), Assessing land-atmosphere coupling using soil moisture from the Global Land Data Assimilation System and observational precipitation, J. Geophys. Res., 113, D17119, doi:10.1029/2008JD009807.

Appendices

A. Variogram analysis

In this thesis, the spatial variability of different fluxes in the coupled water and energy cycles were analyzed using semivariograms. According to *Goovaerts* [1997], the experimental semivariogram for a spatially distributed attribute *z* is calculated as

$$\gamma(h) = \frac{1}{2N(h)} \sum_{\alpha=1}^{N(h)} [z(u\alpha) - z(u\alpha + h)]^2 \quad \text{(A.1)}$$

where *h* is the lag distance, *N* is the number of pairs, and *u* is measurement location. The cross-semivariogram between z_a and z_b is calculated as

$$\gamma_{ab}(h) = \frac{1}{2N(h)} \sum_{\alpha=1}^{N(h)} [z_a(u\alpha) - z_a(u\alpha + h)].[z_b(u\alpha) - z_b(u\alpha + h)] \quad \text{(A.2)}$$

In this study, omni-directional variograms were calculated, which assumes that the data is isotropic.

B. Continuous wavelet transform analysis

The wavelet transform is a useful tool in analyzing time series variability and has been used previously to analyze various geophysical data [e.g., *Andreo et al.*, 2006; *Liu et al.*, 2011; *Perez-Valdivia et al.*, 2012]. Continuous wavelet transform analysis was used in this thesis to show the time localized temporal variance of different processes as a function of frequency. If x_n is a timeseries ($n = 0 \ldots N-1$) with an equal time spacing of δt, according to *Torrence and Compo* [1997], the continuous wavelet transform of x_n can be defined as its convolution with a scaled and translated version of a wavelet function $\psi_0(\eta)$

$$W_n(s) = \sum_{n'=0}^{N-1} x_n \psi_0 * \left[\frac{(n'-n)\delta t}{s} \right] \quad \text{(B.1)}$$

where s is the wavelet scale and (*) denotes the complex conjugate. The wavelet function depends on the non-dimensional time parameter η. In this study, we use the Morlet wavelet as the wavelet function, which can be expressed as

$$\psi_0(\eta) = \pi^{-1/4} e^{i\omega_0 \eta} e^{-\eta^2/2} \quad \text{(B.2)}$$

where ω_0 is the non-dimensional frequency. The global wavelet power is obtained by averaging the wavelet powers over the localized time instances and can be defined as

$$\overline{W}^2(s) = \frac{1}{N} \sum_{n=0}^{N-1} \left| W_n(s) \right|^2 \quad \text{(B.3)}$$

The cross-wavelet spectrum of two time series x and y can be defined as

$$W_n^{xy} = W_n^x(s) W_n^y *(s) \quad \text{(B.4)}$$

where $W_n^x(s)$ and $W_n^y(s)$ denote the wavelet transform of x and y, respectively. According to *Torrence and Compo* [1997], high cross-wavelet power indicates covariance between the time series. *Grinsted et al.* [2004] argued that a phase locked phenomenon with high cross-wavelet power implies a cause and effect relationship between two time series.

C. Atmospheric boundary layer height (ABLH)

The lowest part of the troposphere, which is influenced by the land surface fluxes and has a response time less than an hour is defined as the boundary layer [*Stull*, 1988]. The height of the boundary layer is calculated based on Bulk Richardson Number (BRN). The BRN is computed between ground and a height z as follows:

$$BRN_z = \frac{g(\theta_z - \theta_{ground})(z - z_{ground})}{\theta_z[(u_z - u_{ground})^2 + (v_z - v_{ground})^2]} \quad \text{(C.1)}$$

where g is the acceleration due to gravity (ms^{-2}), θ is the virtual potential (K), u is the zonal wind (ms^{-1}), and v is the meridional wind (ms^{-1}). The ABLH is calculated using this equation assuming a critical BRN_z of 0.33 [*Wetzel*, 1982].

D. Convective Available Potential Energy (CAPE)

The vertically integrated index CAPE is the measure of cumulative buoyant energy between the level of free convection (z_{LFC}) and equilibrium level (z_{EL}) [*Blanchard*, 1998]. z_{LFC} is the level where the temperature of an air parcel exceeds the ambient temperature. At this level the parcels are unstable relative to their ambient. z_{EL} is defined as the level where the ambient temperature exceeds the parcel temperature and the parcels are stable relative to their environment. According to *Doswell and Rasmussen* [1994], CAPE is calculated as follows:

$$CAPE = g.\int_{z_{LFC}}^{z_{EL}} \frac{T_p - T_e}{T_e} dz \qquad \text{(D.1)}$$

Where g is the acceleration due to gravity (ms^{-2}), T_p is the virtual temperature of the air parcel (K), and T_e is the virtual temperature of the environment (K).

BONNER METEOROLOGISCHE ABHANDLUNGEN

Herausgegeben vom Meteorologischen Institut der Universität Bonn durch Prof. Dr. H. FLOHN (Hefte 1-25), Prof. Dr. M. HANTEL (Hefte 26-35), Prof. Dr. H.-D. SCHILLING (Hefte 36-39), Prof. Dr. H. KRAUS (Hefte 40-49), ab Heft 50 durch Prof. Dr. A. HENSE.

Heft 1-49: siehe `http://www.meteo.uni-bonn.de/bibliothek/bma`

Heft 50: ***Petra Friederichs***: Interannuelle und dekadische Variabilität der atmosphärischen Zirkulation in gekoppelten und SST-getriebenen GCM-Experimenten. 2000, 133 S. + VIII. € 25

Heft 51: ***Heiko Paeth***: Anthropogene Klimaänderungen auf der Nordhemisphäre und die Rolle der Nordatlantik-Oszillation. 2000, 168 S.+ XVIII. € 28

Heft 52: ***Hildegard Steinhorst***: Statistisch-dynamische Verbundsanalyse von zeitlich und räumlich hoch aufgelösten Niederschlagsmustern: eine Untersuchung am Beispiel der Gebiete von Köln und Bonn. 2000, 146 S. + XIV. € 25

Heft 53: ***Thomas Klein***: Katabatic winds over Greenland and Antartica and their interaction with mesoscale and synoptic-scale weather systems: three-dimensional numerical models. 2000, 146 S. + XIV. € 25

Heft 54: ***Clemens Drüe***: Experimentelle Untersuchung arktischer Grenzschichtfronten an der Meereisgrenze in der Davis-Straße. 2001, 165 S. + VIII. € 28

Heft 55: ***Gisela Seuffert***: Two approaches to improve the simulation of near surface processes in numerical weather prediction models. 2001, 128 S. + VI. € 25

Heft 56: ***Jochen Stuck***: Die simulierte axiale atmosphärische Drehimpulsbilanz des ECHAM3-T21 GCM. 2002, 202 S. + VII. € 30

Heft 57: ***Günther Haase***: A physical initialization algorithm for non-hydrostatic weather prediction models using radar derived rain rates. 2002, 106S. + IV. € 25

Heft 58: ***Judith Berner***: Detection and Stochastic Modeling of Nonlinear Signatures in the Geopotential Height Field of an Atmospheric General Circulation Model. 2003, 157 S. + VIII. € 28

Heft 59: ***Bernd Maurer***: Messungen in der atmosphärischen Grenzschicht und Validation eines mesoskaligen Atmosphärenmodells über heterogenen Landoberflächen. 2003, 182 S. + IX. € 30

Heft 60: ***Christoph Gebhardt***: Variational reconstruction of Quaternary temperature fields using mixture models as botanical – climatological transfer functions. 2003, 204 S. + VIII. € 30

Heft 61: ***Heiko Paeth***: The climate of tropical and northern Africa – A statistical-dynamical analysis of the key factors in climate variability and the role of human activity in future climate change. 2005, 316 S. + XVI. € 15

Heft 62: ***Christian Schölzel***: Palaeoenvironmental transfer functions in a Bayesian framework with application to Holocene climate variability in the Near East. 2006, 104 S. + VI. € 15

Heft 63: ***Susanne Bachner***: Daily precipitation characteristics simulated by a regional climate model, including their sensitivity to model physics, 2008, 161 S. € 15

Heft 64: ***Michael Weniger***: Stochastic parameterization: a rigorous approach to stochastic three-dimensional primitive equations, 2014, 148 S. + XV. open access[1]

Heft 65: ***Andreas Röpnack***: Bayesian model verification: predictability of convective conditions based on EPS forecasts and observations, 2014, 152 S. + VI. open access[1]

Heft 66: ***Thorsten Simon***: Statistical and Dynamical Downscaling of Numerical Climate Simulations: Enhancement and Evaluation for East Asia, 2014, 48 S. + VII. + Anhänge open access[1]

Heft 67: ***Elham Rahmani***: The Effect of Climate Change on Wheat in Iran, 2014, [erschienen] 2015, 96 S. + XIII. open access[1]

Heft 68: ***Pablo A. Saavedra Garfias***: Retrieval of Cloud and Rainwater from Ground-Based Passive Microwave Observations with the Multi-frequency Dual-polarized Radiometer ADMIRARI, 2014, [erschienen] 2015, 168 S. + XIII. open access[1]

Heft 69: ***Christoph Bollmeyer***: A high-resolution regional reanalysis for Europe and Germany - Creation and Verification with a special focus on the moisture budget, 2015, 103 S. + IX. open access[1]

Heft 70: ***A S M Mostaquimur Rahman***: Influence of subsurface hydrodynamics on the lower atmosphere at the catchment scale, 2015, 98 S. + xvi. open access[1]

Heft 71: ***Sabrina Wahl***: Uncertainty in mesoscale numerical weather prediction: probabilistic forecasting of precipitation, 2015, 108 S. open access[1]

[1]Available at `http://hss.ulb.uni-bonn.de/fakultaet/math-nat/`

METEOROLOGISCHES INSTITUT
MATHEMATISCH NATURWISSENSCHAFTLICHE FAKULTÄT
UNIVERSITÄT BONN

Meteorologisches Institut
Universität Bonn